
# SUPERCONDUCTIVITY AND LOCALIZATION IN DISORDERED SUPERCONDUCTORS

A DISSERTATION SUBMITTED TO GRADUATE PROGRAMS OF ADDIS ABABA UNIVERSITY IN PARTIAL FULFILLMENT OF THE REQUIREMENTS FOR THE DEGREE OF DOCTOR OF PHILOSOPHY IN PHYSICS

BY

ZELEKE DERESSA GERBI

ADDIS ABABA, ETHIOPIA

November 8, 2019

ADDIS ABABA UNIVERSITY

SCHOOL OF GRADUATE STUDIES

DEPARTMENT OF PHYSICS

This is to certify that the dissertation prepared by Zeleke Deressa Gerbi, entitled **Superconductivity and Localization in Disordered Superconductors** and submitted in partial fulfillment of the requirements for the Degree of Doctor of Philosophy in Physics, complies with the regulations of the University and meets the accepted standards with respect to originality and quality.

Dated: November 8, 2019

Chair person of the Department: _____
**Teshome Senbeta (PhD)**

Research Supervisor: _____
**Prof. Pooran Singh**

External Examiner: _____
**Prof. Ranjan Kumar**

Internal Examiner: _____
**Chernet Amente (PhD)**

ADDIS ABABA UNIVERSITY
SCHOOL OF GRADUATE STUDIES
DEPARTMENT OF PHYSICS

Date: **November 8, 2019**

Author: **Zeleke Deressa Gerbi**

Title: **Superconductivity and Localization in Disordered Superconductors**

Department: **Physics**

Degree: **PhD** Convocation Year: **2019**

Permission is herewith granted to Addis Ababa University to circulate and to have copied for noncommercial purpose, at its discretion, upon the request of individuals or institutions.

_____
**Signature**

This work is dedicated to my father Deressa Gerbi and my mother Sedare Sakata.

# Acknowledgements

Above all, I would be grateful to the Almighty God for everything that has been done for me throughout my life career. Next, I would like to express my profound appreciation to my advisor, Prof. Pooran Singh. His continuous supervision, motivation, deep knowledge and friendly approach have proved invaluable to me in my struggle to make the very difficult transition from a student to a researcher.

I would also like to thank Prof. Rajeev Ahuja of Uppsala University for his invitation to visit his Computational Material Theory group. This group introduced me how to perform DFT calculations using VASP and Quantum ESPRESSO software packages. In particular, I have a special thanks for Dr. Sudip and Terapaat for their tutorship during my stay at Uppsala University.

I have likewise a special thanks to staff members Dr. Chernet Amente, Dr. Tesgera Bedassa, Dr. Lemi Demeyou, Dr. Deribie Hirpo, Dr. Teshome Senbeta, and Tsilat Adinew for their academic, morale, technical support and hospitality throughout my stay at AAU. My special thank also goes to all my beloved families and friends for their unlimited support during my study years. I also acknowledge the financial support of Addis Ababa University and Ambo University.

# Contents

# List of Figures

# Abstract

The effect of disorder due to nomagnetic impurities on superconductivity of $Bi_2Sr_2CaCu_2O_{8+x}$ was investegated theoretically employing the matrix Green function in Nambu formalism. The relationship between disorder parameter and superconducting critical temperature has been calculated analytically for each of its possible pairing symmetries. The obtained results indicate that diluted nonmagnetic disorder has no significant effect on superconducting critical temperature of the system when the pairing symmetry is s-wave. On the other hand, the results obtained for the d-wave pairing symmetries show that disorder can significantly suppress the superconducting critical temperature of the system. Moreover, the results reveal that the supression of $T_c$ depends on the strength of the impurity potential, the concentration of scatterers and the anisotropy of the pairing symmetries.

The effect of disorder due to randomness in island potential on superconductivity of thin films was also investigated theoretically based on the hard core boson model developed for superfluid helium. The relationship between superconducting order parameter and disorder paramters was found analytically using the double time retarded Green function formalism. The obtained results indicate that disorder induced due to randomness in island potential enhances decoherence of Cooper pairs and suppresses superconducting order parameter and superfluidity of the system. The results also indicate that increasing the two-body interaction strength suppresses superconductivity of the system. The critical values of disorder and interactin strength at which the system completely ceases its superconductivity was also determined. Below these critical values, the system acts as a superconductor, a system with zero electrical resistance. Above the critical values, it acts as an insulator, a system with infinite electrical resistance.

Finally, the effect of pressure on superconductivity of Pb and $MgB_2$ was investigated theoretically based on density functional theory as implemented in Quantum ESPRESSO

computational package. The electronic and phonon density of states, isotropic Eliashberg spectral density, electron-phonon coupling strength, logarithmic phonon frequency and superconducting critical temperature were calculated for both superconductors using the general framework of Eliashberg formalism. The results obtained for bulk Pb indicate that pressure suppresses its superconducticvity. It was obseved that $T_c$ decreases from 7.86 K at equilibrium structure to almost zero at a pressure of 3500 kbar. The results obtaind for bulk $MgB_2$ indicate that pressure enhances its superconductivity in contrast to that of the bulk Pb. It was observed that at equilibrium, where pressure of the system is almost zero, the calculated $T_c$ value is around 35.67 K. This value is enhanced to around 95 K at pressure of 6500 kbar and then starts to decrease slowly. The investigators emphasize that this approach of strain engineering, with the target of suppressing/enhancing $T_c$ as demonstrated in this work, can be applied to various strain-engineering problems in other functional materials.

# 1

# General Introduction

The difficulty of understanding the features of many-particle systems is central to all the areas of condensed matter physics. In such strongly-correlated many-particle systems, the ground state that emerges can have unexpected properties. One of the most striking examples of this was the discovery of superconductivity. As a loss of electric resistance at a characterstic temperature, called critical temperature $T_c$, superconductivity was first discovered in 1911 by Dutch physicist Heike Kamerlingh Onnes [1] in liquid metallic mercury and understood almost half a century later by American physicists John Bardeen, Leon Cooper and John Robert Schrieffer [2,3] in 1957 through their celebrated BCS theory. The idea behined BCS theory was the understanding of this new state of matter in which electrons are condensed together in a phase-coherent state of pairs. BCS theory was able to explain very well the microscopic mechanisms of many of the properties observed in conventional superconductors. BCS theory is one of the most clebrated theory of the $20^{\text{th}}$ century.

With a huge potential for applications, experimentalists have been searching for the elusive room temperature superconductor since the BCS theory. This resulted famously in the discovery of what is known as high critical temperature superconductivity ($T_c > 30K$) in doped cuprates and iron based compounds [4,5]. Despite its celebrity, the BCS theory has failed to explain the mechanism for the unconventional high transition temperature superconductivity. Although there are theories which qualitatively explain the possible mechanisms of pairing and symmetry of the gap, no one has yet settled on the question of what is the origin of superconductivity in these materials.

Much less publicized and with fewer experimental groups currently working on it, the story of superconductivity has been branched out in to another direction, namely the investigation of dirty superconductors. The investigation of superconductivity in the presence of disorder began in the late 1930s with the work of Alexander Shalnikov [6] at the institute for the physical problems in Moscow. The investigation was revived again in the late 1950s with the Nobel Prize-winning work of Anderson [7] and work of Abrikosov and Gor'kov [8]. Anderson showed that disorder solely by itself can destroy superconductivity and lead to insulating behavior in materials if sufficiently strong. Abrikosov and Gor'kov also showed that magnetic impurities of arbitrary concentration can destroy superconductivity of materials.

The problem of dirty superconductors gives a unique opportunity to study the competition between **superconductivity** which results from pairing of electrons and **localization** which results from scattering effects of nonmagnetic and magnetic impurities [7,8], pair breaking effects of disorder induced Coulomb repulsion, or disorder induced decoherence effects [9,10]. The interest in the field was further increased by the possibility that the disorder driven or magnetic field driven suppression of superconductivity in the limit of zero temperature might be a quantum phase transition [10].

Investigations in this field also revealed that the pair-breaking and decoherence effects of disorder on superconductivity of materials depend on their physical dimension and superconducting pairing symmetry. According to Anderson, weak nonmagnetic disorders (impurities, dislocations, etc) which could not affect the time-reversal symmetry have no significant effect on thermodynamic properties of three-dimensional (3D) s-wave superconductors. In literature, this is well-known by Anderson's theorem. Until the late 1970s, most of the theoretical investigations in this field had been acting according to this theorem. However, the scaling theory of localization developed in 1979 by Abrahams *et al*. [11] revolutionalized the study of dirty superconductors. According to this theory, two-dimensional (2D) systems are supposed to exist in only one of the two states at zero temperature, superconductor or insulator. There is no room for the metallic state to appear at this temperature because all electrons are expected to localize by infinitisimal amount of disorder. Moreover, unlike the case of 3D, infinitesimal amount of disorder can

destroy superconductivity of 2D systems. As a result, 2D superconductors serve as ideal systems to study the less explored problem, the competition between **superconductivity** and **localization**.

Inspired by recent experimental and theoretical works on dirty superconductors, we have made our primary focus on the investigation of the effect of impurity scattering, on-site scalar disorder and pressure on superconductivity of some novel superconductors. Our specific focus is on the effects of impurity scattering on layered high-$T_c$ superconductors with s- and d-wave pairing symmetry, effect of disorder due to randomness in island potential on superconductivity of thin films, and effect of pressure on superconducting properties of strongly coupled and anisotropic superconductors (Pb & $MgB_2$). For the first investigation, we employed the mean-field approximated BCS model with some perturbation term added due to scattering of superconducting quasiparticles by local independent scattering centers. The analytic calculations were carried out using the methods of Greens functions in Nambu formalism. Impurity averaging was performed based on the rules of Feynman diagrams. For the second investigation, we used the tightly-bound hard-core boson model developed for superfluids with an additional term added due to random on-site disorder potential. Analytic calculations of this part were undertaken based on the equation of motion method of Greens functions. In order to study the effect of lattice strain induced pressure on the superconducting state, we have undertaken first-principle calculations based on the concepts of density functional theory (DFT). As a model for this part we employed the Eliashberg theory, which was developed as a remit of BCS theory.

The thesis, in general, is composed of seven chapters and organized as follows. **Chapter 1** presents a more general introduction of the thesis. **Chapter 2** presents the important literature reviewed. It begins with a quick review of the basic concepts in superconductivity. It then follows with a review of the most recent experimental artifacts and widely accepted theoretical paradigms forwarded in the areas of focus. The concept density of fuctional theory (DFT) is also discussed briefly. **Chapter 3** presents the necessary mathematical methods and computational techniques employed. More precisely, the Greens function formalisms used in the thesis were discussed in brief. **Chapter 4**

presents the effect of impurity scattering on superconductivity of unconventional d-wave superconductors. Specific attention is given to the effect of impurity scattering on superconducting critical temperature. **Chapter 5** presents how random on-site scalar potentials suppress the superconductivity of thin superconducting films. Particular attention is paid to the suppression of superconducting order parameter and sperfluid density. **Chapter 6** presents effects of pressure on the superconductivity of some novel superconductors. First-principle calculations were made in this chapter. **Chapter 7** presents the summary, conclusions and future outlooks of the thesis work.

# 2

# Literature Review

## 2.1 Overview of superconductivity

### 2.1.1 Discovery of superconductivity

The phenomenon of superconductivity was discovered in 1911 by Heike Kamerlingh Onnes. Onnes discovered this phenomenon only three years after he succeeded in liquefying helium [12, 13]. This discovery of liquid helium rendered temperatures as low as $1K$ accessible to experimental methods. Using this low temperature conditions, Onnes investigated the relationship between temperature and electrical resistivity of mercury. His investigation revealed that, as the temperature approaches absolute zero, the resistance completely disappeared below 4.2 K [1]. This kind of drop in electrical resistivity is a common property of all superconductors, and the temperature at which this occurs is known as the critical temperature $T_c$ (Figure 2.1). This temperature is the point at which a phase transition occurs between the normal and superconducting states.

The other unexpeted property shown by superconductors was discovered by W. Meissner and R. Ochsenfeld in 1933 [14]. According to their investigation, a superconducting material placed in a weak magnetic field will act as a perfect diamagnet [Figure 2.2]. This phenomenon is known as the Messiner effect. The maximum strength magnetic field in which the superconducting order is maintained is known as the critical field $H_c$. The phenomenon of perfect diamagnetic property of superconductors is applicable nowadays in modern train levitation technologies and for medication purposes.

Following Onnes discovery of superconductivity, theorists struggled for several

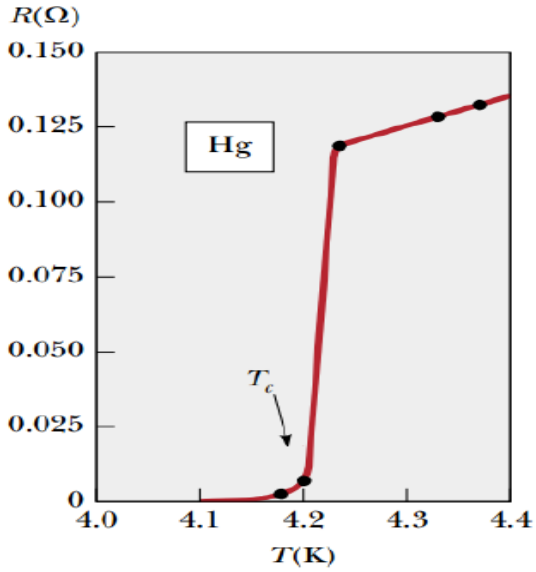


Figure 2.1: Vanishing of electrical resistivity below a critical temperature $T_c$, discovered in mercury. [The figure is taken from [12]].

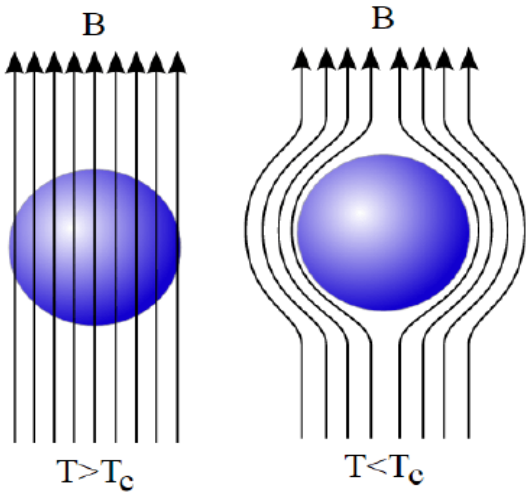


Figure 2.2: The Meissner effect [The figure is taken from [12]].

decades to figure out its origin. Although major advances made through phenomenological theories mainly by London brothers in 1935 [15] and Ginzburg and Landau in 1950 [18], it was John Bardeen, Leon Neil Cooper, and John Robert Schrieffer (BCS) who first gave the microscopic description of superconductivity in 1957 [2]. The basic idea in the BCS theory is that in the superconducting state electrons pair through phonon coupling and these pairs, called as Cooper pairs, condense into a single phase-coherent ground state which allows the electrons to move without scattering and hence dissipationless.

### 2.1.2 London's theory of superconductivity

The London's phenomenological theory of superconductivity was proposed by brothers Fritz and Heinz London 1935 [15] in oreder to describe the observed zero resistance property and diamagnetic properties of superconductors. It explains the perfect conductivity as well as the Meissner effect where they showed that a superconductor produces screening current at the surface which hinders the external magnetic field from entering into the bulk.

Based on their two-fluid model, Fritz and Heinz proposed two equations that govern electromagnetic fields inside a superconductor [16]

$$\frac{\partial \mathbf{j}_s}{\partial t} = \frac{e^2 n_s}{m}\mathbf{E} \tag{2.1}$$

and

$$\nabla \times \mathbf{j}_s = -\frac{e^2 n_s}{m}\mathbf{B} \tag{2.2}$$

These equations are commonly known as the **London equations**. They are able to describe the perfect diamagnetic properties of superconductors. The first equation essentially explains the perfect conductivity through the free acceleration of charges while the second equation explains Meissner effect.

Using the identities in vector calculus and the fourth Maxwell's equation (Ampere's law) in the static case, one can reduce the second equation to

$$\nabla^2 \mathbf{B} = \frac{1}{\lambda_L^2}\mathbf{B} \tag{2.3}$$

where $\lambda_L$ is called as London penetration depth and is defined as $\lambda_L = \sqrt{\frac{mc^2}{4\pi e^2 n_s}}$. Upon the application of magnetic field $\mathbf{B}_{apl} = \mathrm{B}_{\mathrm{apl}}\hat{\mathbf{y}}$ to semi-infinite superconductor, the magnetic field inside the superconductor is given by

$$\mathbf{B}(x) = \mathbf{B}_{apl}\, e^{-x/\lambda_L} \qquad \text{for} \quad x \geq 0. \tag{2.4}$$

This equation reveals that the magnetic field inside the superconductor decreases exponentially and in the bulk one finds $\mathbf{B} \to 0$. This in turn explains the phenomenon of Meissner effect. Again, from the second London equation along with the equation of continuity ($\nabla \times \mathbf{j}_s = 0$) it follows that,

$$\mathbf{j}_s(x) = -\frac{c}{4\pi\lambda_L}\mathbf{B}_{apl}\, e^{-x/\lambda_L} \qquad \text{for} \quad x \geq 0. \tag{2.5}$$

This last equations explains the phenomenon of supercurrent. It indicates that supercurrents flow in the direction parallel to the surface and perpendicular to $\mathbf{B}$ and decrease into the bulk over the same length scale $\lambda_L$.

The nonlocal generalization of London's equations was proposed by Pippard in 1953 [17]. Pippard proposed that superconducting wave function has a characteristic dimension $\xi$. Superconducting properties such as superfluid density changes over the length scale of $\xi$ which can be estimated using the uncertainty principle and is given by $\xi = \alpha\hbar v_F/k_B T_c$ where $\alpha$ is a numeric constant of the order of unity.

### 2.1.3 Ginzburg–Landau theory of superconductivity

The Ginzburg and Landau (GL) [18] theory of superconductivity was proposed in 1950. It describes the phenomenon of superconductivity based on Landau's theory of second-order phase transition. That is, Ginzburg and Landau were tried to describe the phenomenon of conventional superconductivity based on thermodynamic arguments. Ginzburg–Landau theory explains very well the macroscopic phenomenon of both type-I and type-II superconductors. This phenomenological theory is valid near the superconducting critical temperature ($T_c$).

This phenomenological theory introduced a complex pseudo wave function, $\psi =$

$|\psi|\ e^{i\theta}$, as an order parameter. This order parameter describes the properties of the superconducting quasiparticles in the superconducting state. It has defined value below the superconducting critical temperature, and it is zero above the superconducting critical temperature. Ginzburg–Landau equation

$$\frac{1}{2m^*}\left(\frac{\hbar}{i}-\frac{e^*}{c}\mathbf{A}\right)^2\psi+\alpha(T)\psi+\beta|\psi|^2\psi=0 \tag{2.6}$$

can be obtained using the variational principle to minimize the free energy and it has the form analogous to Schrödinger's equation. Here $\alpha$ and $\beta$ are constant coeficients, $m^*=2m_e$ and $e^*=-2e$ are mass and charge of a Cooper pair, respectively, and $\mathbf{A}$ is a vector potential. The corresponding equation for supercurrent is

$$\mathbf{j}_s=\frac{e^*\hbar}{i2m^*}(\psi^*\nabla\psi-\psi\nabla\psi^*)-\frac{(e^*)^2}{m^*c}|\psi|^2\mathbf{A}. \tag{2.7}$$

Using $\psi=|\psi|\ e^{i\theta}$ and (2.7) one can get the equation for supercurrent velocity as

$$\mathbf{v}_F=\frac{\hbar}{2m^*}\left(\nabla\psi-\frac{2e^*}{\hbar c}\mathbf{A}\right). \tag{2.8}$$

It can also be shown that GL order parameter is related to the local density of superelectrons as $n_s^*=|\psi|^2=-\alpha/\beta$.

Ginzburg and landau's theory explained very well the concepts related to phase rigidity (phase stiffness), superconducting coherence length, and superconducting penetration depth. It also explains very well the the phenomenon of type-I and type-II superconductors [19].

### 2.1.4 BCS theory of superconductivity

The BCS theory of superconductivity was proposed in 1957 by J. Bardeen, L. Cooper and R. Schrieffer [2,3]. This theory provided the microscopic theory of superconductivity. BCS theory describes very well almost all the observed phenomenon of conventional superconductivity at the time of its discovery. For the development of this theory, Bardeen, Cooper and Schrieffer won the 1972 Nobel Prize in physics.

According to this theory, a small interaction electrons creates instability in the ground state of free electrons. This small attractive interaction makes the electrons to pair-up and form a bound state. This bound state of electrons called Cooper pair. The idea of Cooper pairing interaction can be explained as follows: an electron of negative charge $-e$ moving in a crystal attracts the stationary positively charged ions and this creates a local lattice distortion. The induced local lattice distortion, in tun, induces excessive positive charge. The induced positive charge attracts attracts another electron which can form abound state with the first electron. Lots of Cooper pairs form in this manner and the system becomes a superconductor below some critical temperature. The cartoon picture showing the phonon-mediated attraction is illustrated in Figure 2.3.

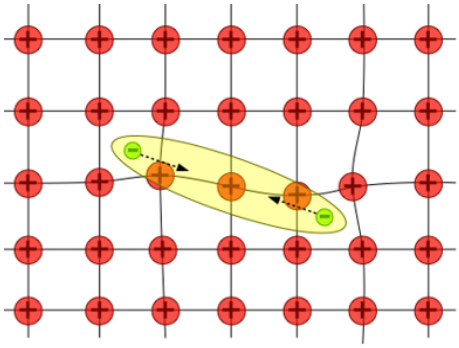

Figure 2.3: The Cartoon picture of Cooper pair, pair of electrons with equal and opposite momentum.

The basic assumptions of BCS theory are the following. Firstly, it assumes that only electrons with energy range $-\hbar\omega_D \leq \xi_{\mathbf{k}} \leq \hbar\omega_D$ participate in the Cooper pairing (Figure 2.4–Right). Cooper explained that the presence of phonon mediated attractive

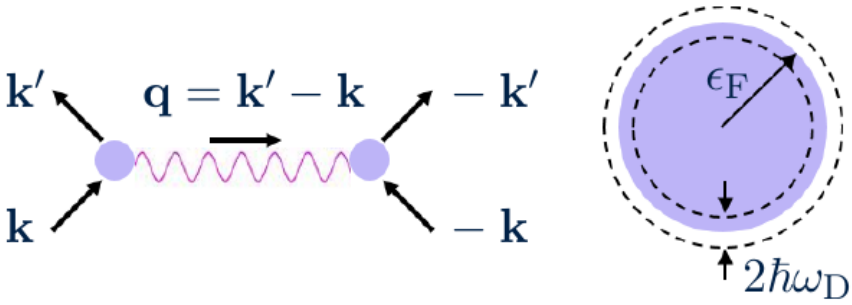


Figure 2.4: The Cartoon picture of Cooper pair, pair of electrons with equal and opposite momenta.

interaction between electrons in this narrow energy range creates Cooper pairs and this results in instability of the Fermi sea. The second assumption is that the Cooper paired electrons have opposite momentum and spin. Therefore, the bound states have zero total momentum, between states $(\mathbf{k}, \sigma =\uparrow)$ and $(-\mathbf{k}, \sigma =\downarrow)$ (Figure 2.4–Left). Thirdly, most real materials show weak coupling and this in turn validates the use of a mean-field theory, where fluctuations can be neglected. This third assumption leads to the BCS ground state wave function

$$|\Psi_0\rangle = \prod_{\mathbf{k}} (u_{\mathbf{k}} + v_{\mathbf{k}} c^{\dagger}_{\mathbf{k}\uparrow} c_{-\mathbf{k}\downarrow})|0\rangle. \tag{2.9}$$

Based on these three assumptions, it is possible to write the reduced mean-field Hamiltonian of conventional superconductors as [16]

$$H_{BCS} = \sum_{\mathbf{k}\sigma} \xi_{\mathbf{k}} c^{\dagger}_{\mathbf{k}\sigma} c_{\mathbf{k}\sigma} + \sum_{\mathbf{k}\mathbf{k}'} \left( \Delta c^{\dagger}_{\mathbf{k}\uparrow} c^{\dagger}_{-\mathbf{k}\downarrow} + \Delta^* c_{-\mathbf{k}'\downarrow} c_{\mathbf{k}'\uparrow} \right) + \frac{|\Delta|^2}{V}. \tag{2.10}$$

Here, $\Delta$ denotes the superconducting energy gap

$$\Delta = -V \sum_{\mathbf{k}} < c_{\mathbf{k}'\uparrow} c_{-\mathbf{k}'\downarrow} > \tag{2.11}$$

and $V$ denotes the strength of the attractive interaction between Cooper paired electrons. The order parameter $\Delta$ characterizes the superconducting state.

The important results of BCS theory are the following: the superconducting order parameter and the superconducting critical temperature are given by

$$\Delta \equiv \Delta_0 = 2\hbar\omega_D e^{-1/\lambda} \tag{2.12}$$

and

$$k_B T_c = 1.13\hbar\omega_D e^{-1/\lambda}. \tag{2.13}$$

with $\lambda = N(0)V$ is called the coupling constant. $N(0)$ is the density of states for normal electrons at Fermi surface. This implies $\Delta_0/k_B T_c \sim 1.76$, another characteristic of BCS systems.

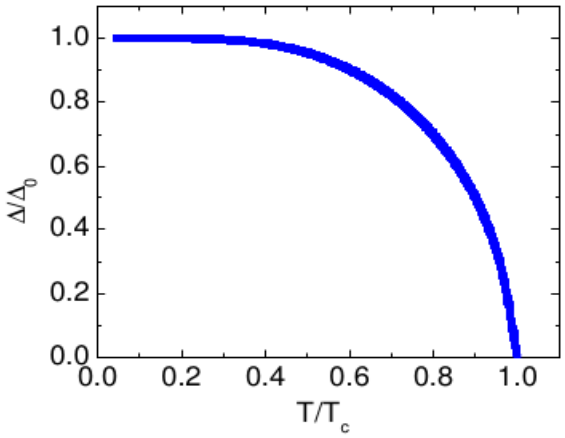


Figure 2.5: Evolution of the superconducting energy gap (normalized by the value at zero temperature) with temperature (normalized by $T_c$) within the BCS theory.

The single particle density of states (DOS) is given by

$$\frac{N_s(E)}{N(0)} = \left\{ \begin{array}{ll} \frac{E}{\sqrt{E^2-\Delta^2}} & \text{if } E > \Delta \\ 0 & \text{if } E < \Delta \end{array} \right\}. \tag{2.14}$$

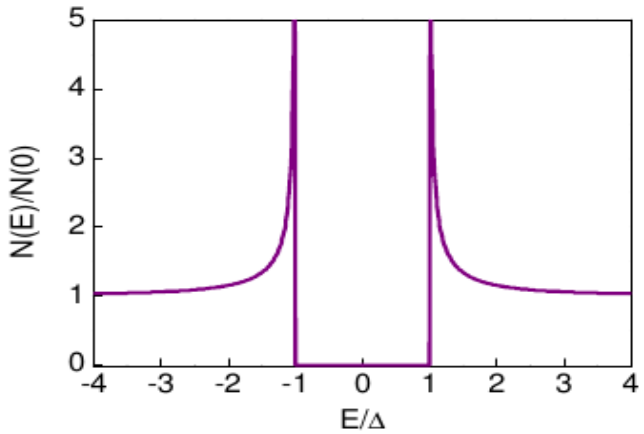


Figure 2.6: Superconducting density of states $N_s(E)$ normalized by the normal state density of states $N_n(0)$ as a function of energy normalized by the gap.

## 2.2 Localization in dirty superconductors

### 2.2.1 Introduction

The interplay of superconductivity and disorder is one of the most intriguing problems of quantum many body physics. Superconducting pairing interactions in a normal metal drives the system into a phase coherent state with zero electrical resistance. In contrast, in a normal metal increasing disorder progressively increases the resistance through disorder scattering eventually giving rise to an insulator at high disorder where all electronic states are localized. Superconductors with large amounts of physical or chemical defects are termed **dirty superconductors**. The first theory addressing the effects of nonmagnetic impurities, including disorder, was published in 1959 by Anderson [7]. He noted that nonmagnetic impurities and disorder which cannot break the time-reversal symmetry do not play a significant role in pair-breaking effects. Anderson also stressed that in the dirty limit the observed gradual destruction of superconductivity is linked to an altered density of states. In literature, this robustness of superconductivity to weak nonmagnetic impurities and disorders is known as **Anderson's theorem**. Experimental work conducted by Lynton et al. [20] on impure Sn also revealed that beyond a sharp initial effect, large quantities of nonmagnetic impurities have very little negative impact on the superconducting state in terms of critical temperature and electronic specific heat. In sharp contrast to the Anderson's theorem of nonmagnetic impurities, Abrikosov and Gor'kov [8] put forth a theory of superconductors containing magnetic impurities. According to their theory, scattering from magnetic impurities leads to broken time-reversal symmetry which causes pair-breaking. An early experimental work by Matthias et al. [21] supports this theory showing that unlike regular impurities, those which carry a magnetic moment result in a rapidly diminished $T_c$ until superconductivity is ultimately extinguished at higher concentrations. In this section, we have provided a brief review of dirty superconductors focussing on localization effects of disorder.

### 2.2.2 Anderson's theorem of localization

The concept of localization was first put forward by Anderson in 1958 [7] to explain the absence of spin diffusion in certain disordered lattices. He showed that sufficiently strong disorder can profoundly alter the nature of the electronic wave functions in the material and ultimately localize them completely so that the modulus of the wave function decays exponentially with distance acording to $|\psi(r)| \sim \exp(-r/\xi)$, where $\xi$ is a localization length.

An intuitive understanding of localization effects can be provided from the analysis of the path of an electron which starts from and returns to a given point $r$. From the principle of quantum mechanics, the total amplitude is given by the sum of all such paths. Since there is time reversal symmetry, the time reversed counterpart of any given path has the exact same magnitude and phase, and thus they interfere constructively increasing the amplitude to return twofold compared to what we would expect classically. This is known as weak localization, and calculations reveal that the total conductivity is given by $\sigma = \sigma_0 - (1/2\pi k_F l)\ln(\tau_0/\tau)$ where $\tau_0$ is a cutoff provided by either inelastic scattering or the system size.

As the disorder is raised, we enter the regime of strong localization. In this situation, the electron eigenstates at the extremeties of the band are localized, bound by deep fluctuations in the random potential profile. However, at a moderate disorder, states near the centre of the band can be extended (in three dimensions), separated from the localized states by a mobility edge. With further increase of disorder, eventually, all states would get localized.

### 2.2.3 Anderson's theorem for dirty superconductors

Although superconductivity as ground state of electronic systems is limited to comparably low energy scales ($T_c \sim 10K$), its ubiquitous appearance as favorable ground state of numerous materials ranging from single crystals to amorphous film results from its insensitivity against disorder. While scaling arguments presented above rules out a $2D$ metal, this insensitivity can qualitatively be seen as a reason for $2D$ superconductors - a

celebrated result first obtained by Anderson [9] and commonly referred to as Anderson's theorem. A comprehensive discussion of Anderson's theorem is lengthy and beyond the scope of this thesis. Instead, we have only sketched the succession of arguments which are very important for our purpose. What follows is based on the more comprehensive discussions provided by Lee in reference [23] and Jian-Xin Zhu in reference [24].

The electron-phonon interaction term of the BCS Hamitonian for clean superconductors reads

$$H = V \sum_{\mathbf{k}} c^{\dagger}_{\mathbf{k}\uparrow} c^{\dagger}_{-\mathbf{k}\downarrow} c_{-\mathbf{k}'\uparrow} c_{\mathbf{k}'\downarrow} \tag{2.15}$$

for pairing states with opposite momenta and spin, i.e. $(\mathbf{k}, \uparrow)$ and $(-\mathbf{k}, \downarrow)$. The BCS meanfield approximation diagonalizes this Hamiltonian and leads to the well known energy spectrum

$$E_{\mathbf{k}} = \sqrt{(\epsilon_{\mathbf{k}} - \mu)^2 + |\Delta|^2} \tag{2.16}$$

with $\epsilon_{\mathbf{k}}$ and $\mu$ the band dispersion and chemical potential. The order parameter $\Delta$ is given by the BCS self-consistency equation

$$\Delta = VN(0) \int d\xi \frac{\Delta}{2\sqrt{(\xi_{\mathbf{k}} - \mu)^2 + |\Delta|^2}}. \tag{2.17}$$

In disordered systems, the lattice translational symmetry is lifted and scattering off impurities violates conservation of momentum such that $\mathbf{k}$ is no longer a good quantum number and Cooper pairs do no longer result from the above pairing scheme. Anderson showed that the BCS condition for pairing can be generalized beyond $(\mathbf{k}, \uparrow)$ and $(-\mathbf{k}, \downarrow)$ to exact eigenstates $|\alpha\rangle$ of the disordered Hamiltonian and their time-reversed counterparts $\hat{T}|\alpha\rangle$ yet restoring the energy spectrum and self-consistency equation above. Starting point is the general electron-phonon interaction operator

$$H = V \sum_{\mathbf{k},\mathbf{k}',\mathbf{q}} \sum_{\sigma,\sigma'} c^{\dagger}_{\mathbf{k}'+\mathbf{q},\sigma'} c^{\dagger}_{\mathbf{k}-\mathbf{q},\sigma} c_{\mathbf{k},\sigma} c_{\mathbf{k}',\sigma'}. \tag{2.18}$$

Transformation of the $\mathbf{k}$-space operators to real-space operators $\psi(\mathbf{r})$ via the Fourier integral

$$c_{\mathbf{k},\sigma} = \int d\mathbf{r} \psi(\mathbf{r}) e^{i\mathbf{k}\cdot\mathbf{r}}, \tag{2.19}$$

subsequent integration and spin summation yields

$$H = 2V \int d\mathbf{r}\psi_{\uparrow}^{\dagger}(\mathbf{r})\psi_{\downarrow}^{\dagger}(\mathbf{r})\psi_{\downarrow}(\mathbf{r})\psi_{\uparrow}(\mathbf{r}). \tag{2.20}$$

In general, the orbitals $\psi(\mathbf{r})$ will be complicated functions of $\mathbf{r}$ for a randomly disordered lattice. For the sake of the argument, however, the actual form is not required given the existence of a set of eigenstates $|\alpha\rangle$ (and corresponding orbitals $\phi_\alpha(\mathbf{r})$) diagonalizing the Hamiltonian for the disordered problem. Transformed into this new basis, the Hamiltonian (2.18) can be cast into the BCS mean-field form with the only difference that the operators create and annihilate (time-reversed) eigenstates $|\alpha\rangle$ instead of momentum eigenstates $|\mathbf{k}\rangle$. After diagonalization and Bogoliubov transformation via the spectral representation

$$\psi_\sigma(\mathbf{r}) = \sum_\alpha \phi_\alpha(\mathbf{r})c_{\alpha,\sigma} \tag{2.21}$$

(that is, introducing new fermionic operators creating and annihilating quasiparticles instead of electrons) one finds a similar spectrum

$$E_\alpha = \sqrt{(\epsilon_\alpha - \mu)^2 + |\Delta|^2} \tag{2.22}$$

which still contains information about the specific choice of eigenstates in terms of the eigenvalues $\epsilon_\alpha$. To obtain the self-consistency equation, however, any reference to the basis is lost when the summation over eigenvalues $\epsilon_\alpha$ is replaced by a continuous integral so that the BCS result (2.16) is exactly restored. Consequently, disorder does not affect the superconducting properties. In other words, if impurity scattering were to destroy a Cooper pair it would need to lift the requirement of time-reversal symmetry. Scattering off a potential, however, preserves the spin orientation and hence no pair-braking takes place, as long as the scatterer does not carry a magnetic moment: in this case, time-reversal symmetry is broken and superconductivity may be strongly suppressed.

However, it has been observed in a number of experiments [25, 26] that sufficiently strong disorder is in fact able to reduce the critical temperature all the way to zero and completely destroy superconductivity. This is because there are a number of disorder related phenomena that the Anderson theory does not account for. These include Coulomb

repulsion, localization of electronic wave functions and fluctuations in the amplitude and phase of the superconducting order parameter.

## 2.3 Superconductor-Insulator transition in disordered thin films

According to scaling theory of localization [11], there is no two dimensional metal at absolute zero. Therefore, if superconductivity of a two dimensional electronic system is destroyed by some mechanism at this temperature, then the resulting phase should be an insulator. This kind of continuous phase transition is known as the superconductor-insulator transition (SIT). It is a prototypical quantum phase transition because it takes place at absolute zero where the classical thermal effects are completely ceased.

Both the Anderson's theorem presented above and the Anderson's theory of localization determine the physics far from the SIT at moderate and extreme amounts of disorder, respectively. As both asymptotic regimes are continuously connected, there must be a regime of disorder, where both paradigms break down and where, pictorially speaking, electrons cannot decide whether to pair up and condense to form a superconducting state or to get trapped and localized to form an insulating state. This breakdown of the two giants (Anderson's theorem of dirty superconductors and Anderson's theorem of localization) at the SIT gives rise to intriguing physics vivified by the interplay of superconductivity (condensed state) and localization. The conceptual explanation how Anderson's theoerm of superconductivity can be invalidated near the quantum critical region of SIT can be given in terms of the Ioffe-Regel [27] criteria on disorder. For marginal disorder, the product of the Fermi wave vector and the electron mean free path becomes $k_F l \gg 1$ and the Anderson theorem holds. For extreme disorder, this product becomes $k_F l \approx 1$ and the system turns insulating signaling the ultimate break down of Anderson's theorem of superconductivity. While this explains the conceptual demand for an SIT, it does not provide an answer to the question how superconductivity actually ceases.

Over the past few decades, large number of theoretical and experimental works have been conducted in this field. In what follows, we will present the recent theoretical and experimental works. For a comprehensive review on this topic, interested body is referred to the reviews made by Gantmakher and Dolgopolov [6] and Lin, Nelson and

Goldman [28].

### 2.3.1 Theoretical paradigms

Although extremely successful in describing conventional bulk superconductors, BCS theory does not provide a satisfactory framework for disordered superconductors of two spatial dimensions (commonly called thin film). This is because BCS theory is simply a mean-field theory which ignores fluctuation. However, in disordered thin film superconductors, fluctuation effects are much stronger due to the low dimensionality and disorder. This necessitates the development of theoretical approaches that modify and/or extend the BCS formulation to incorporate the effects of broken translational symmetry and fluctuations within their framework. While the lack of translational symmetry can be incorporated in the mean field framework itself, inclusion of fluctuations typically requires one to use statistical many body tools, either analytically using perturbation theory, self consistency, etc., or numerically by simulation of model systems. Most of the theoretical works done on this field can be classified broadly into two groups: **Fermionic theories**, which include Coulomb repulsion and explore the destruction of superconductivity due to suppression of the effective pairing interaction, and **Bosonic theories**, which assume performed bosonic pairs and study how phase fluctuations can drive a superconductor-insulator transition.

The fermionic mechanism specifically includes the effect of disorder on the screening process of the material. In a seminal work, Finkelstein [29] has shown that disorder tends to renormalize Coulomb interaction between electrons such that the screening becomes less efficient. Hence, the attractive Cooper interaction pairing up electrons is challenged by the repulsive Coulomb interaction lowering the energy gain upon condensation. At a critical disorder, Coulomb repulsion is strong enough to overcompensate the pairing interaction and the bound state is no longer favorable.

Using a diagrammatic renormalization approach, Finkelstein demonstrated that the amplitude of the order parameter vanishes uniformly at the transition from superconducting to insulating ground states. At the same time, the superfluid density also goes to zero where the latter always remains the greater energy scale. This is depicted in Figure

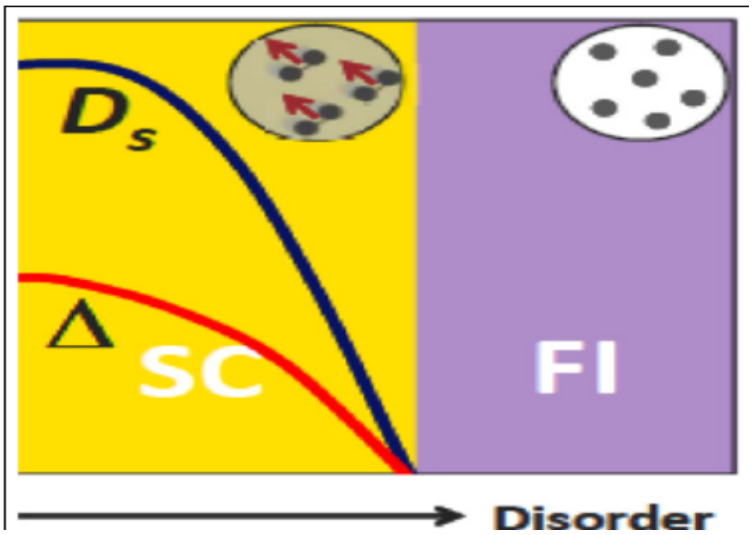


Figure 2.7: Evolution of superconductivity with increasing disorder as postulated by the fermionic mechanism. [66]

2.7. The figure shows that the superconductor consists of coherent pairs with finite order parameter $\Delta$ and superfluid stiffness $D_s$. With increasing disorder both $\Delta$ and $D_s$ decrease due to increasing Coulomb repulsion, until they vanish at the critical point. Beyond this, all pairs are broken, and the system properties are determined by free fermions in a disordered system.

A comprehensive explanation of the disorder induced superconductor-insulator transition based on the bosonic mechanism was provided by Fisher *et al.* [30, 31] and Ghosal *et al.* [32]. They considered a collection of bosons in two dimensions in a random potential with a repulsive Coulomb interaction between them. As the disorder is increased, or the boson number density is decreased, the system undergoes a transition from a superconducting state where the pairs are condensed to a disordered Bose glass state below a critical density $n_c$. In this state, the Cooper pairs are localized and there is no coherence between these localized pairs. Thus, the system ceases to be superconducting, but since the pairs continue to exist, the single particle spectrum remains gapped.

Figure 2.8 shows a schematic figure depicting the evolution of superconductivity with disorder as predicted by the bosonic mechanism. The superconductor consists of coherent pairs with finite order parameter $\Delta$ and phase stiffness $D_s$. With increasing disorder, increasing phase fluctuations results in a decrease in $D_s$, while the gap parameter

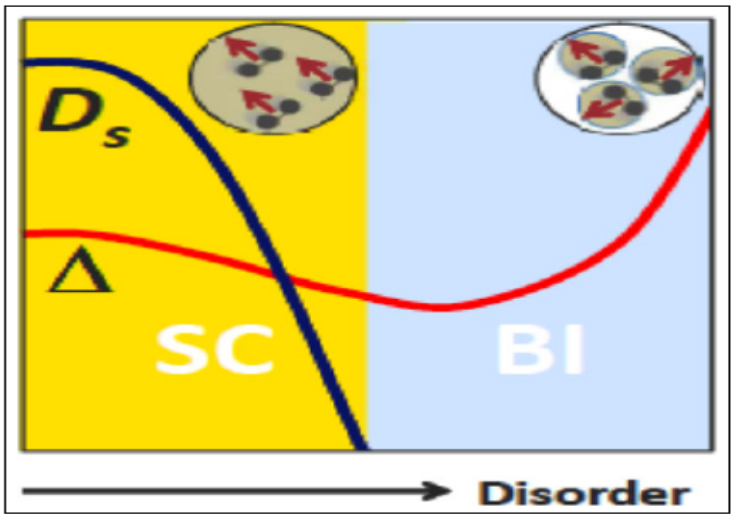


Figure 2.8: Evolution of superconductivity with increasing disorder as postulated by the bosonic mechanism. [66]

$\Delta$ remains the same. The disorder causes the bosonic pairs to lose long range coherence, and increased phase fluctuations among these pairs drives the system insulating. In the insulating regime, the bosonic pairs are incoherent, but the single particle gap persists.

The limited applicability of both models calls for a unified amplitude-phase theory equally capturing Coulomb interactions and phase fluctuations each of which are the central aspects of the respective models. However, such a holistic theory is yet to be developed.

### 2.3.2 Experimental evidences

Much of the experimental works in 2D have involved quench-condensed films, which are amorphous or granular in structure depending on deposition parameters. In most of the cases, thickness is used as a parameter that controls the sheet resistance and the disorder strength is usually characterized by the sheet resistance $R_s$. Increasing the deposition thickness decreases sheet resistance $R_s$, and hence decreases the effective disorder. Chemical doping can also be utilized.

The nature of the observed SIT depends on material and microstructure [6]. In amorphous films with homogeneous disorder on an atomic scale (of materials such as Bi, Al, Pb, and MoGe), the superconductor typically exhibits a BCS-like transition where

$R_s(T)$ is constant above $T_c$ and suddenly drops to zero below $T_c$ , and the insulator is only weakly localized [6,7,33]. Tunneling studies in such films are consistent with the fermionic mechanism, in which the gap closes at the SIT [34].

Conversely, in granular films (Bi, Ga, Al) [35], nanostructured Bi [36], amorphous TiN [37], InOx [38,39], and NbN films [40], the superconducting transition in $R_s(T)$ is much broader, and the insulator exhibits activated transport. Furthermore, it appears that the gap, measured using a tunnel junction or scanning tunneling spectroscopy, remains finite as the SIT is approached, consistent with the bosonic mechanism. Scanning tunneling spectroscopy data, showing significant inhomogeneity of the gap, further supports the aforementioned picture of emergent granularity. Although coherence peaks in the density of states disappear at about $T_c$, a pseudogap persists up to much higher temperatures [40–43], in agreement with theory [44,45].

## 2.4 Brief Overview of Density Functional Theory

In this section, a brief concept of first principles method called Density Functional Theory (DFT) is presented. The concept DFT was introduced by the Nobel Prize winner chemist Walter Kohn around 1965 [51,52]. The most important variable in density functional theory is the charge density. because all the other parameters of DFT can be expressed in terms of the charge density [12]. Nowadays, DFT is is widely applicable method in different fields condensed-matter physics, computational Physics, material science and quantum chemistry to describe properties of condensed matter systems. It allows to study materials even with minimum input parameter like the atomic type and lattice parameters, and that is why the name first principle method is given.

### 2.4.1 The quantum many-body problem in solids

A solid is certainly a quantum mechanical many-body system, consisting atoms or molecules which interact with one another. It is an interacting system of particles consisting of lattice ions and valence electrons. The Hamiltonian of this interacting

many-body system can be put as [12]

$$\hat{H} = -\sum_i \frac{\hbar^2}{2m_e}\nabla_i^2 - \sum_I \frac{\hbar^2}{2M_I}\nabla_I^2 - \frac{1}{4\pi\epsilon_0}\sum_{i,I}\frac{Z_I e^2}{|\mathbf{r}_i - \mathbf{R}_I|} + \frac{1}{2}\frac{1}{4\pi\epsilon_0}\sum_{i\neq j}\frac{e^2}{|\mathbf{r}_i - \mathbf{r}_j|} + \frac{1}{2}\frac{1}{4\pi\epsilon_0}\sum_{I\neq J}\frac{Z_I Z_J e^2}{|\mathbf{R}_I - \mathbf{R}_J|}. \tag{2.23}$$

In this many-body Hamiltonian, $m_e$ and $M_I$ represent the masses of electrons and nuclei, $Z_I$ represent the atomic numbers of the nuclei and $\epsilon_0$ represents the permittivity of free space.

An exact solution for the Schirodinger equation of the overall quantum many-bady problem (2.23) would appear to be impossible. Therefore, an approximation should be used to solve the problem. The front level approximation commonly employed is the Born-Oppenheimer approximation, which ignores the motion of the lattice ions. According to this approximaton, the electrons are considered to move in the field of fixed nuclei [12]. The BO approximation reduces the five term Hamiltonian in (2.23) to three terms, and this boldly simplifies the search for the solution for the problem.

### 2.4.2 The Hohenberg-Kohn (HK) Theorems

**The first HK theorem**: The first HK theorem states that the ground state density $n(r)$ of a many-body quantum system in some external potential $v(r)$ uniquely determines the potential. Therefore, all properties of a many-body system can be determined by the ground state charge density.

$$\psi(r_1, r_2, ..., r_n) \rightarrow n(r) = |\varphi_i(r)|^2 \tag{2.24}$$

**The second HK theorem**: The ground state energy $E$ is uniquely determined by the ground-state charge density: the charge density that minimizes the total energy is the exact ground state density.

$$\begin{aligned} E[n(r)] &= <\psi|T + U|\psi> + <\psi|T + U|\psi> + <\psi|V|\psi> \\ &= F[n(r)] + \int n(r)v(r)dr. \end{aligned} \tag{2.25}$$

Here $H = T + U + V$ , is the many-electron Hamiltonian, $\psi$ is ground state wave function, $T$ is the kinetic energy, $U$ is the electron-electron interaction, $V$ is the external potential, and $n(r)$ is the charge density. The universal functional $F$ of the density is $F[n(r)] =< \psi|T+U|\psi >$. The Functional includes the kinetic energy of the electrons $T_e[n]$, Hartree classical Coulomb repulsion energy $E_H[n]$, and the exchange and correlation energies $E_{xc}[n]$ [107].

### 2.4.3 Kohn–Sham (KS) equations

In 1965, Kohn and Sham [52] showed that it is possible to reduce the many-body quantum mechanical problem to an exactly equivalent set of one-electron equations, solved self-consistently. This is a reformulation of the following idea. The system of interacting electrons is mapped on to an auxiliary system of non-interacting electrons having the same ground state charge density $n(r)$. In Kohn-Sham equation the Schrodingers equation for the system takes the following form:

$$\left[-\frac{\hbar^2}{2m}\nabla^2 + V(r)_{ion} + V(r)_H + V_{XC}[n(r)]\right]\varphi_i(r) = \epsilon_i\varphi_i(r) \tag{2.26}$$

The first term is the energy of non-interacting electrons. The second term $V(r)$ ion is the ionic potential describing the attractive interaction between electrons and nuclei. The third term (called the Hartree potential) contains the electrostatic interactions between clouds of charge.

$$V(r)_H = \int \frac{e^2 n(r')}{r - r'} d^3r'. \tag{2.27}$$

The fourth term is called the exchange and correlation potential.

$$V_{XC}[n(r)] = \frac{\delta E_{XC}}{\delta n(r)}. \tag{2.28}$$

The nature of this external potential defines the physical properties of the system and thus is extremely important. Ground state electronic energies $\epsilon_i$ and wave functions $\varphi_i|i,k >$ can be obtained as the result of the DFT calculation. In many cases very good agreement with experiment is achieved when the exchange and correlation potential is treated using the rather simple local density approximation (LDA). A large variety of important scientific results have been and are still being obtained using LDA and the

generalized gradient approximations (GGA).

The KS equations can be solved self-consistently. This is shown schematically in Figure 2.9.

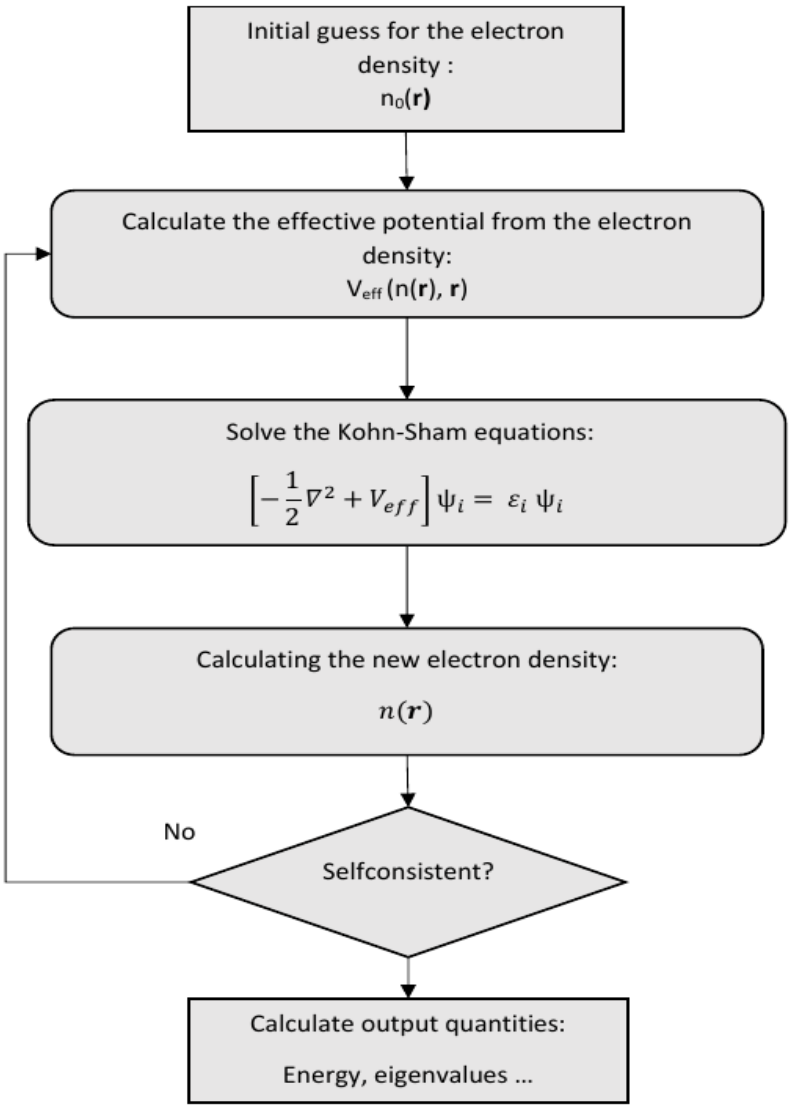


Figure 2.9: Scheme of the self-consistent solution of the Kohn- Sham equations.

### 2.4.4 Quantum ESPRESSO software package

We have seen that DFT can be utilized to reduce the many-body problem. Still, the KS equations are to be solved self-consistently and a sufficiently large basis set has to be selected, as well as an appropriate supercell to implement more complex systems. So,

DFT is implemented numerically in a wide variety of software packages, such as ABINIT, Gaussian, Quantum ESPRESSO, SIESTA, VASP, WIEN2k etc. These differ in several aspects, i.e., the choice of the basis functions, the pseudopotentials, and the algorithms used for diagonalization of the KS Hamiltonian. We used Quantum ESPRESSO for all the calculations performed in the last chapter of this thesis. Quantum ESPRESSO is a suite of open-source computer programs for calculation and modeling of materials parameters. These programs are based on DFT utilizing plane waves and pseudopotentials. Quantum ESPRESSO is developed around the two main programs Pwscf, used to preform self consistent calculations and CP used for preforming molecular dynamics calculations.The best thing about Quantum ESPRESSO project is that it allows the inclusion of modules developed by scientists in the field. Every thing about this software package is available at the website https://www.quantum-espresso.org/.

# 3

# Mathematical Methods

In this chapter, we introduce the important mathematical tools and methods used in the subsequent chapters. For most of the contents, we have used the standard textbooks by W. Nolting [57] and Zubarev [106]. Additional references were given whenever necessary.

## 3.1 Retarded, advanced and causal Greens functions

For the construction of the complete Greens function formalism, we require three types of Greens functions: (i) the retarded Greens functions, (ii) the advanced Greens functions and (iii) the Causal Greens functions defined as

$$G^{R}_{AB}(t,t') = \ll A(t); B(t') \gg_{R} = -i\Theta(t-t') < [A(t), B(t')]_{\pm} >, \tag{3.1}$$

$$G^{A}_{AB}(t,t') = \ll A(t); B(t') \gg_{A} = i\Theta(t'-t) < [A(t), B(t')]_{\pm} >, \tag{3.2}$$

$$G^{C}_{AB}(t,t') = \ll A(t); B(t') \gg_{C} = -i < T_{\pm}(A(t)B(t')) >, \tag{3.3}$$

where $\ll A(t); B(t') \gg_{R,A,}$ are abbreviated notations for the corresponding Green functions. The upper sign (+) is for fermions and the lower sign (−) is for bosons. The operators which generate the Greens functions are given here in their time-dependent Heisenberg representation, i.e. for the case of a Hamiltonian $H$ which is not explicitly time-dependent

$$A(t) = e^{i\mathcal{H}t} A e^{-i\mathcal{H}t}, \qquad B(t') = e^{i\mathcal{H}t'} B e^{-i\mathcal{H}t'}, \tag{3.4}$$

where $\mathcal{H} = H - \mu N$ with $\mu$ and $N$ are the chemical potential and the operator of total number of particles, respectively. The averaging of the operators is carried out over the grand canonical ensemble as

$$< A(t) >= \frac{1}{Z} Tr\left(e^{-\beta\mathcal{H}} A\right) \tag{3.5}$$

where $Z = Tr\left(e^{-\beta\mathcal{H}}\right)$ is the grand canonical partition function and $\beta = 1/k_B T$ with $k_B$ representing the Boltzmann's constant. The step functions $\Theta(t - t')$ and $\Theta(t' - t)$ in equations (3.1) and (3.2) are, respectively, given by

$$\Theta(t - t') = \left\{ \begin{array}{ll} 1 & \text{for } t > t', \\ 0 & \text{for } t < t' \end{array} \right\}, \quad \text{and} \quad \Theta(t' - t) = \left\{ \begin{array}{ll} 0 & \text{for } t > t', \\ 1 & \text{for } t < t' \end{array} \right\}. \tag{3.6}$$

The expression $[A(t), B(t')]_{\pm}$ indicates the commutator or anti-commutator which is expressed by

$$[A(t), B(t')]_{\pm} = A(t)B(t') \pm B(t')A(t). \tag{3.7}$$

The Wick's time-ordering operator $T_{\pm}$, sorts the operators in a product according to their time arguments

$$T_{\pm}(A(t)B(t')) = \Theta(t - t')A(t)B(t') \pm \Theta(t' - t)B(t')A(t)\,. \tag{3.8}$$

In this work, we mostly confine ourselves to the retarded Greens function because it implies the principle of causality, i.e. cause comes before effect.

For the actual computation of the Greens functions, we as a rule will require their equations of motion. Differentiating the retarded Greens function (3.1) with respect to time $t$ gives

$$\frac{d}{dt} \ll A(t); B(t') \gg_R = -i\frac{d}{dt}\Theta(t - t') < [A(t), B(t')]_{\pm} > -i\Theta(t - t') < \left[\frac{d}{dt}A(t), B(t')\right]_{\pm} > . \tag{3.9}$$

Furthermore, using the equation of motion for the Heisenberg operator $A(t)$

$$\frac{d}{dt}A(t) = \frac{i}{\hbar}[\mathcal{H}, A(t)] \tag{3.10}$$

with $\hbar = 1$, gives

$$\frac{d}{dt} \ll A(t); B(t') \gg_R = -i\frac{d}{dt}\Theta(t-t') < [A(t), B(t')]_{\pm} > -i \ll [A(t), \mathcal{H}]; B(t') \gg_R . \tag{3.11}$$

The relation between the Heaviside step function $\Theta(t-t')$ and the Dirac's delta function $\delta(t-t')$ is given by

$$\frac{d}{dt}\Theta(t-t') = \delta(t-t') = -\frac{d}{dt}\Theta(t-t') . \tag{3.12}$$

Employing this relation into (3.11) and multiplying both sides by $i$ gives

$$i\frac{d}{dt} \ll A(t); B(t') \gg_R = \delta(t-t') < [A(t), B(t')]_{\pm} > + \ll [A(t), \mathcal{H}]; B(t') \gg_R . \tag{3.13}$$

In order to solve (3.13), it is convenient to work with its Fourier transform. For Hamiltonians which are not explicitly time-dependent, the Greens functions are homogeneous in time, $G^R_{AB}(t,t') = G^R_{AB}(t-t')$. The Fourier transform and inverse transform of $G^R_{AB}(t-t')$ are given, respectively, by

$$G^R_{AB}(\omega) = \int_{-\infty}^{\infty} dt e^{i\omega(t-t')} G^R_{AB}(t-t'), \tag{3.14}$$

$$G^R_{AB}(t-t') = \frac{1}{2\pi}\int_{-\infty}^{\infty} d\omega e^{-i\omega(t-t')} G^R_{AB}(\omega). \tag{3.15}$$

With this the Fourier transformed equation of motion becomes

$$\omega \ll A; B \gg^R_{\omega} = < [A, B]_{\pm} > + \ll [A, \mathcal{H}]; B \gg^R_{\omega} . \tag{3.16}$$

Similarly, the Fourier transformed equations of motion for the advanced and causal Greens functions become

$$\omega \ll A; B \gg^A_{\omega} = < [A, B]_{\pm} > + \ll [A, \mathcal{H}]; B \gg^A_{\omega}, \tag{3.17}$$

$$\omega \ll A; B \gg^C_{\omega} = < [A, B]_{\pm} > + \ll [A, \mathcal{H}]; B \gg^C_{\omega} . \tag{3.18}$$

These three equations of motion can be expressed in a more compact form as

$$\omega \ll A;B \gg_{\omega}^{\alpha} = < [A,B]_{\pm} > + \ll [A,\mathcal{H}];B \gg_{\omega}^{\alpha} \tag{3.19}$$

with $\alpha = R, A, C$.

We are therefore now no longer dealing with a differential equation, but instead with a purely algebraic equation. However, we again have an infinite chain of such equations of motion, which must be decoupled.

## 3.2 Spectral representations

In order to supplement the system of equations which result from (3.19) with the boundary conditions, it is important to be aware of the so-called spectral (or Lehmann) representations of the Greens functions.

Let $\omega_n$ and $|\omega_n >$ be the energy eigenvalues and the eigenstates of the Hamiltonian $H$ of the physical system under consideration so that

$$H|\omega_n >= \omega_n|\omega_n > . \tag{3.20}$$

The states $|\omega_n >$ are assumed to form a complete, orthonormalised states

$$\sum_n |\omega_n >< \omega_n| = 1, \quad \langle\omega_n|\omega_m\rangle = \delta_{nm}. \tag{3.21}$$

Employing (3.4) and (3.5), we can define the correlation function $< A(t)B(t') >$ as

$$< A(t)B(t') >= \frac{1}{Z}\sum_{n,m} < \omega_n|B|\omega_m >< \omega_m|A|\omega_n > e^{-\beta\omega_n} e^{-i(\omega_n-\omega_m)(t-t')}. \tag{3.22}$$

In our way to this final form, we have inserted the complete set of eigenstates between the operators, rendering the time dependence of the Heisenberg operators trivial and exchanged the indices $n$ and $m$. In a quite analogous manner, we find for the second

correlation function

$$< B(t')A(t) >= \frac{1}{Z}\sum_{n,m} < \omega_n|B|\omega_m >< \omega_m|A|\omega_n > e^{-\beta\omega_n}e^{-\beta(\omega_m-\omega_n)}e^{-i(\omega_n-\omega_m)(t-t')}. \tag{3.23}$$

There is another very important function in many-body theory which we wish to introduce at this point. It is the so-called spectral density, whose information content will prove to be identical to that of the Greens functions

$$S_{AB}(t-t') = \frac{1}{2\pi} < [A(t), B(t')]_{\pm} > \tag{3.24}$$

for Hamiltonians which are not explicitly time-dependent. Upon inserting (3.22) and (3.23) into (3.24) and Fourier transforming, we have

$$S_{AB}(\omega) = \frac{1}{Z}\sum_{n,m} < \omega_n|B|\omega_m >< \omega_m|A|\omega_n > e^{-\beta\omega_n}(e^{-\beta E} \pm 1)\delta[E-(\omega_n-\omega_m)]. \tag{3.25}$$

The arguments of the $\delta$-functions contain the possible excitation energy of the system.

We now wish to express the Greens function in terms of the spectral densities. To this end, we make use of the following representation of the step function

$$\theta(t-t') = \frac{i}{2\pi}\int_{-\infty}^{\infty} dx \frac{e^{-ix(t-t')}}{x+i0^+}. \tag{3.26}$$

With this, the retarded and advanced Greens functions can be rewritten as

$$G^R_{AB}(\omega) = \int_{-\infty}^{\infty} d\omega' \frac{S_{AB}(\omega')}{\omega-\omega'+i0^+}, \tag{3.27}$$

$$G^A_{AB}(\omega) = \int_{-\infty}^{\infty} d\omega' \frac{S_{AB}(\omega')}{\omega-\omega'-i0^+}. \tag{3.28}$$

Equations (3.27) and (3.28) represent the spectral representations of the retarded and advanced Green's functions, respectively. The sign of $i0^+$ is the only – but still important – difference between the retarded and advanced functions, and leads to their differing analytic behaviors. The retarded Greens function can be analytically continued in the upper half-plane while the advanced Greens function can be continued in the lower-half

plane.

Making use of the Dirac identity

$$\frac{1}{x - x_0 \pm i0^+} = \wp \frac{1}{x - x_0} \mp i\pi\delta(x - x_0) \tag{3.29}$$

in which $\wp$ denotes the Cauchy principal value, we can also readily derive the converse

$$S_{AB}(\omega) = \frac{i}{2\pi}\left(G^R_{AB}(\omega + i0^+) - G^A_{AB}(\omega - i0^+)\right). \tag{3.30}$$

If we presume the spectral density $S_{AB}(\omega)$ be real, then it follows that

$$S_{AB}(\omega) = -\frac{1}{\pi}\mathrm{Im}G^R_{AB}(\omega), \quad S_{AB}(\omega) = +\frac{1}{\pi}\mathrm{Im}G^A_{AB}(\omega). \tag{3.31}$$

The spectral function $S_{AB}(\omega)$ satisfies the sum rule $\int_{-\infty}^{\infty} S_{AB}(\omega)d\omega = 1$. Using the spectral representations of the correlation function (3.25) and the spectral density (3.30), we have

$$< B(t')A(t) >= \int_{-\infty}^{\infty} d\omega \frac{S_{AB}(\omega)}{e^{\beta\omega} + 1} e^{-i\omega(t-t')}. \tag{3.32}$$

This fundamental relation is called the ***spectral theorem***. With its aid, arbitrary correlation functions and expectation values ($t = t'$) over suitably defined spectral densities can be computed.

## 3.3 Matsubara Greens functions

In Matsubara formalism, the full imaginary time Greens function is given by

$$\ll A(\tau); B(\tau') \gg \equiv - < [T_\tau A(\tau)B(\tau')]_\mp >= G_{AB}(\tau - \tau'), \tag{3.33}$$

where $T_\tau$ is Wick's time-ordering operator. It orders operators historically with the later time to the left and behaves as

$$T_\tau A(\tau)B(\tau') = \left\{ \begin{array}{ll} A(\tau)B(\tau') & \text{if} \quad \tau > \tau' \\ \mp B(\tau')A(\tau) & \text{if} \quad \tau < \tau' \end{array} \right\}. \tag{3.34}$$

Setting $\tau' = 0$ gives

$$\ll A(\tau); B \gg = - < [T_\tau A(\tau) B] > = - (\Theta(\tau) < A(\tau) B > \pm \Theta(-\tau) < B A(\tau) >) . \tag{3.35}$$

Its equation of motion is given by

$$\frac{d}{d\tau} \ll A(\tau); B \gg = -\delta(\tau) < [A(\tau), B]_\mp > - \ll [A, H(\tau)] B \gg . \tag{3.36}$$

In terms of Matsubara frequency, $\omega_n = 2n\pi/\beta$ for bosons and $\omega_n = (2n+1)\pi/\beta$ for fermions, this can be rewriten as

$$i\omega_n \ll A; B \gg_{\omega_n} = < [A, B]_\mp > + \ll [A, H]; B \gg_{\omega_n} . \tag{3.37}$$

## 3.4 Nambu–Gor'kov formalism

A quantitative theory of the superconductivity can conveniently be formulated within the framework of the Nambu–Gor'kov formalism (also known as Matrix Green function) [58, 59]. In this formalism, one introduces a two-component field operators in the Nambu space as

$$\hat{\phi}_{\mathbf{k}}(\tau) = \begin{pmatrix} c_{\mathbf{k}\uparrow}(\tau) \\ c^\dagger_{-\mathbf{k}\downarrow}(\tau) \end{pmatrix}, \quad \hat{\phi}^\dagger_{\mathbf{k}}(\tau) = \begin{pmatrix} c^\dagger_{\mathbf{k}\uparrow}(\tau) & c_{-\mathbf{k}\downarrow}(\tau) \end{pmatrix} \tag{3.38}$$

where the electronic operators

$$c_{\mathbf{k}\sigma}(\tau) = e^{H\tau} c_{\mathbf{k}\sigma} e^{-H\tau}, \quad c^\dagger_{\mathbf{k}\sigma}(\tau) = e^{H\tau} c^\dagger_{\mathbf{k}\sigma} e^{-H\tau} \tag{3.39}$$

are defined in the imaginary-time space and $H$ is a mean field Hamiltonian. A generalized $2 \times 2$ matrix Green's function, which describes electron quasiparticles and Cooper pairs on an equal footing, is defined as

$$\hat{G}(\mathbf{k}, \tau) = - < T_\tau \hat{\phi}_{\mathbf{k}}(\tau) \hat{\phi}^\dagger_{\mathbf{k}}(0) > . \tag{3.40}$$

Inserting (3.38) into (3.40) gives

$$\hat{G}(\mathbf{k},\tau) = -\begin{pmatrix} < T_\tau c_{\mathbf{k}\uparrow}(\tau)c^\dagger_{\mathbf{k}\uparrow}(0) > & < T_\tau c_{\mathbf{k}\uparrow}(\tau)c_{-\mathbf{k}\downarrow}(0) > \\ < T_\tau c^\dagger_{-\mathbf{k}\downarrow}(\tau)c^\dagger_{\mathbf{k}\uparrow}(0) > & < T_\tau c^\dagger_{-\mathbf{k}\downarrow}(\tau)c_{-\mathbf{k}\downarrow}(0) > \end{pmatrix}. \tag{3.41}$$

Here the diagonal elements correspond to the standard Green's functions for electron quasiparticles and describe the dynamics of single-particle electronic excitations in the material. On the other hand, the off-diagonal elements represent Gorkov's anomalous Green's functions $F(\mathbf{k},\tau)$ and $F^*(\mathbf{k},\tau)$. These functions describe the dynamics of Coopers pairs and are related to the superconducting energy gap [60].

The generalized Green's function $\hat{G}(\mathbf{k},\tau)$ is periodic in imaginary time, therefore it can be Fourier transformed using

$$\hat{G}(\mathbf{k},\tau) = T\sum_{i\omega_n} e^{-i\omega_n}\hat{G}(\mathbf{k},i\omega_n), \quad \hat{G}(\mathbf{k},i\omega_n) = \int_0^\beta d\tau e^{i\omega_n\tau}G(\mathbf{k}\tau) \tag{3.42}$$

where $\omega_n$ stands for the fermion Matsubara frequencies, and $T$ is the absolute temperature. Therefore, the matrix elements of the generalized Green's function read

$$\hat{G}(\mathbf{k},i\omega_n) = \begin{pmatrix} G_{\uparrow\uparrow}(\mathbf{k},i\omega_n) & G_{\uparrow\downarrow}(\mathbf{k},i\omega_n) \\ G_{\downarrow\uparrow}(\mathbf{k},i\omega_n) & G_{\downarrow\downarrow}(\mathbf{k},i\omega_n) \end{pmatrix}. \tag{3.43}$$

Its equation can be put in a matrix form as

$$\begin{pmatrix} i\omega_n - \xi_{\mathbf{k}} & -\Delta \\ -\Delta^* & i\omega_n + \xi_{\mathbf{k}} \end{pmatrix}\begin{pmatrix} G_{\uparrow\uparrow}(\mathbf{k},i\omega_n) & G_{\uparrow\downarrow}(\mathbf{k},i\omega_n) \\ G_{\downarrow\uparrow}(\mathbf{k},i\omega_n) & G_{\downarrow\downarrow}(\mathbf{k},i\omega_n) \end{pmatrix} = \begin{pmatrix} 1 & 0 \\ 0 & 1 \end{pmatrix}. \tag{3.44}$$

Solving for the matrix Green function gives

$$\begin{pmatrix} G_{\uparrow\uparrow}(\mathbf{k},i\omega_n) & G_{\uparrow\downarrow}(\mathbf{k},i\omega_n) \\ G_{\downarrow\uparrow}(\mathbf{k},i\omega_n) & G_{\downarrow\downarrow}(\mathbf{k},i\omega_n) \end{pmatrix} = \frac{1}{(i\omega_n)^2 - \left(\xi^2_{\mathbf{k}} + |\Delta|^2\right)}\begin{pmatrix} i\omega_n + \xi_{\mathbf{k}} & \Delta^* \\ \Delta & i\omega_n - \xi_{\mathbf{k}} \end{pmatrix}. \tag{3.45}$$

Its inverse is given by

$$\hat{G}(\mathbf{k}, i\omega_n)^{-1} = \begin{pmatrix} i\omega_n - \xi_{\mathbf{k}} & -\Delta \\ -\Delta^* & i\omega_n + \xi_{\mathbf{k}} \end{pmatrix}. \tag{3.46}$$

# 4

# Effect of Impurity Scattering on Disordered Superconductors

In this chapter, we have investigated the scattering effects of nonmagnetic impurities on superconductivity of disordered superconductors. We have mainly focused on the suppression of superconductivity by considering the response of the transition temperature in both s-wave and d-wave superconductors. As our model system, we considered the most studied variant of bismuth strontium calcium copper oxide, $Bi_2Sr_2CaCu_2O_{8+x}$, commonly abbreviated as BSCCO-2212. Allowed symmetry of order parameters for this layered superconductor includes s, $d_{x^2-y^2}$ and $d_{xy}$ [61]. These symmetries are compatible symmetry operations that leave BSCCO invariant. The contents of the chapter are organized as follows. In the first section, we have formulated the Hamiltonian and Green's function of a superconductor in the clean limit. In the second section, we have formulated the problem in the dirty limit. In the third section, we have derived the expressions of superconducting critical temperature for s-wave and d-wave pairing symmetries and discussed the effects of impurity scattering on this thermodynamic variable.

## 4.1 Clean superconductors

Our primary objective is to study the effect of impurity scattering within the general framework of BCS theory for disordered superconductors. Therefore, we have started by

defining a model Hamiltonian for our problem as

$$H = H_0 + H_{imp}, \tag{4.1}$$

where the first term $H_0$ represents the Hamiltonian of a clean superconductor while the second represents the perturbative term due to impurity interaction.

For the case of clean superconductors, we have used the usual BCS model Hamiltonian defined by

$$H_0 = \sum_{\mathbf{k}\sigma} \xi_{\mathbf{k}} c^{\dagger}_{\mathbf{k}\sigma} c_{\mathbf{k}\sigma} - \sum_{\mathbf{k}\mathbf{k}'} V_{\mathbf{k}\mathbf{k}'} c^{\dagger}_{\mathbf{k}\uparrow} c^{\dagger}_{-\mathbf{k}\downarrow} c_{-\mathbf{k}'\downarrow} c_{\mathbf{k}'\uparrow}, \tag{4.2}$$

where $c^{\dagger}_{\mathbf{k}\sigma}$ and $c_{\mathbf{k}\sigma}$ are fermion creation and annihilation operators with $\sigma = \uparrow, \downarrow$ being fermion spin indices, $\xi_{\mathbf{k}} = \epsilon_{\mathbf{k}} - \mu$ with $\epsilon_{\mathbf{k}}$ and $\mu$ are band kinetic energy and chemical potential, and $V_{\mathbf{k}\mathbf{k}'}$ is an on-site attractive interaction which creates superconductivity. $\mathbf{k}$ and $\mathbf{k}'$ represent the momentums of the coupled electrons of a Cooper pair through phonon mediation (see Figure 2.4). The second term on the right-hand-side is quartic in fermionic creation and annihilation operators. In order to decouple this quartic term, we have employed a mean-field approximation which consists of replacing products of operators $A$ and $B$ according to

$$AB \simeq < A > B + A < B > - < A >< B > . \tag{4.3}$$

The error introduced by this kind of replacement is

$$AB - < A > B - A < B > + < A >< B >= (A - < A >)(B - < B >). \tag{4.4}$$

The mean-field approximation ignores such kind of fluctuations. A well known mean-field approximation is the Hartree or Stoner approximation, which for our BCS Hamiltonian (4.2) amounts the choice $A = c^{\dagger}_{\mathbf{k}\uparrow} c_{\mathbf{k}'\uparrow}$ and $B = c^{\dagger}_{-\mathbf{k}\downarrow} c_{-\mathbf{k}'\downarrow}$. However, Bardeen, Cooper and Schrieffer [2, 3] realized that superconductivity can be understood with the help of a different choice, namely $A = c^{\dagger}_{\mathbf{k}\uparrow} c^{\dagger}_{-\mathbf{k}\downarrow}$ and $B = c_{-\mathbf{k}'\downarrow} c_{\mathbf{k}'\uparrow}$. This leads to the BCS mean-field

Hamiltonian

$$H_0 = \sum_{\mathbf{k}\sigma} \xi_{\mathbf{k}} c^\dagger_{\mathbf{k}\sigma} c_{\mathbf{k}\sigma} - \sum_{\mathbf{k}\mathbf{k}'} V_{\mathbf{k}\mathbf{k}'} \left( < c^\dagger_{\mathbf{k}\uparrow} c^\dagger_{-\mathbf{k}\downarrow} > c_{-\mathbf{k}'\downarrow} c_{\mathbf{k}'\uparrow} + c^\dagger_{\mathbf{k}\uparrow} c^\dagger_{-\mathbf{k}\downarrow} < c_{-\mathbf{k}'\downarrow} c_{\mathbf{k}'\uparrow} > \right). \tag{4.5}$$

With definitions

$$\Delta = \sum_{\mathbf{k}\mathbf{k}'} V_{\mathbf{k}\mathbf{k}'} < c_{-\mathbf{k}'\downarrow} c_{\mathbf{k}'\uparrow} > \quad \text{and} \quad \Delta^* = \sum_{\mathbf{k}\mathbf{k}'} V_{\mathbf{k}\mathbf{k}'} < c^\dagger_{\mathbf{k}\uparrow} c^\dagger_{-\mathbf{k}\downarrow} >, \tag{4.6}$$

the reduced BCS mean-field Hamiltonian can be put as

$$H_0 = \sum_{\mathbf{k}\sigma} \xi_{\mathbf{k}} c^\dagger_{\mathbf{k}\sigma} c_{\mathbf{k}\sigma} - \sum_{\mathbf{k}} \left( \Delta^*_{\mathbf{k}} c_{-\mathbf{k}\downarrow} c_{\mathbf{k}\uparrow} + \Delta_{\mathbf{k}} c^\dagger_{\mathbf{k}\uparrow} c^\dagger_{-\mathbf{k}\downarrow} \right) \tag{4.7}$$

up to a constant. We have drooped the prime for the purpose of clarity.

### 4.1.1 Greens functions

In order to determine the Greens functions for Hamiltonian (4.7), we have used the Fourier transformed equation of motion (3.16)

$$\omega \ll A; B \gg_\omega = < [A, B] > + \ll [A, H_0]; B \gg_\omega . \tag{4.8}$$

Replacing operators $A$ and $B$ with $c_{\mathbf{k}\uparrow}$ and $c^\dagger_{\mathbf{k}\uparrow}$, respectively, gives

$$\omega \ll c_{\mathbf{k}\uparrow}; c^\dagger_{\mathbf{k}\uparrow} \gg_\omega = < [c_{\mathbf{k}\uparrow}, c^\dagger_{\mathbf{k}\uparrow}] > \delta(t) + \ll [c_{\mathbf{k}\uparrow}, H_0]; c^\dagger_{\mathbf{k}\uparrow} \gg_\omega . \tag{4.9}$$

Performing the commutation $[c_{\mathbf{k}\uparrow}, H_0]$ and rearranging gives

$$(\omega - \xi_{\mathbf{k}}) \ll c_{\mathbf{k}\uparrow}; c^\dagger_{\mathbf{k}\uparrow} \gg_\omega = 1 - \Delta_{\mathbf{k}} \ll c^\dagger_{-\mathbf{k}\downarrow}; c^\dagger_{\mathbf{k}\uparrow} \gg . \tag{4.10}$$

The new Green's function on the right-hand-side of (4.10) is given by

$$\omega \ll c^\dagger_{-\mathbf{k}\downarrow}; c^\dagger_{\mathbf{k}\uparrow} \gg_\omega = < [c^\dagger_{-\mathbf{k}\downarrow}, c^\dagger_{\mathbf{k}\uparrow}] > + \ll [c^\dagger_{-\mathbf{k}\downarrow}, H_0]; c^\dagger_{\mathbf{k}\uparrow} \gg_\omega . \tag{4.11}$$

Again, performing the commutation $[c^{\dagger}_{-\mathbf{k}\downarrow}, H_0]$ and rearranging gives

$$\ll c^{\dagger}_{-\mathbf{k}\downarrow}; c^{\dagger}_{\mathbf{k}\uparrow} \gg_{\omega} = -\frac{\Delta}{\omega + \xi_{\mathbf{k}}} \ll c_{\mathbf{k}\uparrow}; c^{\dagger}_{\mathbf{k}\uparrow} \gg_{\omega} . \tag{4.12}$$

Inserting (4.12) into (4.10) and rearranging results

$$G(\mathbf{k}, \omega) = \ll c_{\mathbf{k}\uparrow}; c^{\dagger}_{\mathbf{k}\uparrow} \gg_{\omega} = \frac{\omega + \xi_{\mathbf{k}}}{\omega^2 - \xi^2_{\mathbf{k}} - \Delta^2_k}. \tag{4.13}$$

In order to evaluate the order parameter $\Delta_{\mathbf{k}}$ we require the Gorkov's abnormal Green's function $\ll c^{\dagger}_{-\mathbf{k}\downarrow}; c^{\dagger}_{\mathbf{k}\uparrow} \gg$. Substituting (4.13) into (4.12) and rearranging gives

$$F(\mathbf{k}, \omega) = \ll c^{\dagger}_{-\mathbf{k}\downarrow}; c^{\dagger}_{\mathbf{k}\uparrow} \gg_{\omega} = -\frac{\Delta_{\mathbf{k}}}{\omega^2 - \xi^2_{\mathbf{k}} - \Delta^2_k}. \tag{4.14}$$

### 4.1.2 Order parameter and critical temperature

In order to obtain the expression for the superconducting order parameter we have used the anomalous Green's function defined in (4.14). The corresponding spectral density (3.25) is given by

$$S(\mathbf{k}, E) = \frac{\Delta}{2E_{\mathbf{k}}} \left(\delta\left(E + E_{\mathbf{k}}\right) - \delta\left(E - E_{\mathbf{k}}\right)\right). \tag{4.15}$$

Using the spectral theorem (3.32) and the spectral density (4.15) into the self-consistency condition (4.6) gives

$$\Delta = V \sum_{\mathbf{k}} < a^{\dagger}_{\mathbf{k}\uparrow} a^{\dagger}_{-\mathbf{k}\downarrow} >= V \sum_{\mathbf{k}} \frac{\Delta}{2E_{\mathbf{k}}} \tanh(\beta E_{\mathbf{k}}/2). \tag{4.16}$$

Cancelling $\Delta$ from both sides and converting the summation into integral results

$$1 = \frac{V}{(2\pi)^2} \int_{1BZ} d\mathbf{k} \frac{1}{2E_{\mathbf{k}}} \tanh(\beta E_{\mathbf{k}}/2) \tag{4.17}$$

with $\int_{\mathbf{k}} = \int_{1BZ} \frac{d\mathbf{k}}{(2\pi)^2}$. Here we have used constant attractive interaction ($V_{\mathbf{k}\mathbf{k}'} = -V$) for clean s-wave superconductors. For a normal state single-particle energy dispersion, $\xi_{\mathbf{k}} = \frac{\hbar^2 k^2}{2m_e} - E_F$, the integral over momentum amplitude $k$ can be changed to the integral

over energy as

$$\frac{1}{(2\pi)^2}\int dk \to \int N(\epsilon)d\epsilon, \tag{4.18}$$

where $N(\epsilon) = m_e\epsilon/2\pi\hbar^2$ denotes the density of states for electrons of one spin orientation for two-dimensional systems.

In the BCS-type weak-coupling theory of superconductivity, the pairing interaction is limited to a range of $[-\hbar\omega_c, \hbar\omega_c]$ around the Fermi surface (see Figure 2.4). The cutoff $\omega_c$ is the Debye frequency of phonons in conventional superconductors. Now the self-consistency condition (4.17), for the non-trivial $\Delta \neq 0$, becomes

$$1 = N_0 V \int_0^{\hbar\omega_c} d\xi \frac{1}{\sqrt{\xi_{\mathbf{k}}^2 + \Delta^2}} \tanh\left(\frac{\beta}{2}\sqrt{\xi_{\mathbf{k}}^2 + \Delta^2}\right). \tag{4.19}$$

Here we have employed the assumption that the density of states changes slightly in the range of $[-\hbar\omega_c, \hbar\omega_c]$ around the Fermi surface and can be approximated by that at the Fermi energy, i.e., $N_0$.

The zero-temperature order parameter $\Delta_0$ and the mean-field critical temperature $T_c$ can be obtained by setting $T = 0$ and $\Delta = 0$, respectively, in the self-consistency equation (4.19). When $T = 0$, it becomes

$$\frac{1}{\lambda} = \int_0^{\hbar\omega_c} d\xi \frac{1}{\sqrt{\xi_{\mathbf{k}}^2 + \Delta^2}}, \tag{4.20}$$

where $\lambda = N(0)V$. Rearranging this equation gives

$$\frac{1}{\lambda} = \int_0^{\hbar\omega_c} d\xi \frac{1}{\Delta\sqrt{1 + \left(\frac{\xi}{\Delta}\right)^2}}. \tag{4.21}$$

Employing the substitution $x = \xi/\Delta$ and using the standard integral

$$\int dx \frac{1}{\sqrt{1 + x^2}} = \sinh^{-1}(x) \tag{4.22}$$

gives

$$\frac{1}{\lambda} = \sinh^{-1}\left(\frac{\hbar\omega_c}{\Delta}\right) = \ln\left(\frac{\hbar\omega_c}{\Delta} + \sqrt{\left(\frac{\hbar\omega_c}{\Delta}\right)^2 + 1}\right). \tag{4.23}$$

Expanding the term under square root on the right-hand-side using Taylor series expansion and rearrnging gives

$$\Delta_{sc} = 2\hbar\omega_c \exp\left(-\frac{1}{\lambda}\right). \tag{4.24}$$

Similarly, the mean field transition temperature $T_c$ can be obtained by setting $\Delta = 0$ in equation (4.19)

$$\frac{1}{\lambda} = \int_0^{\hbar\omega_c} d\xi_{\mathbf{k}} \frac{1}{2\xi_{\mathbf{k}}} \tanh\left(\frac{\xi_{\mathbf{k}}}{2k_B T_c}\right). \tag{4.25}$$

Employing integration by substitution ($x = \xi_{\mathbf{k}}/2k_B T_c$) gives

$$\frac{1}{\lambda} = \int_0^{\hbar\omega_c/2k_B T_c} \frac{\tanh(x)}{x} dx = \ln\left(1.13\frac{\hbar\omega_c}{k_B T_c}\right). \tag{4.26}$$

Therefore, the expression for mean field critical temperature becomes

$$T_c = 1.13\omega_c \exp\left(-\frac{1}{\lambda}\right). \tag{4.27}$$

From (4.24) and (4.27), the ratio of $\Delta_0$ and $T_c$ gives a univerasl constant

$$\frac{2\Delta_0}{k_B T_c} = 3.50. \tag{4.28}$$

This is true for all weakly correlated BCS-type conventional superconductors.

The most important results of the calculations made in this section are equations (4.13), (4.14) and (4.27). We have used equations (4.13) and (4.14) for calculations of normal and anomalous self-energies which appear due to the interaction between Cooper paired electrons and the scatterng centers. Moreover, we have used equation (4.27) for comparison purposes. That is, we have discussed the effect of disorder due to scattering by impurity potential on superconducting critical temperature ($T_c$) of disordered superconductors by comparing to this expression.

## 4.2 Dirty superconductors

In a real material, a great variety of processes fall under the umbrella of scattering by impurities, and the result in general depends on the geometry involved and the particular character of the impurities. In this section, we have considered nonmagnetic impurities from which electrons can scatter elastically. For this type of impurity scattering, energy is conserved while momentum is not.

We have defined a short-ranged impurity potential due to interaction between conduction electrons and nonmagnetic impurities as

$$V(\mathbf{r}) = \sum_i u\left(\mathbf{r} - \mathbf{R}_i\right), \tag{4.29}$$

where $u(\mathbf{r} - \mathbf{R}_i)$ denotes strength of the scattering potential due to individual impurities, and $\mathbf{R}_i$ represents position of the impurities. The pertubative term, $H_{imp}$, in Hamiltonian (4.1) is due to this interaction potential. In the first quantization notation, this pertubative term is given by

$$H_{imp} = \sum_\sigma \int d^2\mathbf{r}\psi^\dagger_\sigma(\mathbf{r})\psi_\sigma(\mathbf{r})V(\mathbf{r}), \tag{4.30}$$

where $\psi^\dagger_\sigma(\mathbf{r})$ and $\psi_\sigma(\mathbf{r})$ are the usual fermionic creation and annihilation operators. In the basis of plane waves, these operators can be expressed as

$$\psi_\sigma(\mathbf{r}) = \frac{1}{\sqrt{\Omega}}\sum_{\mathbf{k}} e^{i\mathbf{k}.\mathbf{r}}c_{\mathbf{k}\sigma}, \quad \psi^\dagger_\sigma(\mathbf{r}) = \frac{1}{\sqrt{\Omega}}\sum_{\mathbf{k}} e^{-i\mathbf{k}.\mathbf{r}}c^\dagger_{\mathbf{k}\sigma}, \tag{4.31}$$

where $\Omega$ is volume of the system, and $c^\dagger_{\mathbf{k}'\sigma}$ and $c_{\mathbf{k}\sigma}$ are the usual fermionic creation and annihilation operators. With this the pertubative Hamiltonian becomes (see Appendix A.1)

$$H_{imp} = \sum_{\mathbf{k}\mathbf{k}',\sigma} u(\mathbf{k}' - \mathbf{k})\rho(\mathbf{k}' - \mathbf{k})c^\dagger_{\mathbf{k}',\sigma}c_{\mathbf{k}\sigma} \tag{4.32}$$

where

$$u(\mathbf{k}' - \mathbf{k}) = \frac{1}{\Omega}\int d^2\mathbf{r}' e^{-i(\mathbf{k}'-\mathbf{k}).\mathbf{r}'}, \quad \rho(\mathbf{k}' - \mathbf{k}) = \sum_i e^{-i(\mathbf{k}'-\mathbf{k}).\mathbf{R}_i}. \tag{4.33}$$

Therefore, upon using (4.7) and (4.32) into (4.1), the model Hamiltonian of our disordered system reads

$$H = \sum_{\mathbf{k}\sigma} \xi_{\mathbf{k}} c^{\dagger}_{\mathbf{k}\sigma} c_{\mathbf{k}\sigma} - \sum_{\mathbf{k}} \left( \Delta^{*}_{\mathbf{k}} c_{-\mathbf{k}\downarrow} c_{\mathbf{k}\uparrow} + \Delta_{\mathbf{k}} c^{\dagger}_{\mathbf{k}\uparrow} c^{\dagger}_{-\mathbf{k}\downarrow} \right) + \sum_{\mathbf{k}\mathbf{k}',\sigma} u(\mathbf{k}' - \mathbf{k}) \rho(\mathbf{k}' - \mathbf{k}) c^{\dagger}_{\mathbf{k}',\sigma} c_{\mathbf{k}\sigma}. \tag{4.34}$$

This Hamiltonian is assumed to be perturbative and quadratic in fermionic quasiparticle operators. It can be expanded in perturbation series as

$$\begin{aligned} \langle \mathbf{k}| \frac{1}{H_0 + H_{imp}} |\mathbf{k}'\rangle &= \langle \mathbf{k}| \frac{1}{H_0} |\mathbf{k}'\rangle + \sum_{\mathbf{k}_1 \mathbf{k}_2} \langle \mathbf{k}| \frac{1}{H_0} |\mathbf{k}_1\rangle \langle \mathbf{k}_1| H_{imp} |\mathbf{k}_2\rangle \langle \mathbf{k}_2| \frac{1}{H_0} |\mathbf{k}'\rangle \\ &+ \sum_{\mathbf{k}_1 \mathbf{k}_2 \mathbf{k}_3 \mathbf{k}_4} \langle \mathbf{k}| \frac{1}{H_0} |\mathbf{k}_1\rangle \langle \mathbf{k}_1| H_{imp} |\mathbf{k}_2\rangle \langle \mathbf{k}_2| \frac{1}{H_0} |\mathbf{k}_3\rangle \langle \mathbf{k}_3| H_{imp} |\mathbf{k}_4\rangle \langle \mathbf{k}_4| \frac{1}{H_0} |\mathbf{k}'\rangle + \dots \end{aligned} \tag{4.35}$$

Hence, its Green's function can be put as [62, 63]

$$\begin{aligned} G(\mathbf{k}, \mathbf{k}') &= G_0(\mathbf{k}) \delta_{\mathbf{k}\mathbf{k}'} + G_0(\mathbf{k}) u_{\mathbf{k}\mathbf{k}'} \rho_{\mathbf{k}\mathbf{k}'} G_0(\mathbf{k}') \\ &+ \sum_{\mathbf{k}_1} G_0(\mathbf{k}) u_{\mathbf{k}\mathbf{k}_1} \rho_{\mathbf{k}\mathbf{k}_1} G_0(\mathbf{k}_1) u_{\mathbf{k}_1\mathbf{k}'} \rho_{\mathbf{k}_1\mathbf{k}'} G_0(\mathbf{k}') + \dots, \end{aligned} \tag{4.36}$$

where $G_0(\mathbf{k})$ is Green's function of a superconductor in the clean limit.

### 4.2.1 Impurity averaging and Feynmann diagrams

The Green's function $G(\mathbf{k}, \mathbf{k}')$, defined in (4.36), is a function of the location of all the individual impurities, i.e. it is not diagonal in $\mathbf{k}$-space. However, averaging $G(\mathbf{k}, \mathbf{k}')$ over all possible impurity configurations restore its $\mathbf{k}$-space diagonality. Here we have assumed that the location of the various impurities are independent of each other so that the probability distributions for the impurity configuration is simply a product of probability distributions for the location of individual impurities, which will be taken as a uniform in space. Therefore, the impurity average simply consists of averaging the positions of the $N$ impurities. Denoting the impurity averaged Green's function by $< G(\mathbf{k}, \mathbf{k}') >$ thus we have

$$< G(\mathbf{k}, \mathbf{k}') >= \prod_{i=1}^{N} \left( \frac{1}{\Omega} \int d^2 \mathbf{R}_i \right) G(\mathbf{k} - \mathbf{k}'). \tag{4.37}$$

Being simply an integral over all impurity coordinates, the impurity average is clearly a linear operation, and can therefore be carried out for each term in the perturbation series of (4.36) separately (i.e. the average of the sum is the sum of the averages), giving

$$< G(\mathbf{k},\mathbf{k}') >= \sum_{n=0}^{\infty} < G^{(n)}(\mathbf{k},\mathbf{k}') > . \tag{4.38}$$

The only factors in the series expansion which depend on the impurity positions are the function $\rho(\mathbf{k})$. Thus to find the impurity averaged Green function we need to calculate the quantity $< \rho(\mathbf{k}-\mathbf{k}_1)\rho(\mathbf{k}_1-\mathbf{k}_2)\cdots\rho(\mathbf{k}_{n-1}-\mathbf{k}') >$. The detail of this calculation is given in Appendix A.2. Now, the impurity averaged Green's function $< G(\mathbf{k},\mathbf{k}') >$ is diagonal in $\mathbf{k}$-space

$$< G(\mathbf{k},\mathbf{k}') >=< G(\mathbf{k}) > \delta_{\mathbf{k}\mathbf{k}'}. \tag{4.39}$$

This is a consequence of the fact that the impurity averaging makes the system translationally invariant, i.e. electrons see the same average environment everywhere in the system. This $\mathbf{k}$-space diagonality is an important simplification resulting from the impurity averaging.

Apart from this, however, performing this configurational averaging does not make our task much easier since the complexity and diversity of the terms increase with the order of $n$. Hence, in order to escape from this difficulty, we should represent each term by Feynman diagrams and apply Feynman rules for translating the diagram version of the term into its corresponding mathematical expression (for the diagrams see Figure 4.1). The details of Feynman diagrams rules are given in Appendix A.3. The diagrams will give us an intuitive physical interpretation of the terms in the perturbation expansion. The corresponding mathematical expressions are written below.
For $n = 1$ we only have one term:

$$G^{(0)}(\mathbf{k})Nu(0)G^{(0)}(\mathbf{k}) \qquad \text{(term 1)} \tag{4.40}$$

For $n = 2$ there are two terms:

$$G^{(0)}(\mathbf{k})Nu(0)G^{(0)}(\mathbf{k})Nu(0)G^{(0)}(\mathbf{k}) \qquad \text{(term 2a)} \tag{4.41}$$

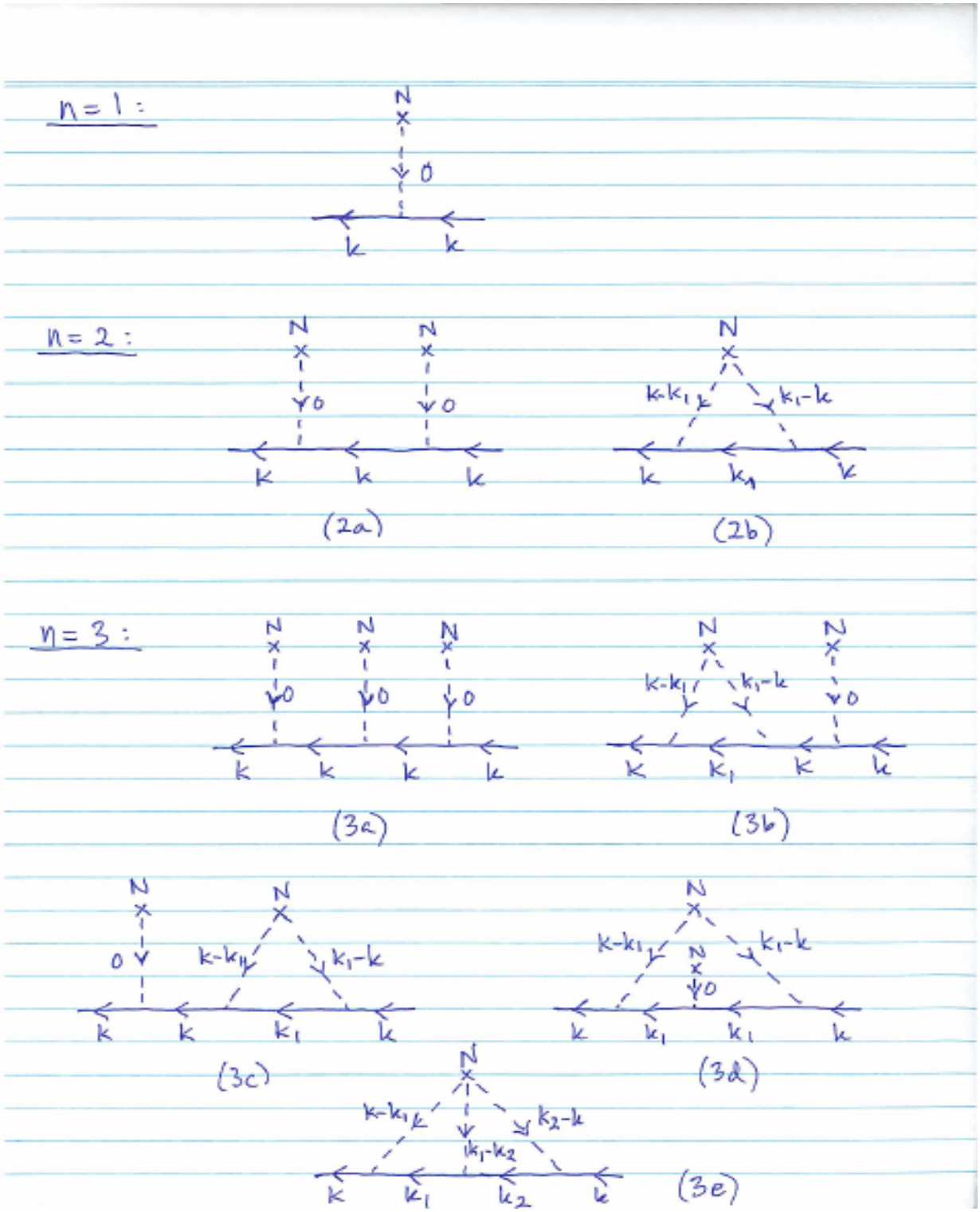


Figure 4.1: Feynman diagrams for orders $n = 1, 2$, and 3.

and

$$\sum_{\mathbf{k}_1} G^{(0)}(\mathbf{k}) Nu(\mathbf{k}-\mathbf{k}_1) G^{(0)}(\mathbf{k}_1) Nu(\mathbf{k}_1-\mathbf{k}) G^{(0)}(\mathbf{k}) \qquad \text{(term 2b)} \tag{4.42}$$

For $n = 3$ there are five terms:

$$G^{(0)}(\mathbf{k}) Nu(0) G^{(0)}(\mathbf{k}) Nu(0) G^{(0)}(\mathbf{k}) Nu(0) G^{(0)}(\mathbf{k}) Nu(0) G^{(0)}(\mathbf{k}) \qquad \text{(term 3a)}, \tag{4.43}$$

$$\sum_{\mathbf{k}_1} G^{(0)}(\mathbf{k}) Nu(\mathbf{k}-\mathbf{k}_1) G^{(0)}(\mathbf{k}_1 u(\mathbf{k}_1-\mathbf{k})) G^{(0)}(\mathbf{k}) Nu(0) G^{(0)}(\mathbf{k}) \qquad \text{(term 3b)}, \tag{4.44}$$

$$\sum_{\mathbf{k}_1} G^{(0)}(\mathbf{k}) Nu(0) G^{(0)}(\mathbf{k}) Nu(\mathbf{k}-\mathbf{k}_1) G^{(0)}(\mathbf{k}_1) u(\mathbf{k}_1-\mathbf{k}) G^{(0)}(\mathbf{k}) \qquad \text{(term 3c)}, \tag{4.45}$$

$$\sum_{\mathbf{k}_1} G^{(0)}(\mathbf{k}) Nu(\mathbf{k}-\mathbf{k}_1) G^{(0)}(\mathbf{k}_1) Nu(0) G^{(0)}(\mathbf{k}_1 u(\mathbf{k}_1-\mathbf{k}) G^{(0)}(\mathbf{k}) \qquad \text{(term 3d)} \tag{4.46}$$

and

$$\sum_{\mathbf{k}_1,\mathbf{k}_2} G^{(0)}(\mathbf{k}) Nu(\mathbf{k}-\mathbf{k}_1) G^{(0)}(\mathbf{k}_1) u(\mathbf{k}_1-\mathbf{k}_2) G^{0}(\mathbf{k}_2) u(\mathbf{k}_2-\mathbf{k}) G^{(0)}(\mathbf{k}) \qquad \text{(term 3e)}. \tag{4.47}$$

### 4.2.2 Irreducible diagrams and self-energy

By inspecting the terms in the perturbation series and the corresponding diagrams, one can see that some diagrams are composed by essentially concatenation, in various ways, diagrams appearing at a lower order in the expansion. This implies that there exist diagrammatic building blocks which can be utilized to generate all the diagrams and thus the entire perturbation expansion. In order to express the whole perturbation expansion in terms of these **building blocks**, we use the concept of an irreducible diagram. It is a diagram that cannot be stopped in to two pieces by only cutting a single internal electron line. The leftmost and rightmost electron lines in a diagram are called external. All other electron lines are called internal.

The next important concept is a self energy diagram. It is an irreducible diagram with the two external electron lines removed. Thus from Figure 4.1 one finds one self energy diagram at the leading order, one at the second, and two at the third order. We can figure out a mathematical expression for the self energy diagram by using the Feynman rules.

Finally, we define the selfenergy $\Sigma(\mathbf{k})$ as the sum of all self energy diagrams (there are an infinite number of such diagrams). Denoting self energy diagrams as $\Sigma^{(i)}(\mathbf{k})$, $i = 1, 2, 3, ...$, the self energy can be written as

$$\Sigma(\mathbf{k}) = \sum_i \Sigma^{(i)}(\mathbf{k}). \tag{4.48}$$

The self-energy up to and including terms of order $n = 3$ is shown in Figure 4.2.

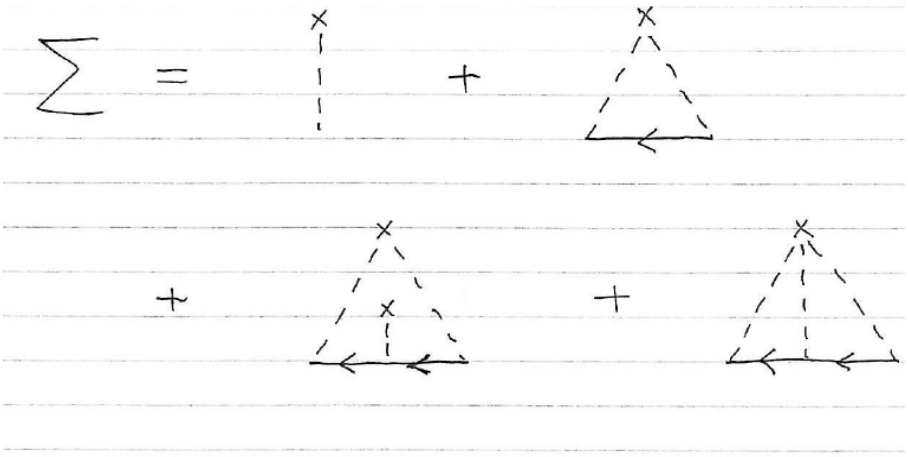

Figure 4.2: Self-energy up to and including terms of order $n = 3$.

An arbitrary term in $< G(\mathbf{k}) >$ can now be written in the form

$$G^{(0)}(\mathbf{k})\Sigma^{(i)}(\mathbf{k})G^{(0)}(\mathbf{k})\Sigma^{(j)}(\mathbf{k})G^{(0)}(\mathbf{k})\cdots G^{(0)}(\mathbf{k})\Sigma^{(l)}(\mathbf{k})G^{(0)}(\mathbf{k}). \tag{4.49}$$

The number of self-energy factors here can be $0, 1, 2, ...$ depending on the term. Note that there is a factor of $G^{(0)}(\mathbf{k})$ on both sides of every self-energy factor, and that the momenta of all Green functions and self-energy factors are the same $\mathbf{k}$. The entire perturbation expansion for $< G(\mathbf{k}) >$ can then be obtained by summing over all such terms and over all the self-energy diagrams in each term

$$\begin{aligned} < G(\mathbf{k}) > &= G^{(0)}(\mathbf{k}) + \sum_i G^{(0)}(\mathbf{k})\Sigma^{(i)}(\mathbf{k})G^{(0)}(\mathbf{k}) + \sum_{i,j} G^{(0)}(\mathbf{k})\Sigma^{(i)}(\mathbf{k})G^{(0)}(\mathbf{k})\Sigma^{(j)}(\mathbf{k})G^{(0)}(\mathbf{k}) \\ &+ \sum_{i,j,k} G^{(0)}(\mathbf{k})\Sigma^{(i)}(\mathbf{k})G^{(0)}(\mathbf{k})\Sigma^{(j)}(\mathbf{k})G^{(0)}(\mathbf{k})\Sigma^{(k)}(\mathbf{k})G^{(0)}(\mathbf{k}) + \cdots \\ &= G^{(0)}(\mathbf{k}) + G^{(0)}(\mathbf{k})\Sigma(\mathbf{k})\left(G^{(0)}(\mathbf{k}) + G^{(0)}(\mathbf{k})\Sigma(\mathbf{k})G^{(0)}(\mathbf{k}) + \cdots\right). \end{aligned} \tag{4.50}$$

The expression inside bracket is the expansion of $< G(\mathbf{k}) >$ itself, so that we finally get

$$< \hat{G}(\mathbf{k}) >= \hat{G}^{(0)}(\mathbf{k}) + \hat{G}^{(0)}(\mathbf{k})\hat{\Sigma}(\mathbf{k}) < \hat{G}(\mathbf{k}) > . \tag{4.51}$$

This equation is the well-known Dyson's equation. Solving this equation gives

$$< \hat{G}(\mathbf{k},\omega) >= \frac{1}{\left(\hat{G}^{(0)}(\mathbf{k},\omega)\right)^{-1} - \hat{\Sigma}(\mathbf{k},\omega)}. \tag{4.52}$$

Here $\hat{G}^{(0)}(\mathbf{k},\omega)$ is the matrix Green function for the nonperturbative term. It is defined in (3.46). We define the the self-energy matrix $\hat{\Sigma}(\mathbf{k},\omega)$ as

$$\hat{\Sigma}(\mathbf{k},\omega) = \begin{pmatrix} \Sigma_{\uparrow\uparrow}(\mathbf{k},\omega) & \Sigma_{\uparrow\downarrow}(\mathbf{k},\omega) \\ \Sigma_{\downarrow\uparrow}(\mathbf{k},\omega) & \Sigma_{\downarrow\downarrow}(\mathbf{k},\omega) \end{pmatrix} \tag{4.53}$$

Hence, the impurity averaged Green fnction matrix $< \hat{G}(\mathbf{k},\omega) >$ becomes

$$< \hat{G}(\mathbf{k},\omega) >= \frac{1}{D}\begin{pmatrix} i\omega_n + \xi_{\mathbf{k}} - \Sigma_{\downarrow\downarrow}(\mathbf{k},\omega) & \Delta^* + \Sigma_{\downarrow\uparrow}(\mathbf{k},\omega) \\ \Delta + \Sigma_{\uparrow\downarrow}(\mathbf{k},\omega) & i\omega_n - \xi_{\mathbf{k}} - \Sigma_{\uparrow\uparrow}(\mathbf{k},\omega) \end{pmatrix} \tag{4.54}$$

where $D$ is given by

$$D = \left(i\omega_n + \xi_{\mathbf{k}} - \Sigma_{\downarrow\downarrow}(\mathbf{k},\omega)\right)\left(i\omega_n - \xi_{\mathbf{k}} - \Sigma_{\uparrow\uparrow}(\mathbf{k},\omega)\right) - \left(\Delta^* - \Sigma_{\downarrow\uparrow}(\mathbf{k},\omega)\right)\left(\Delta - \Sigma_{\uparrow\downarrow}(\mathbf{k},\omega)\right). \tag{4.55}$$

In the limit of low impurity density $n_i \equiv N/\Omega$ and weak scattering potential $V(\mathbf{r})$, the self-energy $\Sigma(\mathbf{k},\omega)$ can be approximated by considering the first two diagrams in Figure 4.2. From the Feynman rules, the self energy due to the first diagram neither depends on $\mathbf{k}$ nor $\omega$. Hence, when introduced into the Dyson equation, it contributes only to a constant energy shift. Therfore, without loss of generality, we can ignore it in our subsequent calculations. The self energy due to the second diagram is given by

$$\Sigma^{(2)}(\mathbf{k},\omega) = \frac{n_i}{(2\pi)^2}\int |u(\mathbf{k}-\mathbf{k}_1)|^2 G^{(0)}(\mathbf{k}_1,\omega) d^2\mathbf{k}_1. \tag{4.56}$$

## 4.3 Order parameter and critical temperature

In this section, we have derived the expressions for transition temperature of both s-wave and d-wave dirty superconductor by considering different possible pairing symmetries. For the calculations of the order parameter and the critical temperature, we make use of the BCS self-consistency condition defined in (4.6) and the off-diagonal terms of the impurity averaged Green function defined in (4.54). In Matsubara frequency domain, the self-consistency condition is defined as

$$\Delta_{\mathbf{k}} = \frac{T}{(2\pi)^2} \sum_{\omega_n} \int V_{\mathbf{k}\mathbf{k}'} < G_{\downarrow\uparrow}(\mathbf{k}', \omega) > d^2\mathbf{k}' \tag{4.57}$$

where $T$ is temperature and $< G_{\downarrow\uparrow}(\mathbf{k}', \omega) >$ is the off-diagonal (anomalous) term in the impurity averaged Green function matrix (4.54). Moreover, for the calculations of the self-energies, we have defined the square of the impurity potential $u(\mathbf{k} - \mathbf{k}')$ as

$$|u(\mathbf{k} - \mathbf{k}')|^2 = u_0^2 + u_1^2 \cos(\phi_{kk'}) + u_2^2 \cos(2\phi_{kk'}) \tag{4.58}$$

where $u_0$, $u_1$ and $u_2$ are real constants. Here we have used $\phi_{kk'} = \phi - \phi'$ for notation convenience. This has experimental precedent, and can be thought of in terms of the Born approximation expansion including an infinite series of $P_n \cos(\phi_{kk'})$ terms [64].

The profile of the energy gap around the Fermi surface for these two types of pairing symmetry is depicted in Figure 4.3. For the isotropic s wave pairing symmetry, the quasiparticle gap is uniform along the Fermisurface. For the anisotropic $d_{x^2-y^2}$ wave pairing symmetry, the quasiparticle gap is closed at some special momentum directions $\phi = \frac{\pi}{4}, \frac{3\pi}{4}, \frac{5\pi}{4}, \frac{7\pi}{4}$. These gapless quasiparticles are called nodal quasiparticles.

### 4.3.1 Disordered s-wave superconductors

For an isotropic s-wave pairing symmetry, we use the ansatz [24]

$$V_{\mathbf{k}\mathbf{k}'} = V \tag{4.59}$$

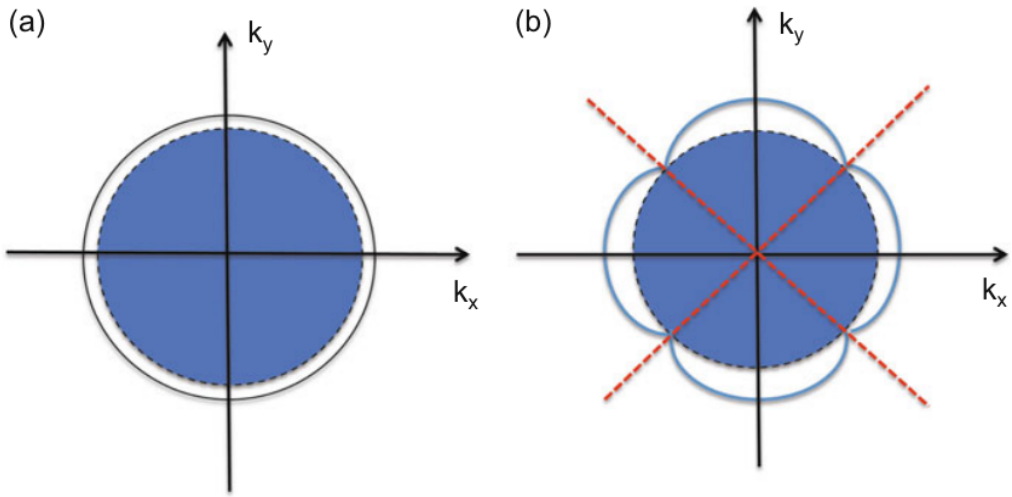


Figure 4.3: A schematic drawing of quasiparticle excitation gap for an s wave (a) and a $d_{x^2-y^2}$ wave (b) pairing symmetries [24].

and correspondingly

$$\Delta(\mathbf{k}, T) = \Delta(T) \tag{4.60}$$

where $\Delta(T)$ is a complex-valued function of the temperature $T$ and $V$ is a constant pairing interaction.

Upon substituting (4.14) and (4.58) into (4.56), the anomalous self energy component $\Sigma_{\downarrow\uparrow}(\mathbf{k}, i\omega_n)$ becomes (Appendix B.1)

$$\begin{aligned}\Sigma_{\downarrow\uparrow}(\mathbf{k}, i\omega_n) &= \frac{n_i}{(2\pi)^2}\int |u(\mathbf{k}-\mathbf{k}')|^2 G^{(0)}_{\downarrow\uparrow}(\mathbf{k}', \omega) d^2\mathbf{k}' \\ &= \frac{\Delta^*}{2\tau\sqrt{\omega_n^2 + |\Delta|^2}},\end{aligned} \tag{4.61}$$

where the scatering time $\tau$ is defined by $\tau = 1/n_i m u_0^2$. Similarly, upon substituting (4.13) and (4.58) into (4.56), the normal self-energy component $\Sigma_{\uparrow\uparrow}(\mathbf{k}, i\omega_n)$ becomes (Appendix B.1)

$$\begin{aligned}\Sigma_{\uparrow\uparrow}(\mathbf{k}, i\omega_n) &= \frac{n_i}{(2\pi)^2}\int |u(\mathbf{k}-\mathbf{k}')|^2 G_{\uparrow\uparrow}(0)(\mathbf{k}', \omega) d^2\mathbf{k}' \\ &= -\frac{i\omega_n}{2\tau\sqrt{\omega_n^2 + |\Delta|^2}}.\end{aligned} \tag{4.62}$$

Here, we note that

$$\Delta + \Sigma_{\downarrow\uparrow}(\omega_n) = \eta_\omega \Delta \quad \text{and} \quad i\omega_n - \Sigma_{\uparrow\uparrow}(\omega_n) = i\eta_\omega \omega_n \tag{4.63}$$

where

$$\eta_\omega = 1 + \frac{1}{2\tau\sqrt{\omega_n^2 + |\Delta|^2}}. \tag{4.64}$$

Hence, the effect of scattering on the Greens functions is to make the substitutions $\omega \to \eta_\omega \omega$ and $\Delta \to \eta_\omega \Delta$. For convenience, we have defined $\tilde{\omega} \equiv \eta_\omega \omega$ and $\tilde{\Delta} \equiv \eta_\omega \Delta$. Therefore, with this modification, the normal and anomalous Greens functions become

$$G_{\uparrow\uparrow}(\mathbf{k}, i\omega_n) = -\frac{i\tilde{\omega}_n}{\tilde{\omega}^2 + \xi^2 + |\tilde{\Delta}|^2}, \quad G_{\downarrow\uparrow}(\mathbf{k}, i\omega_n) = \frac{\tilde{\Delta}}{\tilde{\omega}^2 + \xi^2 + |\tilde{\Delta}|^2}. \tag{4.65}$$

Substituting the anomalous Green function (4.65) into the self-consistency condition (4.57) gives (Appendix B.1)

$$\begin{aligned} \Delta^* &= \frac{T}{(2\pi)^2} \sum_{\omega_n} \int V_{\mathbf{k}\mathbf{k}'} G_{\downarrow\uparrow}(\mathbf{k}', i\omega_n) d^2\mathbf{k}' \\ &= \frac{VTm}{2} \sum_{\omega_n} \frac{\Delta^*}{\sqrt{\omega_n^2 + |\Delta|^2}}. \end{aligned} \tag{4.66}$$

Dividing both sides of (4.66) by $\Delta^*$ results

$$1 = \frac{VTm}{2} \sum_{\omega_n} \frac{1}{\sqrt{\omega_n^2 + |\Delta|^2}}. \tag{4.67}$$

At $T = T_c$, the gap is zero. With this, equation (4.67) educes to

$$1 = \frac{VT_c m}{2} \sum_{\omega_n} \frac{1}{|\omega_n|}. \tag{4.68}$$

The sum over the Matsubara frequency $\omega_n$ in this equation is divergent, and must be cut off at some finite (but large) frequency $\omega_c$ in order to obtain physical results. With this cut

off, the self-consistency equation (4.68) can be put as

$$1 \simeq \frac{VT_c m}{2} \sum_{n=-\infty}^{\omega_c/2\pi T_c - 1/2} \frac{1}{|(2n+1)\pi T_c|}. \tag{4.69}$$

where the relation $(2n_{max}+1)\pi T_c = \omega_c$ was employed. In terms of the digamma function $\psi(x)$, which satisfies

$$\psi(x+N+1) - \psi(x) = \sum_{n=0}^{\infty} \left( \frac{1}{n+x} - \frac{1}{n+x+N+1} \right) = \sum_{n=0}^{N} \frac{1}{n+x}, \tag{4.70}$$

the last equation becomes

$$1 \approx \frac{Vm}{2\pi} \left[ \psi\left( \frac{1}{2} + \frac{\omega_c}{2\pi T_c} \right) - \psi\left( \frac{1}{2} \right) \right] \tag{4.71}$$

due to the largeness of $\omega_c$. Employing the property of digamma function,

$$\psi\left( \frac{\omega_c}{2\pi T_c} + \frac{1}{2} \right) \approx \ln\left( \frac{\omega_c}{2\pi T_c} \right), \tag{4.72}$$

for $\omega_c \to \infty$ gives

$$1 = \frac{Vm}{2\pi} \left[ \ln\left( \frac{\omega_c}{2\pi T_c} \right) - \psi\left( \frac{1}{2} \right) \right]. \tag{4.73}$$

The digamma function $\psi\left(\frac{1}{2}\right)$ is given by

$$\psi\left( \frac{1}{2} \right) = -\gamma - 2\ln 2 = -C, \tag{4.74}$$

where $\gamma$ is the Euler constant. Using this into (4.73) and rearranging finally gives

$$T_c = 1.13\omega_c \exp\left(-1/\lambda\right), \tag{4.75}$$

where $\lambda = Vm/2\pi$ is the coupling constant.

### 4.3.2 Disordered d-wave supercoductors

As it has been mentioned in the introduction, the system we have considered for our investigation is the most studied variant of bismuth strontium calcium copper oxide $Bi_2Sr_2CaCu_2O_{8-x}$. Its allowed d-wave pairing symmetry are $d_{x^2-y^2}$ and $d_{xy}$. Here in this subsection, we consider the $d_{x^2-y^2}$ pairing symmetry and investigate the effect of disorder which comprises of nonmagnetic impurities by calculating the transition temperature, $T_c$.

For the $d_{x^2-y^2}$ pairing symmetry, the pairing interaction can be written as

$$V_{\mathbf{k}\mathbf{k}'} = V\cos(2(\phi-\phi')), \tag{4.76}$$

where the angle $\phi = \tan^{-1}(k_{Fy}/k_{Fx})$ with $k_{Fx(y)}$ the two components of the Fermi wave vector and V is a constant. Correspndingly, the superconducting pair potential is of the form

$$\Delta(\mathbf{k},T) = \Delta(T)\cos(2\phi), \tag{4.77}$$

where $\Delta(T)$ is a complex-valued function of the temperature $T$.

Upon substituting equations (4.14), (4.58) and (4.77) into (4.56), the self-energy $\Sigma_{\downarrow\uparrow}(\mathbf{k}, i\omega_n)$ becomes (Appendix B.2)

$$\begin{aligned}\Sigma_{\downarrow\uparrow}(\mathbf{k},\omega_n) &= \frac{n_i}{(2\pi)^2}\int |u(\mathbf{k}-\mathbf{k}')|^2 G^{(0)}_{\downarrow\uparrow}(\mathbf{k},\omega_n)d^2\mathbf{k}' \\ &= \frac{n_i m u_2^2 \Delta^* \cos(2\phi)}{4}\frac{1}{|\omega_n|}.\end{aligned} \tag{4.78}$$

Similarly, the self-energy $\Sigma_{\uparrow\uparrow}(\mathbf{k},\omega_n)$ becomes (Appendix B.2)

$$\begin{aligned}\Sigma_{\uparrow\uparrow}(\mathbf{k},\omega_n) &= \frac{n_i}{(2\pi)^2}\int |u(\mathbf{k}-\mathbf{k}')|^2 G^{(0)}_{\uparrow\uparrow}(\mathbf{k},\omega_n)d^2\mathbf{k}' \\ &= -i\omega_n \frac{n_i m u_0^2}{2}\left(\frac{1}{|\omega_n|} - \frac{|\Delta|^2}{4|\omega_n|^3}\right).\end{aligned} \tag{4.79}$$

Defining $1/\tau_1 \equiv n_i m u_0^2$ and $1/\tau_2 \equiv n_i m u_2^2$, we get

$$i\omega_n - \Sigma_{\uparrow\uparrow}(\mathbf{k},\omega_n) = i\eta_{\omega 1}\omega_n \tag{4.80}$$

and

$$\Delta^*(\mathbf{k}) + \Sigma_{\downarrow\uparrow}(\mathbf{k}, \omega_n) = \eta_{\omega 2}\Delta^*(\mathbf{k}) \tag{4.81}$$

where

$$\eta_{\omega 1} \equiv 1 + \frac{1}{2\tau_1}\left(\frac{1}{|\omega_n|} - \frac{|\Delta|^2}{4|\omega_n|^3}\right), \quad \eta_{\omega 2} \equiv 1 + \frac{1}{2\tau_2|\omega_n|}. \tag{4.82}$$

Therefore, the effect of scattering on the Green functions is simply to make the substitutions $\omega_n \rightarrow \eta_{\omega 1}\omega_n$ and $\Delta(\mathbf{k}) \rightarrow \eta_{\omega 2}\Delta(\mathbf{k})$. Here for convenience, we define $\tilde{\omega} \equiv \eta_{\omega 1}\omega_n$ and $\tilde{\Delta} \equiv \eta_{\omega 2}\Delta(\mathbf{k})$.

Now we will calculate the effect of disorder on $T_c$ using the BCS self-consistency condition (4.57). Substituting (4.65), (4.76) and (4.77) into the self-consistency condition (4.57) gives (Appendix B.2)

$$\begin{aligned}\Delta^*(\mathbf{k}) &= \frac{T}{(2\pi)^2}\sum_n \int V_{\mathbf{k}\mathbf{k}'} G_{\downarrow\uparrow}(\mathbf{k}', \omega_n) d^2\mathbf{k}' \\ &= \frac{VTm\Delta^*(\mathbf{k})}{4}\sum_n \eta_{\omega 2}\frac{1}{|\tilde{\omega}_n|}.\end{aligned} \tag{4.83}$$

Dividing both sides by $\Delta^*(\mathbf{k})$ results

$$1 = \frac{VTm}{4}\sum_n \frac{1 + \frac{1}{2\tau_2|\omega_n|}}{\left(1 + \frac{1}{2\tau_1}\left(\frac{1}{|\omega_n|} - \frac{|\Delta|^2}{4|\omega_n|^3}\right)\right)|\omega_n|}. \tag{4.84}$$

At the phase transsition, $\Delta = 0$, this last equation reduces to the form

$$1 = \frac{T_c Vm}{4}\sum_n \frac{|\omega_n| + \frac{1}{2\tau_2}}{\left(|\omega_n| + \frac{1}{2\tau_1}\right)|\omega_n|}. \tag{4.85}$$

After some algebra analogous to the s-wave case [65], we get the result

$$\ln\left(\frac{T_c}{T_{c0}}\right) = \left(\frac{\tau_1}{\tau_2} - 1\right)\left[\psi\left(\frac{1}{2} + \frac{(1/2\tau_1)}{2\pi T_c}\right) - \psi\left(\frac{1}{2}\right)\right]. \tag{4.86}$$

For the diluted short range scattering potential, we can consider only the first term of the Born approximated scattering potential defined in equation (4.58). Based on this assumption,we can set $1/\tau_2 \approx 0$ and $\tau_1 \equiv \tau$. With this, equation (4.86) reduces to the

well-known Abrikosov-Gorkov expression [8]

$$\ln\left(\frac{T_c}{T_{c0}}\right) = \psi\left(\frac{1}{2}\right) - \psi\left(\frac{1}{2} + \frac{1}{4\pi\tau T_c}\right). \tag{4.87}$$

Taking exponent on both sides and rearranging gives

$$\frac{T_c}{T_{c0}} = 0.14 \exp\left[-\psi\left(\frac{1}{2} + \frac{1}{4\pi\tau T_c}\right)\right]. \tag{4.88}$$

Defining a disorder strength parameter $\delta$ as $\delta = 1/4\pi\tau T_c$ and using in (4.88) gives

$$\frac{T_c}{T_{c0}} = 0.14 \exp\left[-\psi\left(\frac{1}{2} + \delta\right)\right]. \tag{4.89}$$

### 4.3.3 Discussion of the results

The expression of superconducting critical temperature derived for isotropic disordered s-wave superconductor (equation (4.75)) indicates that the factors which represent the effect of impurity scattering are completely absent. Moreover, equation (4.75) is completely identical to the expression of $T_c$ derived in the clean limit (equation(4.27)), where there is no impurity scattering. This indicates that impurity scattering has no bearing on the thermodynamic parameters, such as superconducting order parameter and critical temperature, of s-wave superconductors. This insensitivity of superconductivity to dilute nonmagnetic impurities agrees with the well-known Anderson's theorem [7]. The theorem states that because the superconductivity arises from the instability of the Fermi surface upon the pairing of time-reversed electronic states, any perturbation that cannot reverse the time reversal symmetry should not affect the mean-field superconducting order parameter and the transition temperature of conventional superconductors.

The expression for superconducting critical temperature of disordered d-wave superconductor was also derived (equation (4.89)) and numerically plotted as depicted in Figure 4.4. As it has been clearly shown in the figure, the impurity scattering in this case supresses the superconducting critical temperature of disordered d-wave superconductors. The supression of the critical temperature depends on the concentration of scattering centers ($\delta \sim n_i$) and the strength of the impurity scattering potential ($\delta \sim u_0^2$). Therefore,

increasing the concentration of the scattering centers and the strength of the impurity potental supresses superconductivity of the system by decreasing the scattering time and enhancing resistance of the sytem.

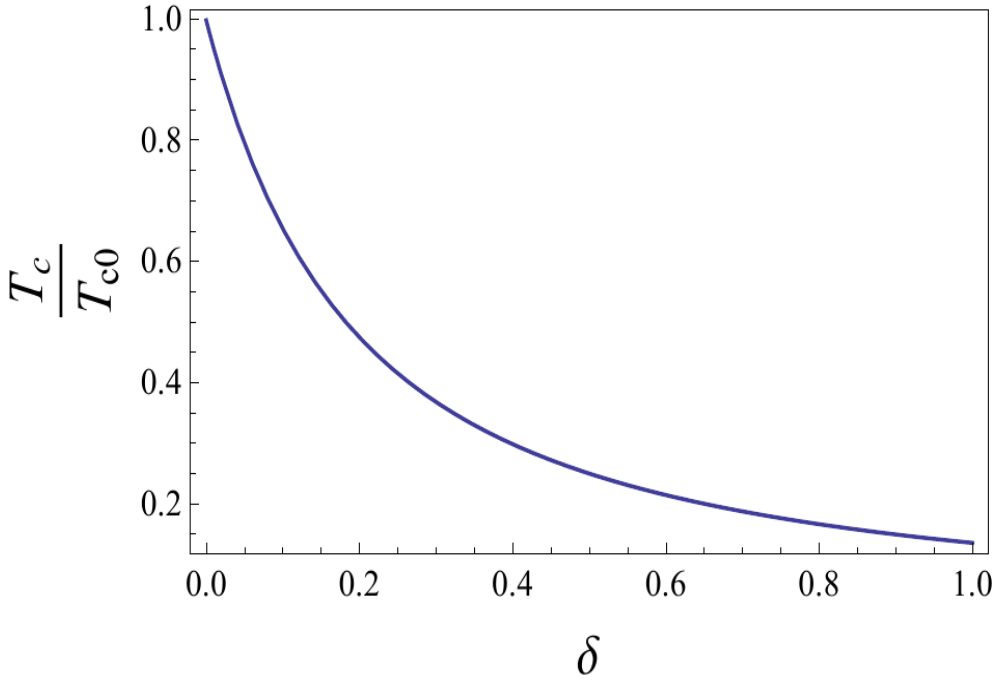


Figure 4.4: Supression of superconducting critical temperature by disorder.

The $T_c$ suppression equations (4.75) and (4.89) were derived for extreme limits of completely isotropic s-wave and completely anisotropic d-wave pairing symmetries, for which the isotropy parameters are $\chi = 0$ and $\chi = 1$, respectively. However, the anisotropy parameter for some superconductors can lie in between these extreme limits ($0 < \chi < 1$). For such pairing symmetries, equation (4.87) takes the form

$$\ln\left(\frac{T_c}{T_{c0}}\right) = \chi\left[\psi\left(\frac{1}{2}\right) - \psi\left(\frac{1}{2} + \frac{1}{4\pi\tau T_c}\right)\right], \tag{4.90}$$

and the $T_c$ suppression equation (4.89) can be put as

$$\frac{T_c}{T_{c0}} = \exp\left(\chi\left[\psi\left(\frac{1}{2}\right) - \psi\left(\frac{1}{2} + \delta\right)\right]\right). \tag{4.91}$$

The graph in Figure 4.5 was plotted based on equation (4.91) and shows the dependence of the suppression of superconducting critical temperature on the degree of anisotropy

of a superconductor. The graph clearly indicates that the effect of impurity scattering is more dominant in those superconductors having high degree of anisotropy in pairing symmetry.

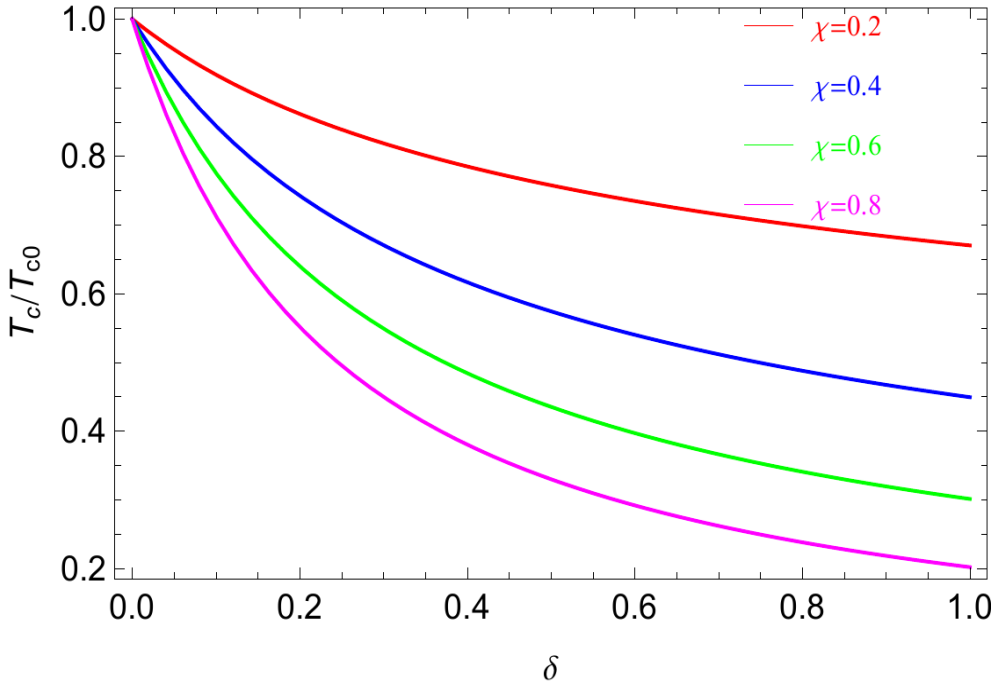


Figure 4.5: Dependence of $T_c$ supression on anisotropy of the pairing symmetry.

# 5

# Disorder-Induced Superconductor-Insulator Transition

In this chapter, we study the effect of disorder due to randomness in island potential on superconductivity of superconducting granular thin films based on the bosonic hard-core model. The chapter has two parts. In the first part, we have investigated the effect of disorder owing to variation in island size on the superconducting order parameter using the equation of motion methods of Greens functions. Specifically, we have studied how superconducting order parameter varies with strength of disorder and two-body interaction. In the second part, we have investigated the effect of phase fluctuation on superconductivity of the thin film using the phase fluctuation scenario of Josephson Junction Arrays model. We mainly focused on the effect of fluctuation in the phase of the order parameter induced due to disorder on superfluid density of the system. We have determined the superfluid density of the system as a cross-check for the validity of our hard-core boson model. For this part, we have employed the path integral formalism of quantum field theory.

Practically, superconducting granular thin films can be manufactured by repeated small increments of materials onto substrates held at low temperatures in an ultra-high vacuum. Such systems are found to form superconducting islands separated by thin insulating regions as clearly shown in Figure 5.1. They are strongly disordered due to distribution of island sizes and the coupling between islands.

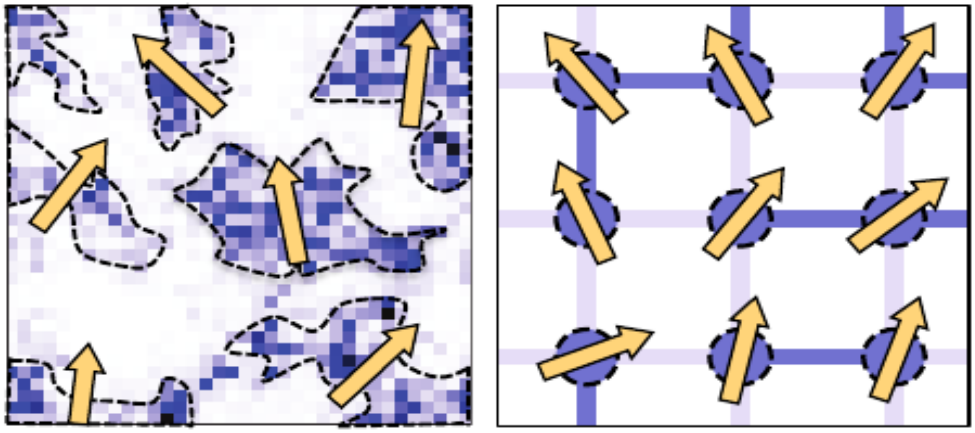

Figure 5.1: Superconducting islands (blue regions) separated by insulating matrix (white regions). For very thin films the islands are assumed to be on lattice sites (Right) [66].

## 5.1 Suppression of superconductivity due to randomness in an on-site potential and two-body interaction

### 5.1.1 Model Hamiltonian

In low dimensional superconductors, the effect of disorder can be either pair breaking or phase decoherence [7]. The pair breaking effect is known by fermionic model [29] and the decoherence effect is known by bosonic model [31]. For our granular film, the widely accepted scenario is the bosonic model [7, 30–34]. According to this model, in the presence of strong disorder the superconducting order parameter becomes inhomogeneous, spontaneously segregating into superconducting domains, dispersed in an insulating matrix (as indicated in Figuere 5.1). Superconducting islands of different sizes will be induced, and these random sized islands can in turn create randomness in chemical potentials which can potentially disturb the coherence between Cooper pairs on different islands. At some disorder strength, the coherence is entirely lost and the system becomes a gaped insulator. By gaped insulator, we mean that there is superconducting gap (also known as pseudogap) but no superconductivity. Figure 5.1, which was plotted by K. Bouadim et al. [66] based on Quantum Monte Carlo simulation, depicts this model.

Based on this bosonic scenario, we have developed a Bose-Hubbard [57] type model

Hamiltonian of the form

$$H = -t\sum_{i,a} b_i^+ b_{i+a} + \hat{b}_i b_{i+a}^+) + U\sum_{i,a} n_i n_{i+a} - \sum_i v_i n_i \tag{5.1}$$

where $b_i^+$, $b_i$ and $n_i$ represent the creation, annihilation and number operators of Cooper pairs on the i-th lattice point, respectively. $a$ denotes the vector to the four nearest neighbours. $U$ and $t$ denote the repulsive interaction and the hopping integral for bosons on the nearest neighbour sites, respectively. $v_i$ represents the randomness in the single-site potential due to variation in the island sizes. Deviation of the chemical potential $\Delta v_i$ from its average value $v$, $\Delta v_i = v_i - v$, is mainly due to distribution of island size.

In the case of infinite on-site repulsive interaction, our bosonic model becomes an hard-core boson model and double occupancy of bosons is completely restricted. Therefore, the hard-core boson system is isomorphic to spin-half system. Hence, employing the hard-core boson spin transformation rule [67], we have mapped our bosonic Hamiltonian into Heisenberg type of the form

$$H = -\frac{J_{xy}}{2}\sum_{i,a}(S_i^+ S_{i+a}^- + S_i^- S_{i+a}^+) + J_z\sum_{i,a} S_i^z S_{i+a}^z - \sum_i v_i S_i^z. \tag{5.2}$$

In this model, the order in spin operators $< S^{\pm} >$ represent the superconducting order parameters and $< S^z >$ represents the crystalline order. Therfore, one can give a qualitative judgement whether the system is superconducting or insulating by calculating the averages in spin operators.

### 5.1.2 Calculation of superconducting order paramter

In this subsection, the orders in spin operators which describe the Cooper pairs on each island have been calculated. The retarded Green's function defined in section (3.1), for operators $S_i^+(t)$ and $S_j^-(t')$, is given by

$$G^R(t,t') \equiv\ll v_i S_i^+(t); S_j^-(t') \gg_R = -i\Theta(t-t') < [v_i S_i^+(t), S_j^-(t')] > . \tag{5.3}$$

Its Fourier transformed equation of motion is

$$\omega \ll v_i S_i^+, S_j^- \gg_\omega = < [v_i S_i^+, S_j^-] > + \ll [v_i S_i^+, H]; S_j^- \gg_\omega . \tag{5.4}$$

Inserting the Hamiltonin (5.2) into (5.4), employing the standard commutation rules of spin operators [57, 64] and rearranging gives

$$\begin{aligned} \omega \ll v_i S_i^+; S_j^- \gg_\omega = & < [v_i S_i^+, S_j^-] >_\omega + \ll v_i^2 S_i^+; S_j^- \gg_\omega \\ & + \sum_a J_z \ll v_i S_i^+ S_{i+a}^z; S_j^- \gg_\omega - J_{xy} \ll v_i S_i^z S_{i+a}^+; S_j^- \gg_\omega . \end{aligned} \tag{5.5}$$

The random on-site potential $v_i$ was averaged based on the simple Born approximation

$$< v_i > = < v \pm \Delta v_i > = v, \quad < v_i v_j > = v^2 + \Delta v^2 \delta_{ij}. \tag{5.6}$$

Using (5.6) into (5.5) and applying the decoupling approximations

$$\ll S_i^+ S_{i+a}^z; S_j^- \gg \simeq < S^z > \ll S_i^+; S_j^- \gg, \quad \ll S_i^z S_{i+a}^+; S_j^- \gg \simeq < S^z > \ll S_{i+a}^+; S_j^- \gg, \tag{5.7}$$

gives

$$\begin{aligned} \omega \ll S_i^+; S_j^- \gg_\omega = & \, 2 < S^z > + \frac{v^2 + \Delta v}{v} \ll S_i^+; S_j^- \gg_\omega \\ & + \sum_a J_z < S^z > \ll S_i^+; S_j^- \gg_\omega - \sum_a J_{xy} < S^z > \ll S_{i+a}^+; S_j^- \gg_\omega . \end{aligned} \tag{5.8}$$

In **k** -space representation [57], this becomes

$$G(k, \omega) = \ll S_{\mathbf{k}}^+; S_{-\mathbf{k}}^- \gg = \frac{2 < S^z >}{\omega - 4 < S^z > \omega_{\mathbf{k}} - V}, \tag{5.9}$$

where

$$\omega_{\mathbf{k}} = J_z - \frac{J_{xy}}{4} \sum_a e^{i\mathbf{k}.\mathbf{a}} \quad \text{and} \quad V = v + \frac{\Delta v^2}{v}. \tag{5.10}$$

The correlation function $< \hat{S}_j^- \hat{S}_i^+ >$ was calculated using the spectral theorem (3.23)

$$< S_j^- S_i^+ >= \frac{1}{(2\pi)^3} \int_{-\pi}^{\pi} d\mathbf{k} e^{i\mathbf{k}.(\mathbf{R}_J - \mathbf{R}_i)} \int_{-\infty}^{\infty} d\omega \left( G_{\mathbf{k}}^R(\omega) - G_{\mathbf{k}}^A(\omega) \right) \frac{1}{e^{\frac{\omega}{T}} - 1}, \tag{5.11}$$

where $G_{\mathbf{k}}^R(\omega)$ and $G_{\mathbf{k}}^A(\omega)$ represent the retarded and advanced Greens functions. Their difference can be obtained using the Dirac identity (3.29)

$$G_{\mathbf{k}}^R(\omega) - G_{\mathbf{k}}^A(\omega) = -4\pi i < S^z > \delta(\omega - 4 < S^z > \omega_k - V). \tag{5.12}$$

Using (5.12) into (5.11) and integrating the right hand side with respect to $\omega$ gives

$$1 = \frac{< S^z >}{\pi} \int_0^{\pi} k dk \coth \left( \frac{4 < S^z > \omega_k + V}{2T} \right). \tag{5.13}$$

For this small $\mathbf{k}$ region, $\omega_k$ can be approximated as

$$\omega_k \simeq \frac{1}{4} J_{xy} k^2 + J_z - J_{xy} \tag{5.14}$$

and the excitation energy can be put as

$$\omega =< S^z > J_{xy} k^2 + 4 < S^z > (J_z - J_{xy}) + V. \tag{5.15}$$

The second and the third terms on the right-hand side of (5.15) represent the gap of spin wave excitation $\Delta$ at $\mathbf{k} = 0$

$$\Delta = 4 < S^z > (J_z - J_{xy}) + V, \tag{5.16}$$

which is caused by anisotropy and randomness. Two conditions must be satisfied in order that the ground state is superconducting. The first condition is that the gap of the spin wave excitation must be sufficiently small as compared to $T$ so that $\Delta = 4 < S^z > (J_z - J_{xy}) + V \ll T$, and the second condition is $J_{xy} \gg J_z$. The integration on the right-hand side of (5.13) was evaluated at low temperature using the above mentioned two conditions. The integration gives

$$< S^z >= \frac{V \left( e^{\frac{\pi J_{xy}}{T}} - 1 \right)}{\pi^2 J_{xy} - 4 \left( J_z - J_{xy} \right) \left( e^{\frac{\pi J_{xy}}{T}} - 1 \right)} \simeq \frac{V}{4 \left( e^{\frac{\pi J_{xy}}{T}} - 1 \right)}. \tag{5.17}$$

This last equation depicts that increasing the randomness in an on-site potential $V$ increases $< S^z >$ which in turn assists the localization of superconducting quasiparticles. This can be explained in our hard-core boson model as localization of bosons by randomness in island potential. The random potential fixes the Cooper pairs on the lattice sites and favors the transition from superconducting ground state to insulating ground state. It has to be noted here that the effect of disorder in this case is not pair breaking but pair localization.

The crystalization order $< S^z >$ and the superconducting order $< S^x >$ at $T = 0$ are related by the expression

$$< S^z >^2 + < S^x >^2 = \frac{1}{4}. \tag{5.18}$$

This relation corresponds to the assumption that the size of spin in our system is certainly 1/2 at $T = 0$. Due to rotation symmetry of spin in x-y plane, we can select the x-axis as the direction of superconducting order. Substituting (5.18) into (5.17) and rearranging gives the relation between superconducting order parameter and randomness $V$

$$< S^x >= \sqrt{(\frac{1}{2})^2 - (< S^z >)^2} \simeq \frac{1}{2}\sqrt{1 - \frac{V^2}{4(J_z - J_{xy})^2}}. \tag{5.19}$$

We introduced normalized variables such as strength of randomness, strength of two body interaction, and strength of the average chemical potential, respectively, as

$$\alpha \equiv \frac{\Delta v}{J_{xy}}, \quad \beta \equiv \frac{J_z}{J_{xy}}, \quad \gamma \equiv \frac{v}{J_{xy}}. \tag{5.20}$$

Substituting these variables into (5.19) gives

$$< S^x > \simeq \frac{1}{2}\sqrt{1 - \frac{(\gamma^2 + \alpha^2)^2}{4\gamma^2(1 - \beta)^2}}. \tag{5.21}$$

This last equation describes how superconducting order parameter $< S^x >$ depends on the strength of randomness in an on-site potential and strength of the two-body interaction.

Again, expanding (5.21) in the power of $\alpha$ gives

$$< S^x > \simeq \frac{1}{2}\sqrt{1-\frac{\gamma^2}{4(1-\beta)^2}}\left(1-\frac{\alpha^2}{4(1-\beta)^2\gamma^2}\right). \tag{5.22}$$

Setting $< S^x >= 0$ results

$$\alpha_c = \sqrt{2\gamma(1-\beta)-\gamma^2}. \tag{5.23}$$

Here, $\alpha_c$ represents the value of disorder strength at which the transition from superconducting state to insulating state takes place.

### 5.1.3 Results and Discussions

Discussions of the results for this subsection were made based on the plots generated numerically from equation (5.21) using MATHEMATICA. The plot in Figure 5.2 indicates the relationship between disorder strength and superconducting order parameter. As

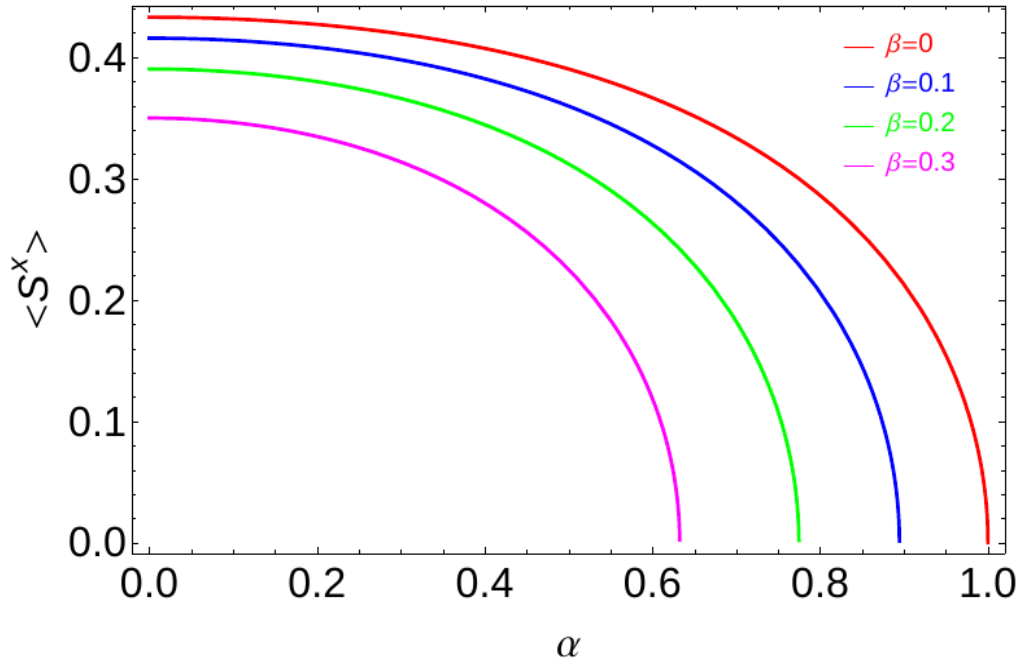


Figure 5.2: The behavior of superconducting order $< S^x >$ with increasing randomness $\alpha$.

it is clearly indicated, disorder supresses superconductivity and at some critical point the system entirely loses its superconductivity. At this critical value, Cooper pairs stop tunneling from one island to the other. Therefore, the system is regarded as an

insulator for $\alpha > \alpha_c$. This point divides the superconducting and insulating phases of the system. Moreover, the plot reveals that increasing the strength of repulsive interaction advances the transition. The most important part of this result is the possibility of tuning superconductivity simply by changing the size of the system. That is, increasing the size decreases rondomness in chemical potential, and in turn, increase conductivity of the system. Conversely, decreasing size of the system increases randomness in chemical potential by enhancing granularity and decreases conductivity of the system. This quantum size effect is experimentaly supported by the work of Goldman et al. [37].

The plot in Figure 5.3 shows the relationship between superconducting order parameter and the strength of two-body interaction. Two-body interaction, in this case, means the repulsive interaction between the Cooper pairs of neighbouring islands. The plot clearly shows that increasing the strength of repulsive interaction between Cooper pairs supresses superconductivity of the thin films. Therefore, the two-body interaction strength can also be regarded as a parameter of the phase transition.

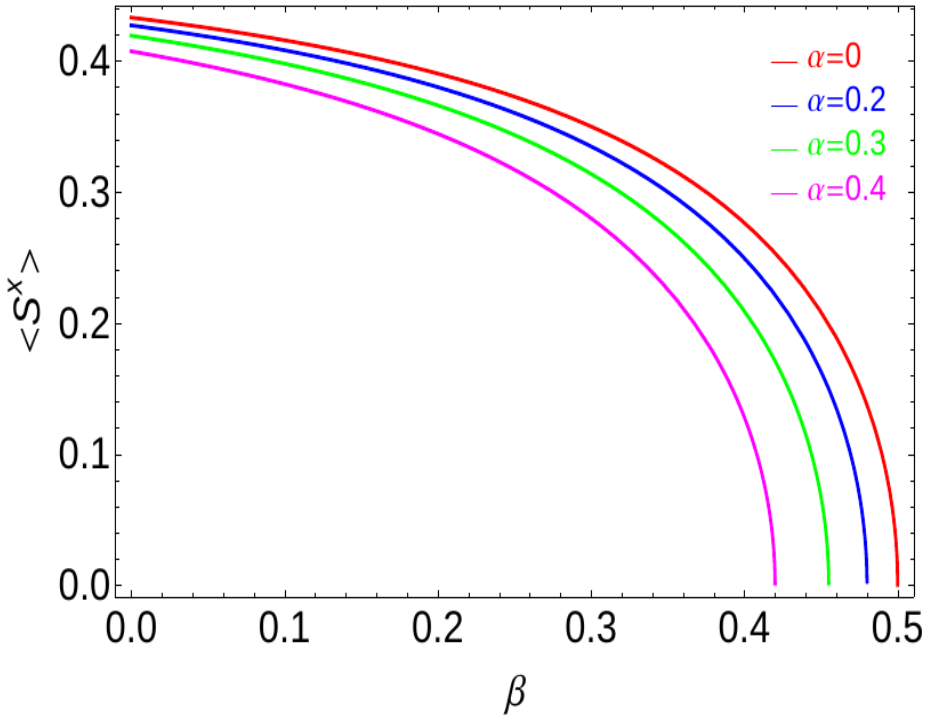


Figure 5.3: The behavior of superconducting order $< S^x >$ with increasing interaction strength $\beta$.

The graph in Figure 5.4 was plotted by setting the order parameter $< S^x >= 0$ in equation (5.21) and changing the values of both $\alpha$ and $\beta$. The plot indicates the point of zero superconducting order parameter. Hence, it can be considered as the a line separating the superconducting and insulating state of the system. Region to the left is superconducting and the region to the right is insulating. Therefore, the graph represents the phase diagram of the system in disorder-interaction plane.

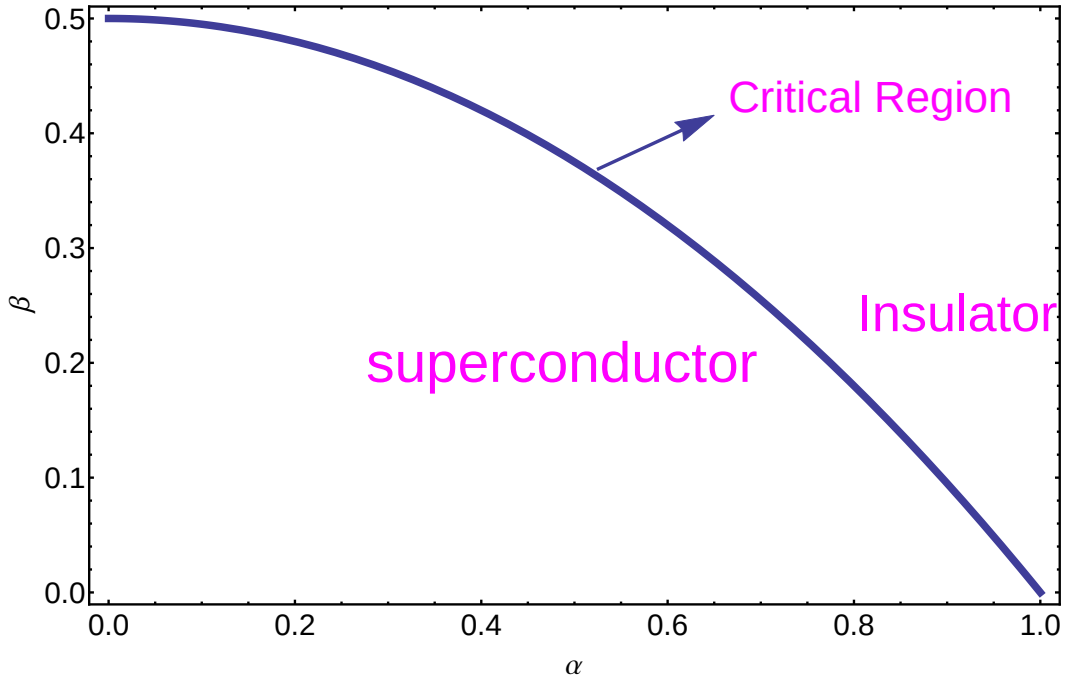


Figure 5.4: The phase diagram of SIT with respect to randomness $\alpha$ and two-body interaction $\beta$.

## 5.2 The phase fluctuation model

In this section, we study the effect of phase fluctuations on superconductivity of granular thin films employing the self-consistent harmonic approximation [9, 68]. In order to incorporate phase fluctuations on the order parameter, we have chosen the 2D Josephson Junction array model which defines phase variable of the order parameter with two dimensional planar degree of freedom at each lattice site with a Josephson type coupling between them (Figure 5.1-Right). This model describes the dynamics of the phase variable on a lattice.

### 5.2.1 Model Hamiltonian

The Hamiltonian for the 2D Josephson Junction arrays is given by [66,68]

$$H = \frac{U}{2}\sum_i n_i^2 - J\sum_{<ij>}\cos(\theta_i - \theta_j) = E_c + E_J. \tag{5.24}$$

Here $n_i$ is the number operator for Cooper pairs on the $i$-th grain and $U$ is the effective charging energy related to the inverse of the capacitance of the assembly of superconducting islands. The second term is the Josephson energy specified by the Josephson coupling strength $J$, with $\theta_i$ being the phase angle on the i-th grain. The charging energy $E_c$ favors insulating behaviour as it arises due to the fact that it costs energy to transfer a Cooper pair from one superconducting island to another. This term restricts hopping of Cooper pairs from one superconducting island to another by increasing fluctuation in the phase of the order parameter. The Josephson coupling energy, $E_J$, establishes a global phase coherence among the islands and thus gives rise to a superconducting ground state. This term plays a crucial role in establishing the phase ordering between various superconducting islands which emerge in the limit of large disorder. Thus, the phase variable continues to be a smoothly varying function with the phase difference between the superconducting islands being negligibly small.

Without loss of generality, the Hamiltonian (5.24) can be rewritten as

$$H_\theta = \frac{U}{2}\sum_i n_i^2 + J\sum_{<ij>}\Big(1 - \cos(\theta_i - \theta_j)\Big). \tag{5.25}$$

Here, a constant term has been added to the Josephson term just to follow the standard conventions of the quantum rotor model. Harmonic approximation (small-angle approximation) of the cosine term in (5.25) gives a trial Hamiltonian

$$H_{tr} = \frac{U}{2}\sum_i n_i^2 + \frac{K}{2}\sum_{<ij>}\Big(\theta_i - \theta_j\Big)^2 \tag{5.26}$$

where $K = D_s/4$. Here, $D_s$ represents a renormalized superfluid stiffness. The number

and phase are conjugate variables [68]

$$[n_j, \theta_j] = i\delta_{ij}, \quad n_i = -i\frac{\partial}{\partial\theta_i}. \tag{5.27}$$

Using this relation, the Hamiltonian (5.24) can also be rewritten in terms of the phase only variables as

$$H_\theta = -\frac{U}{2}\sum_i \left(\frac{\partial}{\partial\theta_i}\right)^2 - J\sum_{<ij>}\cos(\theta_i - \theta_j). \tag{5.28}$$

### 5.2.2 Calculations

The thermodynamics of a quantum mechanical system with Hamiltonian $H$ depends on the calculation of the quantum partition function

$$Z = Tr\left(e^{-\beta H}\right) \tag{5.29}$$

where $\beta = 1/T$ is the inverse temperature. The free energy of this quantum mechanical system is given in terms of the partition function as

$$F = -\frac{1}{\beta}\log Z. \tag{5.30}$$

All the thermodynamic quantities of interest can be calculated from the partion function. For example, any observable $A$ can be calculated as

$$< A >= \frac{1}{Z}Tr\left(Ae^{-\beta H}\right). \tag{5.31}$$

Therefore, the expectation value of $(H_\theta - H_{tr})$ in the trial basis is given by

$$< H_\theta - H_{tr} >=< J\sum_{<ij>}\left(1 - \cos(\theta_{ij})\right) - \frac{D_s}{8}\theta_{ij}^2 >_{tr} \tag{5.32}$$

where $\theta_{ij} = \theta_i - \theta_j$. According to Gibbs-Bogoliubov inequality, the relation between the free energies corresponding to $H_\theta$ and $H_{tr}$ is given by

$$F_\theta \leq F_{tr} + < H_\theta - H_{tr} > \tag{5.33}$$

where $F_{tr}$ is the free energy of the system described by the trial Hamiltonian defined in (5.26). With this relation, equation (5.32) becomes

$$< H_\theta - H_{tr} >= \sum_{<ij>} \left( J - J\, e^{-<\theta_{ij}^2>_{tr}/2} - \frac{D_s}{8} < \theta_{ij}^2 >_{tr} \right). \tag{5.34}$$

The stiffness constant $D_s$ can be obtained using a variational approach. Hence, one should determine $\partial F_{tr}/\partial D_s$ using the partition function

$$Z_{tr} = \int D\theta \exp\left(-S_{tr}[\theta]\right) \tag{5.35}$$

where the action, $S_{tr}[\theta]$, is defined as

$$S_{tr}[\theta] = \int_0^\beta d\tau H_{tr}[\theta] = \int_0^\beta d\tau \left( \frac{U}{2} \sum_i n_i^2 + \frac{D_s}{8} \sum_{ij} \theta_{ij}^2 \right). \tag{5.36}$$

Defining $n_i = (\hbar/2U)\partial\theta_i/\partial\tau$ and using equations (5.36) and (5.35) into equation (5.30) gives

$$F_{tr} = -\frac{1}{\beta} \ln \int D\theta \exp\left( - \int_0^\beta d\tau \left( \frac{1}{8U} \sum_i \left( \frac{\partial\theta_i}{\partial\tau} \right)^2 + \frac{D_s}{8} \sum_{ij} \theta_{ij}^2 \right) \right). \tag{5.37}$$

Taking derivative of this trial free energy with respect to $D_s$ results

$$\frac{\partial F_{tr}}{\partial D_s} = \frac{1}{8\beta} \int_0^\beta d\tau \sum_{<ij>} < \theta_{ij}^2 >_{tr} . \tag{5.38}$$

Equation (5.33) can also be rewritten as

$$F_\theta \leq F_{tr} + \frac{1}{\beta} < S_\theta - S_{tr} >_{tr} = F^* \tag{5.39}$$

where

$$\frac{1}{\beta} < S_\theta - S_{tr} >_{tr} = \frac{1}{\beta} \int_0^\beta d\tau \sum_{<ij>} \left( J - J\, e^{-<\theta_{ij}^2>_{tr}/2} \right) - \frac{D_s}{8} < \theta_{ij}^2 >_{tr} . \tag{5.40}$$

The free energy (5.39) can be minimized by considering the infinitesimal variation in $F^*$

$$\left(\frac{\partial F^*}{\partial D_s}\right)_{\langle\theta_{ij}^2\rangle_{tr}} + \left(\frac{\partial F^*}{\partial < \theta_{ij}^2 >_{tr}}\right)_{D_s} \left(\frac{\partial < \theta_{ij}^2 >_{tr}}{\partial D_s}\right) = 0. \tag{5.41}$$

The first partial derivative is

$$\left(\frac{\partial F^*}{\partial D_s}\right)_{<\theta_{ij}^2>_{tr}} = \frac{\partial F_{tr}}{\partial D_s} + \frac{1}{\beta}\left(\frac{\partial < S_\theta - S_{tr} >_{tr}}{\partial D_s}\right)_{<\theta_{ij}^2>_{tr}} = 0. \tag{5.42}$$

The first term of the second partial derivative is given by

$$\left(\frac{\partial F^*}{\partial < \theta_{ij}^2 >_{tr}}\right)_{D_s} = \frac{1}{\beta}\left(\frac{\partial < S_\theta - S_{tr} >_{tr}}{\partial < \theta_{ij}^2 >_{tr}}\right)_{D_s} = \frac{1}{2\beta}\int_0^\beta d\tau \sum_{<ij>}\left(Je^{-\frac{<\theta_{ij}^2>_{tr}}{2}} - \frac{D_s}{8}\right). \tag{5.43}$$

Inserting this into (5.41) and integrating finally gives

$$D_s = J\exp\left(-\frac{< \theta_{ij}^2 >_{tr}}{2}\right). \tag{5.44}$$

The detailed calculation of $< \theta_{ij}^2 >_{tr}$ is given Appendix C. Its bond averaged form is given by (C.23)

$$\langle\bar{\theta}_{ij}^2\rangle_{tr} \simeq 1.2\left(\frac{U}{D_s}\right)^{1/2} \tag{5.45}$$

Introducing this into (5.44) results

$$\kappa = \exp\left(-0.6\left(\frac{U}{J\kappa}\right)^{1/2}\right) \tag{5.46}$$

where $\kappa = D_s/J$ is known as the stiffness constant. Finally, defining a parameter $\alpha = 2U/J$, equation (5.46) can be rewritten as

$$\kappa = \exp\left(-0.85\left(\frac{\alpha}{\kappa}\right)^{1/2}\right). \tag{5.47}$$

### 5.2.3 Discussion of the result

In this section, the effect of inclusion of disorder induced phase fluctuations on superconductivity of very thin films has been investigated employing the JJA model. Discussion of the result obtained in this section was made based on the plot generated from equation (5.47) using MATHEMATICA. The plot in Figure 5.5 depicts the relationship between strength of disorder and superfluid stiffness (the energy cost of spatially twisting the phase of the condensate). As it has been clearly shown in the plot, increasing disorder strength suppresses the superflud stiffness of the superconductor. At some critical value of disorder, the Cooper pairs on the separate islands entirely loose their coherence and the system becomes an insulator. Here, increasing disorder reduces the pair size of the Cooper pairs and increases the insulating region between the islands. This, in turn, results in substantial rise in phase fluctuations of the order parameter and finally the Cooper pairs loose their phase coherence. This result is very important because it gives a clue to the source of pseudo gaps that appear in the immediate vicinity of the superconducting phase transtions of most high-Tc superconductors. The origin of pseudogap and its relationship with superconductivity has been the field of active research for more than two decades.

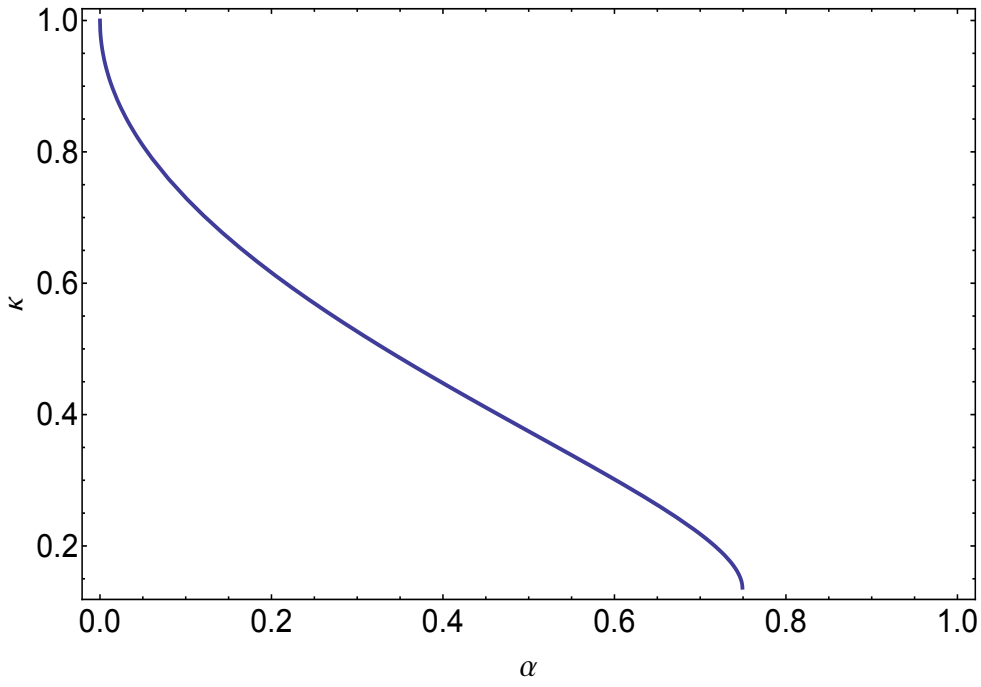


Figure 5.5: Supression of superfluid stiffness with disorder.

# 6

# First-principle Investigation of Superconductivity of Pb and $MgB_2$ Under Pressure

## 6.1 Introduction

Prediction of superconducting properties such as the critical temperature and the superconducting gap remains one of the outstanding challenges in contemporary condensed matter theory. Resulting from the complex nature of the superconducting state, a quantitative understanding of the pairing mechanism in superconductors requires a very detailed knowledge of the electronic structure, the phonon dispersions, the interaction between electrons and phonons, and the repulsive electron-electron interaction. Superconductors with strong electron-phonon coupling violate the universal BCS relation $2\Delta_0/T_c = 3.53$ of conventional superconductors. BCS theory [2,3] was derived based on the assumption of weak electron-phonon interaction and fail to explain the cases of strong coupling. Deviations from this universal relations contributed to the need to improve BCS theory and its underlying approximations.

In this chapter, we report the results of first-principle calculations made in order to investigate the effect of hydrostatic pressure on superconducting properties of lead (Pb) and magnesium diboride ($MgB_2$) by employing the Migdal–Eliashberg formalism. We have chosen Pb because it is a prototypical example of elemental superconductors with strong electron-phonon coupling. Moreover, we have chosen magnesium diboride to

address the issue of anisotropy in superconductors. Besides the issue of anisotropy, $MgB_2$ is a simple intermetallic compound with relatively higher $T_c$ and can be prepared easily. Due to these reasons, it has been opted as one of the most promising candidates for application in lossless electric power transmission and levitated train transportation.

The contents of the chapter are organized as follows. Section 6.2 presents the Migdal–Eliashberg formalism. Sections 6.3 and 6.4 present the first-principle calculations made on superconducting properties of Pb and $MgB_2$, respectively.

## 6.2 Migdal–Eliashberg formalism

A very accurate description of the superconducting state can be achieved using this formalism. It is a Greens function approach which extends the remit of BCS theory to describe the superconductivity of materials having strong electron-phonon coupling. Unlike the BCS theory which models a non-local instantaneous interaction, the Migdal–Eliashberg formalism is local in space and retarded in time to more properly reflect the time delay in the lattice overscreening. A key strength of this formulation is that only normal state properties enter, and these can be obtained via the first principles approaches to electron-phonon coupling.

The study of the superconducting properties of anisotropic superconductor $MgB_2$ using Migdal–Eliashberg formalism involves practical calculations of the following anisotropic expressions [69–71]

$$Z(\mathbf{k}, i\omega_n) = 1 + \frac{\pi T}{\omega_n} \sum_{\mathbf{k}', n'} W_{\mathbf{k}'} \frac{\omega_{n'}}{\sqrt{R(\mathbf{k}', i\omega_{n'})}} \lambda(\mathbf{k}, \mathbf{k}', n - n'), \tag{6.1}$$

$$Z(\mathbf{k}, i\omega_n)\Delta(\mathbf{k}, i\omega_n) = \pi T \sum_{\mathbf{k}', n'} W_{\mathbf{k}'} \frac{\Delta(\mathbf{k}', i\omega_{n'})}{\sqrt{R(\mathbf{k}', i\omega_{n'})}} [\lambda(\mathbf{k}, \mathbf{k}', n - n') - N_F V(\mathbf{k} - \mathbf{k}')], \tag{6.2}$$

where $R(\mathbf{k}, i\omega_n)$ and $W_{\mathbf{k}}$ are given by

$$R(\mathbf{k}, i\omega_n) = \omega_n^2 + \Delta^2(\mathbf{k}, i\omega_n) \quad \text{and} \quad W_{\mathbf{k}} = \delta(\epsilon_{\mathbf{k}})/N_F. \tag{6.3}$$

Here $N_F$ denotes the density of states per spin at the Fermi level, and $\lambda(\mathbf{k}, \mathbf{k}', n - n')$ is an

auxiliary function describing the anisotropic electron-phonon coupling and defined as

$$\lambda(\mathbf{k},\mathbf{k}',n-n') = \int_0^\infty d\omega \frac{2\omega}{(\omega_n-\omega_{n'})^2+\omega^2}\alpha^2F(\mathbf{k},\mathbf{k}',\omega). \tag{6.4}$$

The Eliashberg electron-phonon spectral function, $\alpha^2F(\mathbf{k},\mathbf{k}',\omega)$, is defined as

$$\alpha^2F(\mathbf{k},\mathbf{k}',\omega) = N_F\sum_\nu |g_{\mathbf{k}\mathbf{k}'\nu}|^2\delta(\omega-\omega_{\mathbf{k}-\mathbf{k}',\nu}). \tag{6.5}$$

Including the Coulomb interaction in the Eliashberg equations is typically dealt with by use of the Morel–Anderson [19,107] pseudopotential

$$\mu_c^* = \frac{\mu_c}{1+\mu_c\ln(\epsilon_F/\omega_c)}, \tag{6.6}$$

where $\mu_c$ is a dimensionless parameter describing the double Fermi surface average of the matrix element of the screened Coulomb interaction times the density of states at the Fermi level

$$\mu_c = N_F\langle\langle V(\mathbf{k}-\mathbf{k}')\rangle\rangle_{FS}. \tag{6.7}$$

In practice $\mu_c^*$ replaces the $N_FV(\mathbf{k}-\mathbf{k}')$ term in (2), and is set as a material dependent parameter. This dimensionless parameter is usually in the range of $0.05-0.2$.

The isotropic versions Eliashberg equations can be obtained by averaging $\mathbf{k}$ over the Fermi surface in (1) and (2). This results in the following isotropic expressions for the mass renormalisation and superconducting gap

$$Z(\mathbf{k},i\omega_n) = 1+\frac{\pi T}{\omega_n}\sum_{n'}\frac{\omega_{n'}}{\sqrt{(\omega_{n'})^2+\Delta(i\omega_n)}}\lambda(\omega_n-\omega_{n'}), \tag{6.8}$$

and

$$Z(i\omega_n)\Delta(i\omega_n) = \pi T\sum_{n'}\frac{\Delta(i\omega_{n'})}{\sqrt{(\omega_{n'})^2+\Delta^2(i\omega_{n'})}}\left(\lambda(\omega_n-\omega_{n'})-\mu_c^*\right) \tag{6.9}$$

where the isotropic electron-phonon coupling strength $\lambda(\omega_n)$ and the isotropic Eliashberg

spectral function $\alpha^2F(\omega)$ are, respectively, given by

$$\lambda(\omega_n) = \int_0^\infty d\omega \alpha^2F(\omega) \frac{2\omega}{\omega_n^2 + \omega^2}, \tag{6.10}$$

$$\alpha^2F(\omega) = \frac{1}{N_F} \sum_{nm\nu} \int \frac{d\mathbf{k}}{\Omega_{BZ}} \int \frac{d\mathbf{q}}{\Omega_{BZ}} |g_{mn\nu}(\mathbf{k}, \mathbf{q})|^2 \delta(\omega - \omega_{\mathbf{q}\nu}) \delta(\varepsilon_{n\mathbf{k}} - \varepsilon_F) \delta(\varepsilon_{m\mathbf{k}+\mathbf{q}} - \varepsilon_F). \tag{6.11}$$

The quasiparticle density of states in the superconducting state is

$$\frac{N_S(\omega)}{N_F} = R_e \left[ \frac{\omega}{\sqrt{\omega^2 - \Delta^2(\omega)}} \right]. \tag{6.12}$$

The superconducting critical temperature can be calculated using McMillan emperical formula

$$T_c = \frac{\theta_D}{1.45} \exp\left( -\frac{1.04(1+\lambda)}{\lambda - \mu_c^*(1 + 0.62\lambda)} \right) \tag{6.13}$$

where $\theta_D$ is the Debye temperature and the number $\lambda$ has the same meaning as the electron-phonon coupling parameter. Later, this formula was refined by Allen and Dynes [81], who substituted the factor $\theta_D/1.45$ with $\Omega_{\log}/1.2$, with the much more representative frequency

$$\Omega_{log} = exp\left[ \frac{2}{\lambda} \int d\Omega \log \Omega \frac{\alpha^2F(\Omega)}{\Omega} \right] \tag{6.14}$$

which is a weighted average of the phonon frequencies.

## 6.3 Superconductivity of Pb under pressure

### 6.3.1 Computational details

First principle (ab initio) calculations were carried out employing the plane wave pseudopotential method based on the basis of density functional theory as implemented in Quantum ESPRESSO [77] computational package. The local density approximation (LDA) basis of density functional theory was employed for the calculations of convergence tests and electronic properties. A norm conserving fully relativistic scalar pseudopotential where the $5d^{10}6s^26p^2$ electrons were regarded as valence electrons was used. Fully optimized plane wave energy cutoff of 60 Ry and a $9 \times 9 \times 9$ Γ-centered k-point mesh were

utlized in all the subsequent calculations. A Methfessel–Paxton (m-p) [78] Fermi-surface smearing of 0.05 Ry was employed in the BZ integration. Using these optimized parameters, structural optimization calculation was performed for the fcc Pb and an optimized lattice parameter of 9.270 bohr was obtained.

For the calculation of phonon matrix, density-functional perturbation theory was applied and the electron-phonon coupling was calculated using Fourier interpolation method. A $3 \times 3 \times 3$ $\Gamma$-centered q-point mesh was used. The superconducting transition temperature $T_c$, the electron-phonon coupling strength $\lambda$, the Eliashberg spectral function $\alpha^2F(\omega)$ and the logarithmic phonon frequency $< \omega >_{\log}$ were determined using the isotropic Eliashberg equations described in section 6.2.

### 6.3.2 Convergence tests

Most quantities that can be computed using DFT (total energy, equilibrium structure, band structures, density of states, vibrations, etc.) depend critically on the kinetic energy cutoff employed for the calculations. Therefore, one should always perform ecutwfc convergence test before running the calculations. The use of very small values of ecutwfc greatly affects the results of DFT calculations. Likewise, one should also avoid the use of very large values of ecutwfc. This is because of the fact that calculations with higher cutoff values are highly time consuming. Hence, a judicious choice of ecutwfc can save us from errors as well as computer run time problems. Based on these notions, a serious ecutwfc convergence test calculations were undertaken for bulk fcc Pb. The result obtained from these calculations was plotted and depicted in Figure 6.1. A 60 Ry ecutwfc value was chosen and employed in all the subsequent calculations.

As it has been clearly described in section 2.4, in DFT calculations all quanties are derived from electron density. This electron density, in principle, should be integrated over k-space in the first Brillouin zone owing to periodicity of the lattice, and it is continuous in this restricted reciprocal lattice space (1BZ). However, integration over continuous variables is impossible in numerical calculations. Therefore, a k-point grid shoud be constructed in order to sample the first BZ and hence facilitate the numirical calculations. Based on this fact, a thoughtful selection of k-point grid was made and the corresponding

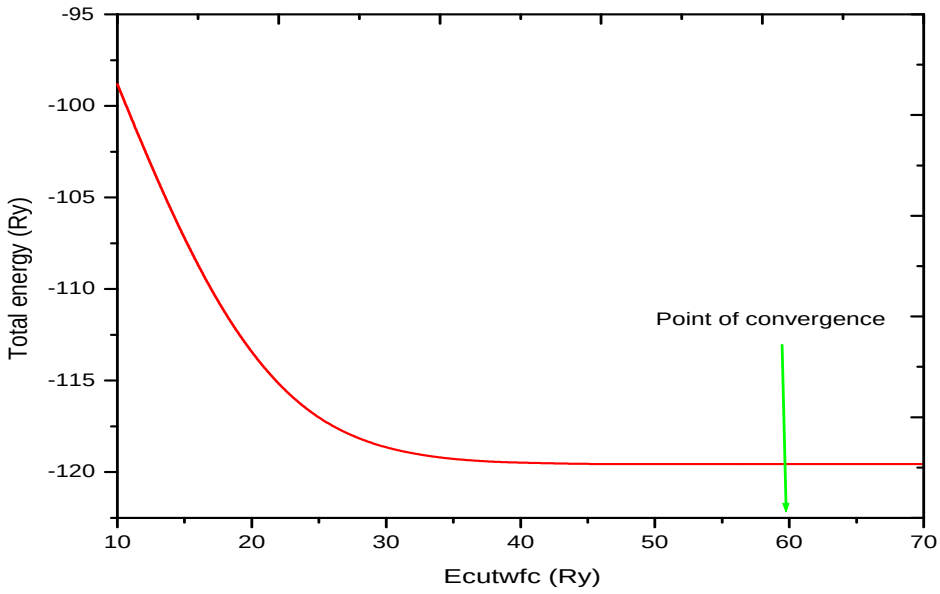


Figure 6.1: Ecutwfc convergence test

convergence test was performed. The result of the optimization calculations performed was plotted and shown in Figure 6.2. The plot clearly indicates that the optimized value of k-point grid is $9 \times 9 \times 9$. This result was used in all the subsequent calculations.

For bulk crystals, we often get information about the structure from X-Ray Diffraction (XRD) measurements. Accordingly, bulk Pb crystal belongs to face centered cubic (fcc) structure with the space group Fm3m[225]. This information simplifies drastically the calculation of the equilibrium structure. In order to achieve the equilibrium structure, one has to calculate the lattice parameter that minimizes the DFT total energy. The result of calculations performed for lattice parameter optimization was shown in Figure 6.3. As it has been clearly indicated in the plot, the lattice parameter that minimizes the DFT total energy is 9.270 bohr. This result agrees well both with experimental and theoretical values reported by P. Haas et al. (2009) [99]. The slight difference observed is attributed to different approximation schemes considered in our DFT calculations. This lattice parameter was used in all the subsequent calculations.

Figure 6.4 depicts the optimized structure of bulk fcc Pb for conventional unit cell.

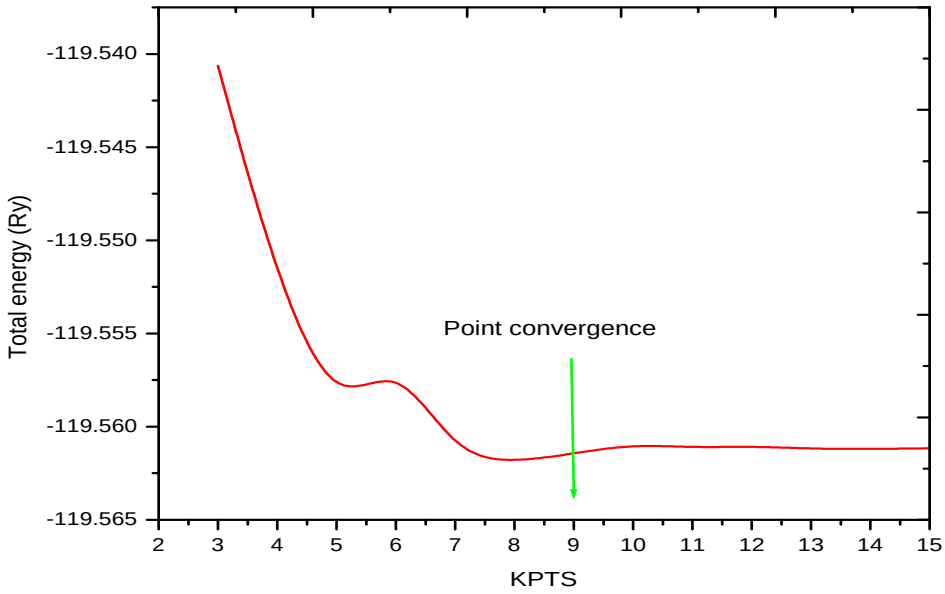


Figure 6.2: KPTS convergence test

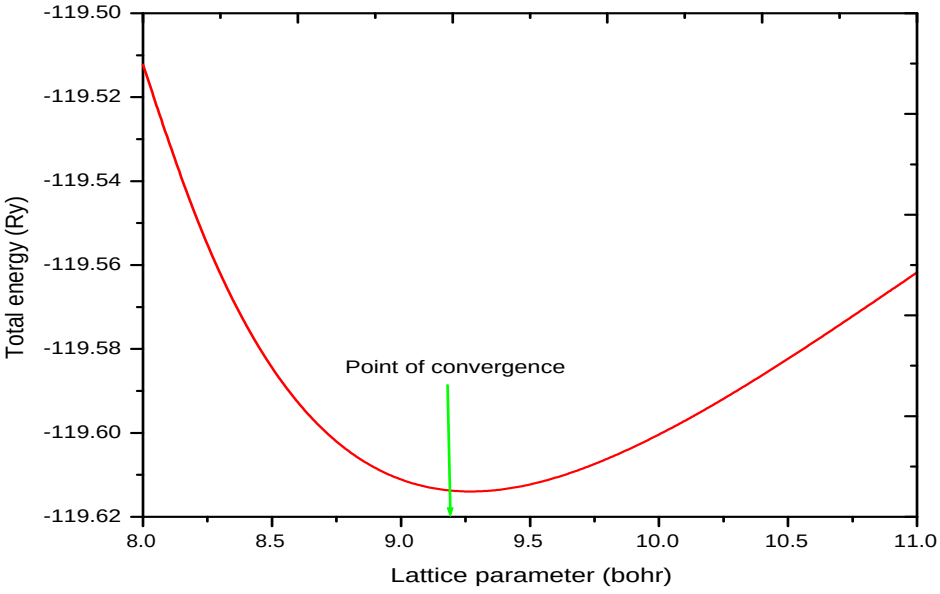


Figure 6.3: Lattice parameter convergence test

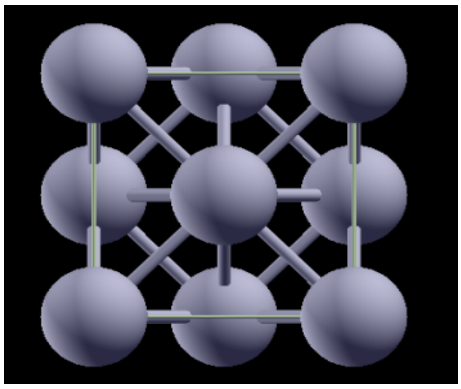

Figure 6.4: Conventional cubic unit cell of bulk fcc Pb

### 6.3.3 Results and discussions

In DFT calculations, pressure can be applied simply by varying the lattice constant of the system or by changing the position of atoms in the system. For this calculation, the first method was used as it is simple and straightforward. The lattice parameter was varied in steps of 0.5 bohr starting from the optimized value of 9.270 bohr at equilibrim. By doing so, the hydrostaic pressure on the system was increased from 0 at equilibrium to 3500 kbar at a lattice parameter of 7.0 bohr. The obtained result was plotted and depicted in Figure 6.5. As the plot clearly reveals, pressure and lattice parameter have inverse relationship. That is, decreasing the lattice parameter increases pressure exerted on the system and vicevera. In all of the subsequent calculations, application of pressure has been made through the change of lattice parameters.

The electronic and phonon densities of states were calculated at different values of pressure, and the obtained result was plotted in Figures 6.6 and 6.7. As it has been clearly indicated in the plots, pressure suppresses both electron and phonon density of states near the Fermi surface. This in turn has an effect on superconducting properties of the system which have direct relationship with both electronic and phonon DOS.

Eliashberg spectral function $\alpha^2F(\omega)$ was also calculated using the isotropic Eliashberg equation (**??**) and the obtained result was plotted in Figure 6.8. As the plot clearly indicates, increasing the value of pressure suppresses the Eliashberg spectral density. Suppression of Eliasberg density $\alpha^2F(\omega)$ in turn implies the supression of electron-phonon

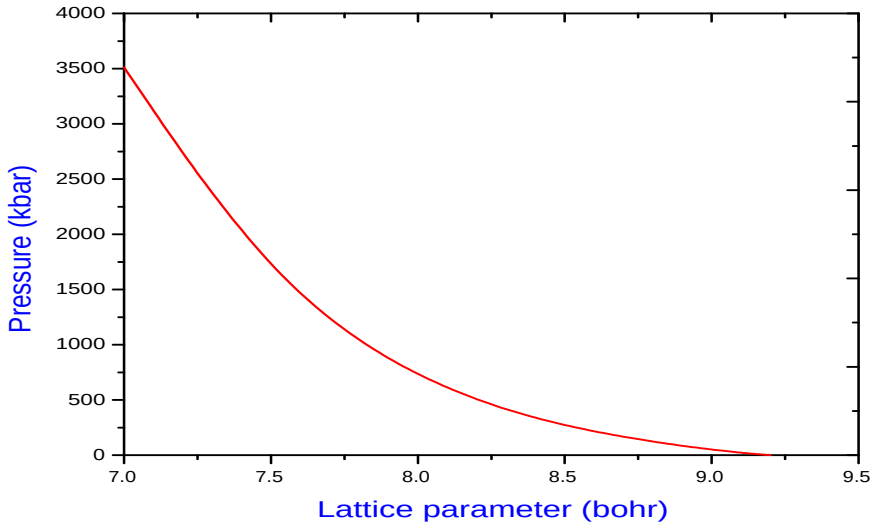


Figure 6.5: Pressure versus lattice parameter

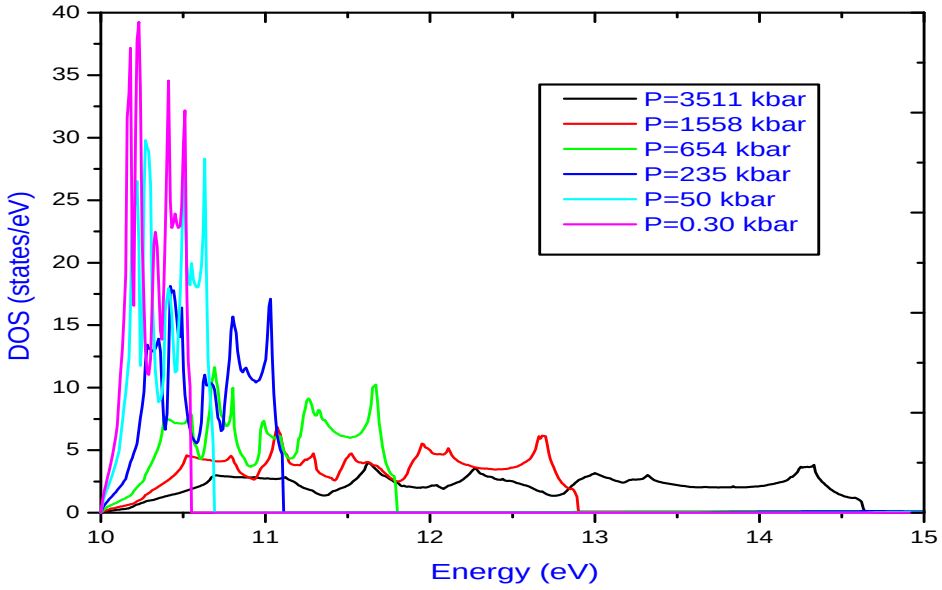


Figure 6.6: Suppression of electronic density of states by pressure

coupling strength $\lambda$ according to the isotropic Eliashberg equation (**??**). This also has an effect on the superconducting properties such as critical temperature and gap parameter, which are directly related to electron-phonon coupling strength $\lambda$. This supression of

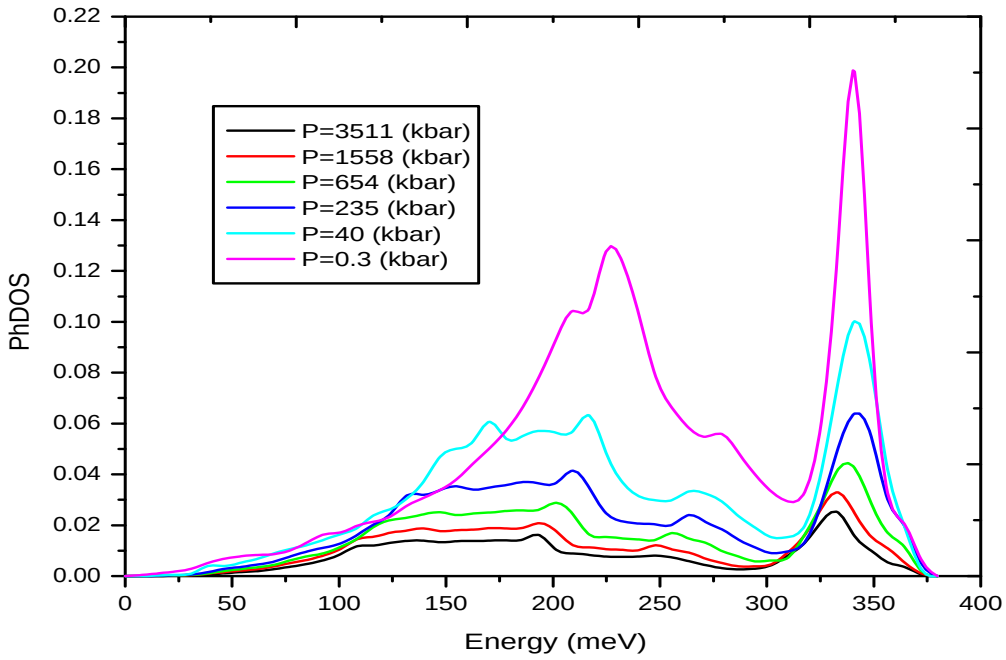


Figure 6.7: Suppression of phonon density by pressure

superconductivity of Pb under pressure was reported by theoretical works of P. Vashishta and P. Carbotte (1975) [79] and experimental work of P. Franck and J. Keeler (1968) [80]. As noted by R. C. Dynes [100], this suppression of Eliashberg spectral density is tied to the phase variation created due to change in lattice paramater and instablity of phonon modes around Fermi surface.

Superconducting critical temperature $T_c$ was computed using the McMillan formula given in equation (**??**). At equilibrium, where the pressure of the system is almost zero, the calculated $T_c$ value is 7.86 K. It is relatively nearer to the experimental value of 7.2 K. The slight overestimation of $T_c$ is attributed to the approximations used in DFT calculations. A series of $T_c$ calculations were performed at different values of pressure and the obtained result is plotted in Figure 6.9. The plot clearly reveals, pressure suppresses the critical temperature of bulk fcc Pb. This suppression of $T_c$ was also reported by works of J. P. Carbotte and P. Vashishta [79], Robert E. Hodder [101], and J. Bennett [102]. The suppression of $T_c$ observed is tied to suppression of $\lambda$ and the Eliashberg spectral function $\alpha^2F(\omega)$.

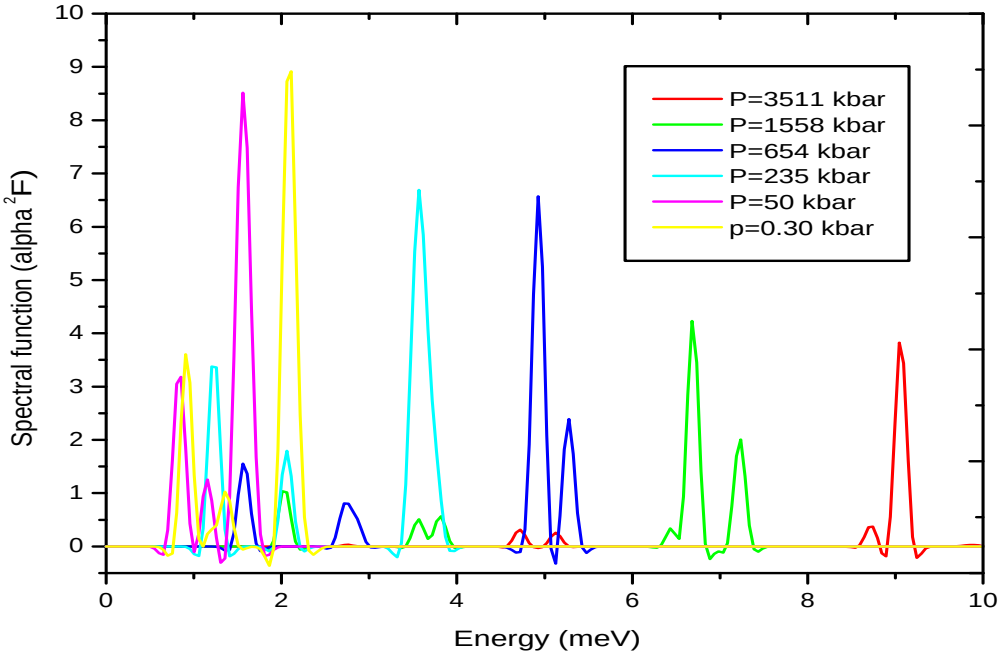


Figure 6.8: Suppression of spectral density by pressure

The plot in Figure 6.10 depicts the effect of pressure on electron-phonon coupling strength $\lambda$ of the system. This reduction of electron-phonon coupling strength was reported in the work of J. P. Franck and W. J. Keeler [80]. As they noted, the supression of $\lambda$ is tied to the reduction of electronic density of states around Fermi level $N(0)$ and increment of phonon frequency. Here, we note that this suppression of coupling strength has effect on superconducting properties of phonon mediated superconductors. Figure 6.11 shows the effect of pressure on phonon frequency of the system. As it has been clearly indicated, pressure enhances the logarithmic phonon frequency. The effect was also reported in the work of J. P. Franck and W. J. Keeler [80].

## 6.4 Superconductivity of $MgB_2$ under pressure

### 6.4.1 Computational details

First principle calculations were performed within the local density approximation to density functional theory. The valence electronic wave functions were expanded in plane

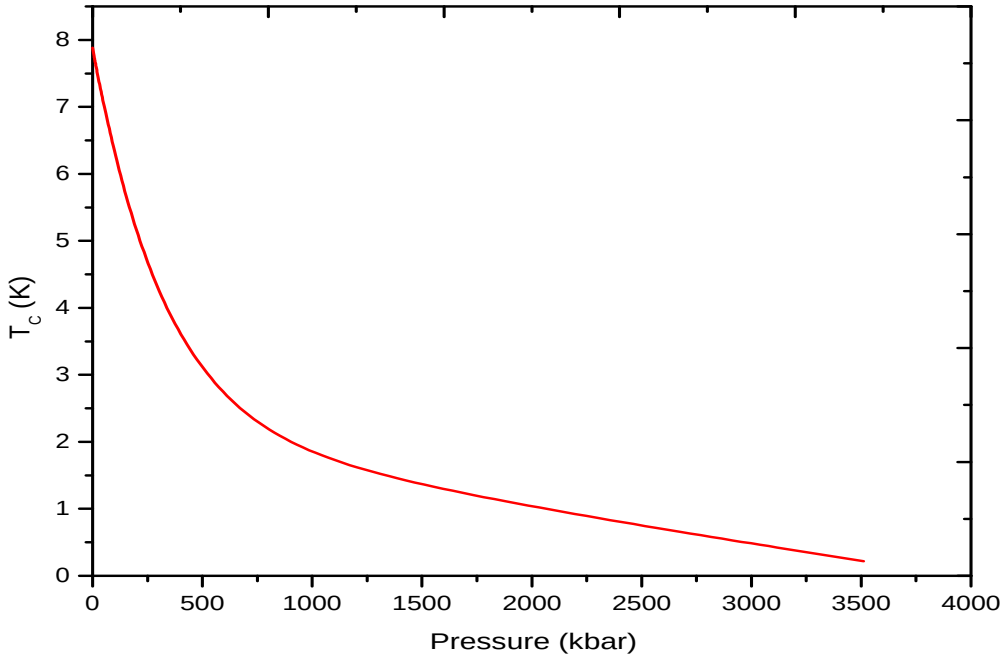


Figure 6.9: Suppression of critical temperature by pressure

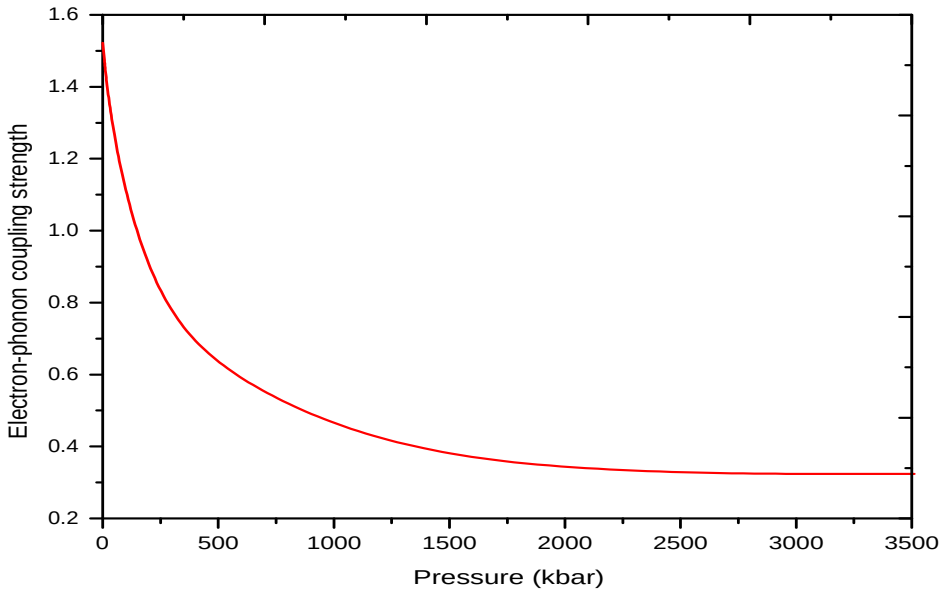


Figure 6.10: Supression of coupling constant by pressure

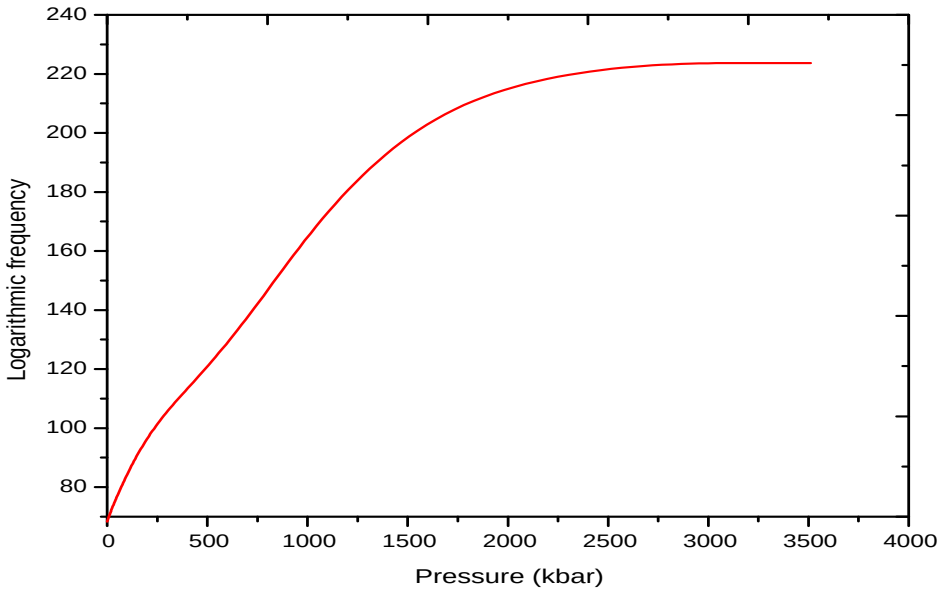


Figure 6.11: Enhancement of logarithmic phonon frequency by pressure

wave basis sets with optimized kinetic energy cutoff 60 Ry and the charge density was computed using a 6×6×6 Γ-centered k-point mesh. The core–valence interaction was taken into account by employing norm conserving pseudopotentials. A Methfessel–Paxton Fermi surface smearing of 0.02 Ry was employed in the BZ integration. An optimized lattice parameter of $a = 5.723$ bohr with $c/a = 1.142$ was used in all the calculations.

For the phonon calculations, the density functional perturbation theory was applied. For this calculation, a fully optimized $3 \times 3 \times 3$ Γ-centered q-point grid was utilized. Superconducting critical temperature ($T_c$), electron–phonon coupling strength ($\lambda$), Eliasberg spectral function ($\alpha^2F(\omega)$), phonon density of states (PhDOS) and superconducting gap ($\Delta$) were calculated based on the general formalis of Eliashberg theory described briefly in section 6.2. The calculculations were performed employing the Wannier–Fourier interpolation method as implemented in EPW software package fully integrated in Quantum ESPRESSO.

### 6.4.2 Calculation results for convergence tests

Optimization calculations were performed in order to obtain the converged values of the plane wave kinetic energy cutoff (ecutwfc), lattice parameter and k-point grid for hexagonal bulk $MgB_2$. The results of the respective calculations were ploted and depicted in Figures 6.12–6.15. The plot shown in Figure 6.12 clearly indicates that the optimized value of ecutwfc is 60 Ry. Figure 6.13 indicates that the optimized value of lattice parameter is $a = 5.723$ bohr for $c/a = 1.142$. Moreover, Figure 6.14 shows that the optimized value for k-point grid is $6 \times 6 \times 6$ and Figure 6.15, the equilibrium structure for a unit cell of hexagonal bulk $MgB_2$. These optimzed values were employed in all the calculations performed for $MgB_2$.

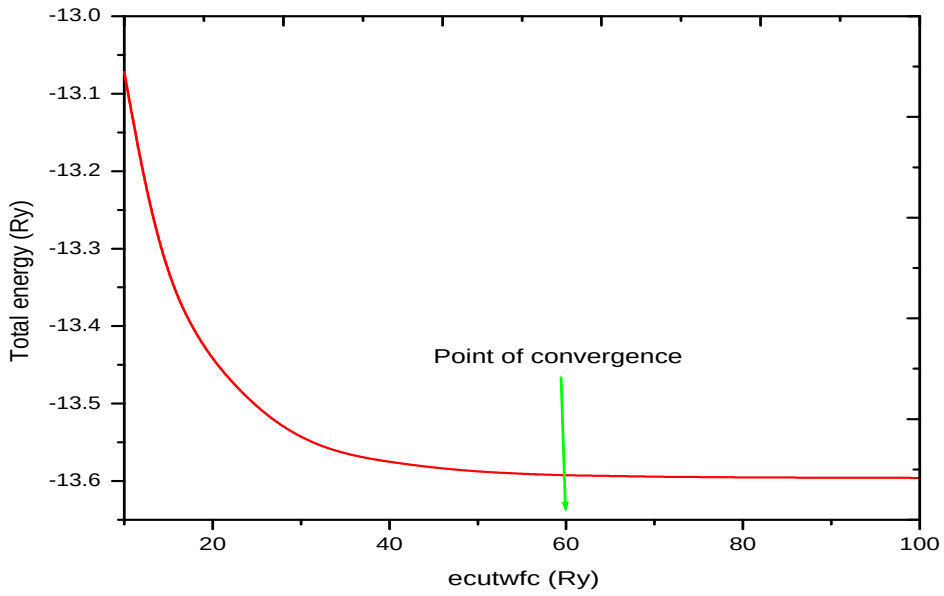


Figure 6.12: Ecutwfc convergence test

### 6.4.3 Results and discussions

Figures **??–??** depict the plots of the results obtained from the calculations performed in order to investigate the effects of pressure on superconductivity of $MgB_2$. The plot in Figure 6.16 shows the variation of hydrostatic pressure with change in lattice parameter of

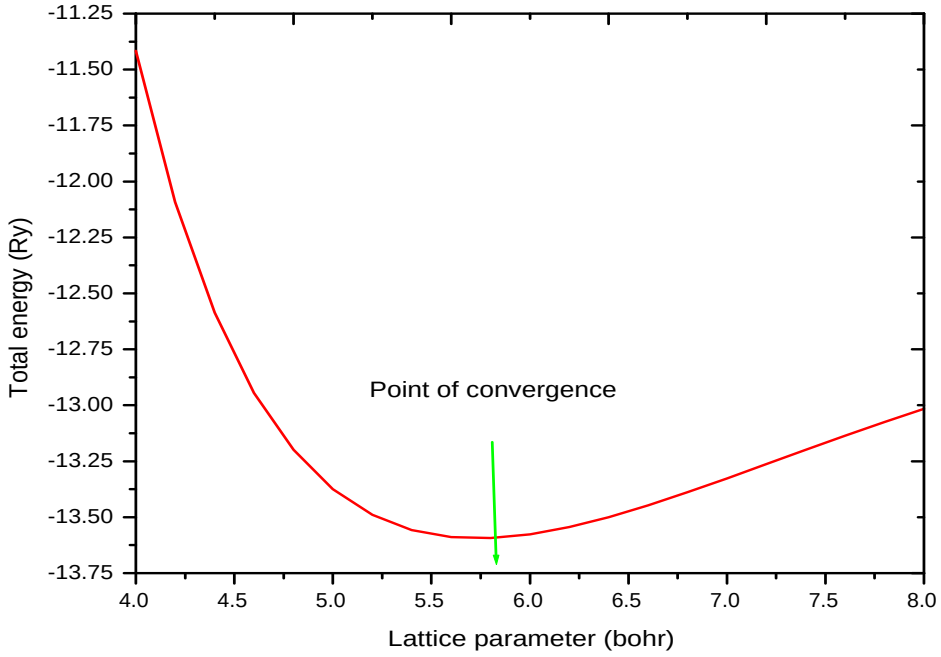


Figure 6.13: Lattice parameter convergence test

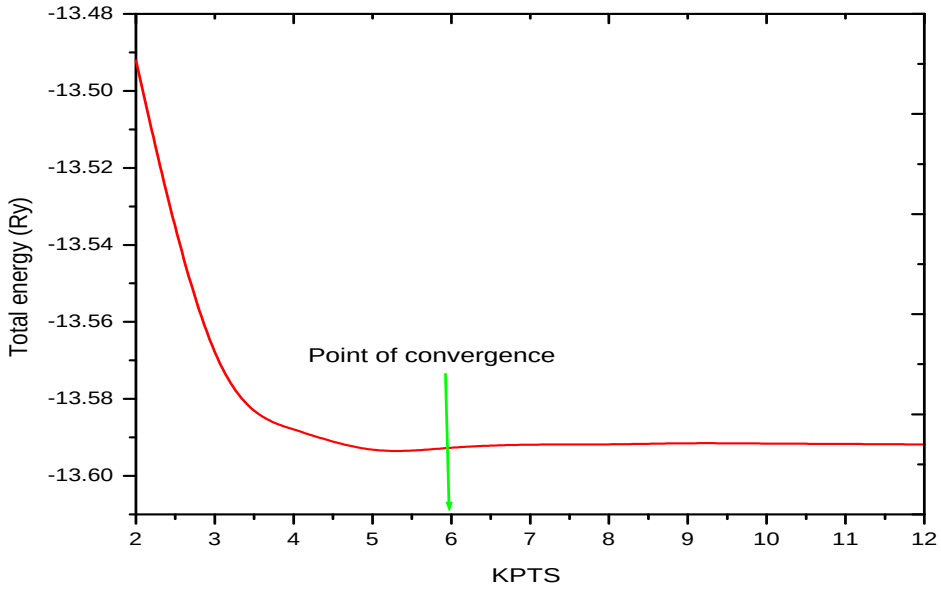


Figure 6.14: KPTS convergence test

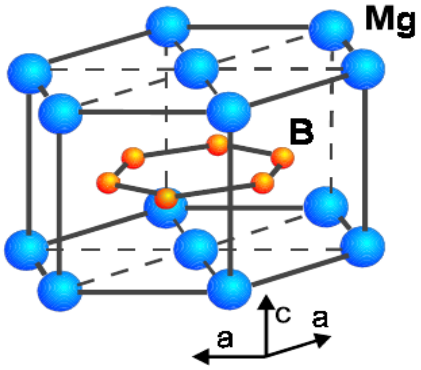


Figure 6.15: Hexagonal conventional unit cell of $MgB_2$

bulk hexagonal $MgB_2$. As it has been clearly indicated in the plot, small negative values of pressure were measured for lattice parameters set above the equilibrium structure ($a > 5.723$ bohr) and no significant variation in pressure is observed. However, for lattice parameters set below the equilibrium structure ($a \leq 5.723$ bohr), the pressure increases rapidly. This implies that the effect of pressure results from the contraction of the system's volume. The reduction in volume increases the hydrostatic pressure of the system. However, the expanding volume creates a negligible hydrostatic pressure. The plot in Figure 6.17 shows the relationship between hydrostatic pressure and electron–phonon coupling strength ($\lambda$). It indicates that pressure enhances the electron–phonon coupling and hence superconductivity.

The plots in Figures 6.18 and Figure 6.19 indicate the variation of phonon density of states and Eliashberg spectral density with pressure, respectively. As it has been clearly indicated, pressure enhances PhDOS and the Eliashberg spectral density of $MgB_2$ in sharp contrast to that of Pb. The plot in Figure 6.20 indicates the relationship between pressure and the critical temperature of bulk $MgB_2$. As it has been clearly indicated in the plot, increasing pressure enhances the critical temperature. Similar result was reported by Jin-Cheng Zheng and Yimei Zhu [105] for bulk $MgB_2$ under lattice strain. The calculated critical temperature is 36.7 K at equilibrium. This value is enhanced to around 95 K at hydrostatic pressure of 6500 kbar.

Figures 6.21 and 6.22 depict the effect of pressure on superconducting gap parameter. The plot in Figure 6.21 indicates the enhancement of superconducting gap parameter

measured along the imaginary frequency axis, while the plot in Figure 6.22 shows the enhancement of the order parameter measured along the real frequency axis. The order parameter was evaluated along the real frequency axis using the Pade approximation.

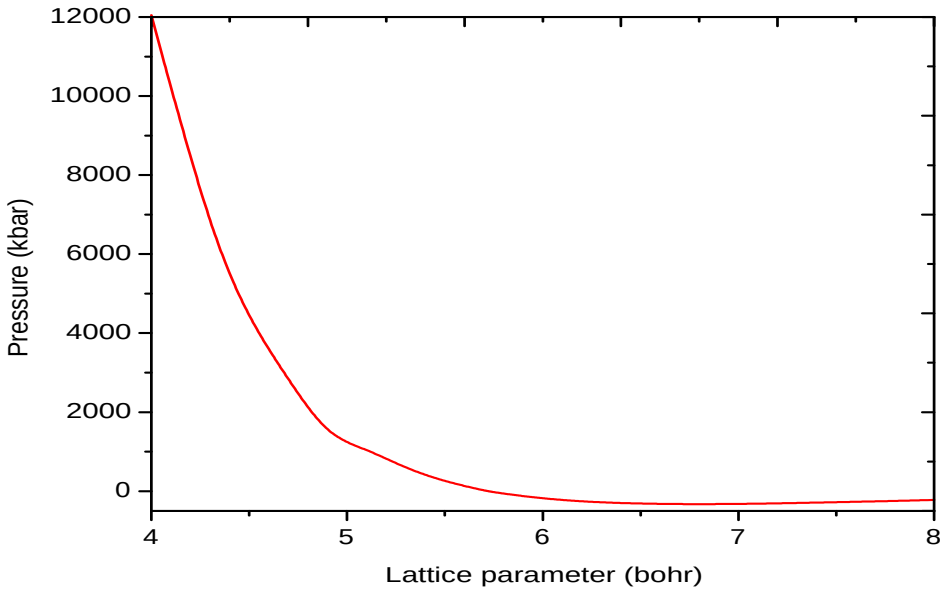


Figure 6.16: Pressure versus lattice parameter

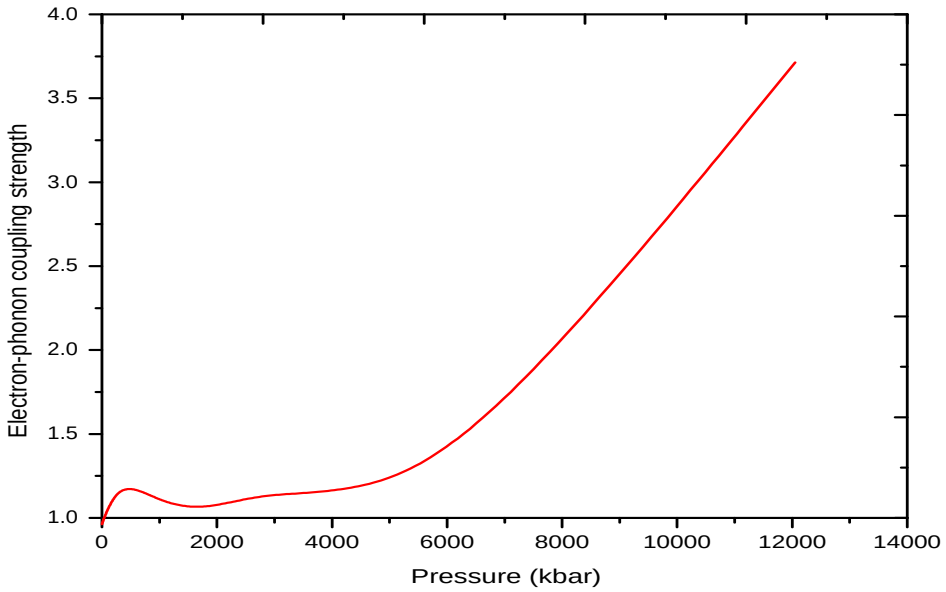


Figure 6.17: Enhancement of electron-phonon coupling constant by pressure

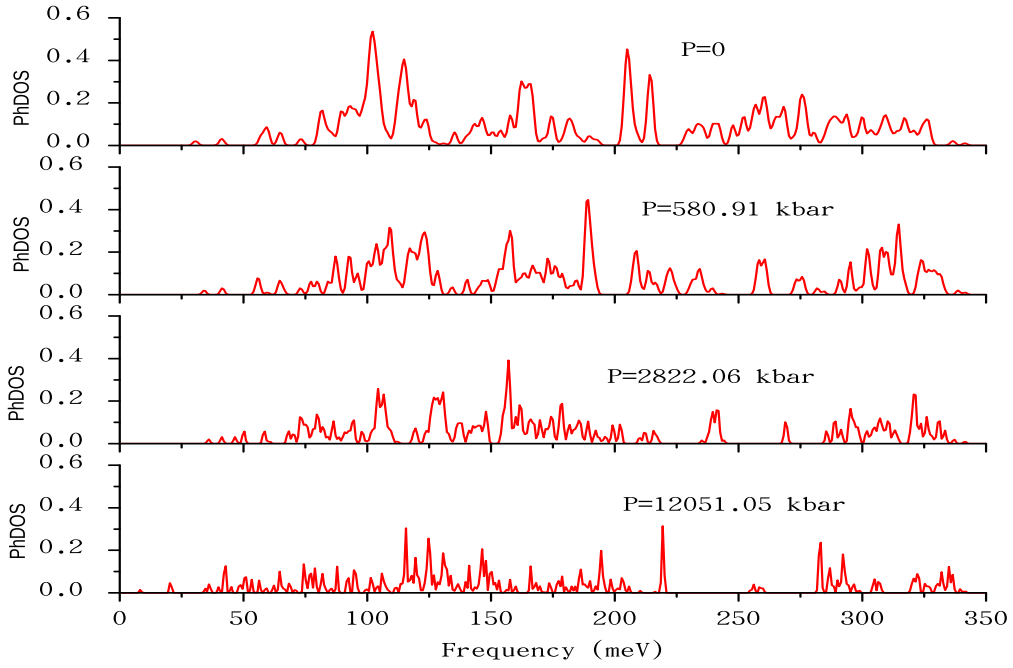


Figure 6.18: Supression of phonon density by pressure

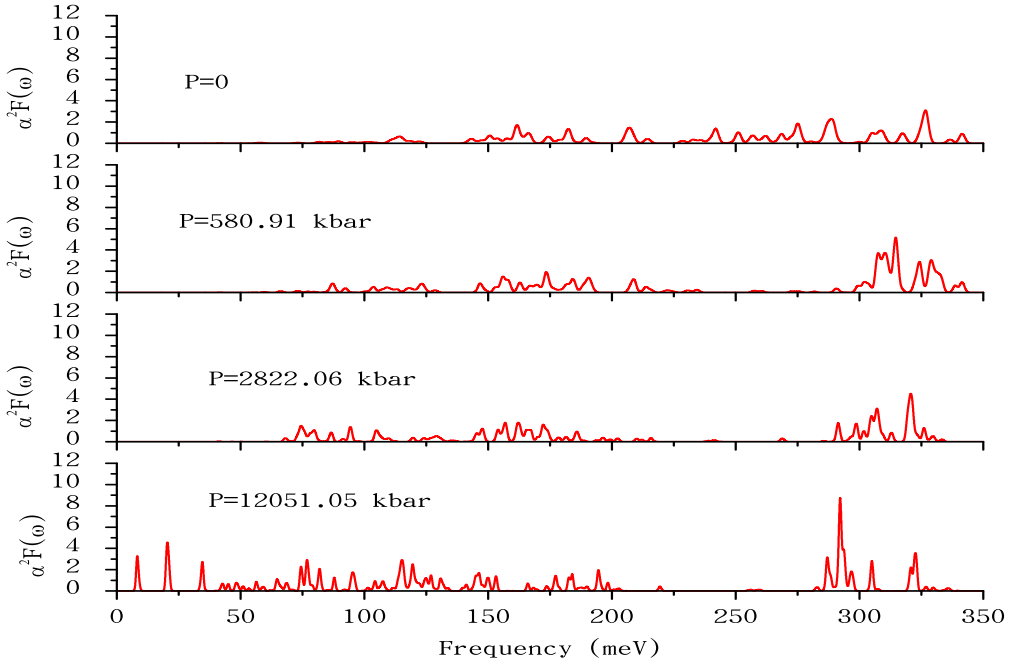


Figure 6.19: Enhancement of spectral function by pressure

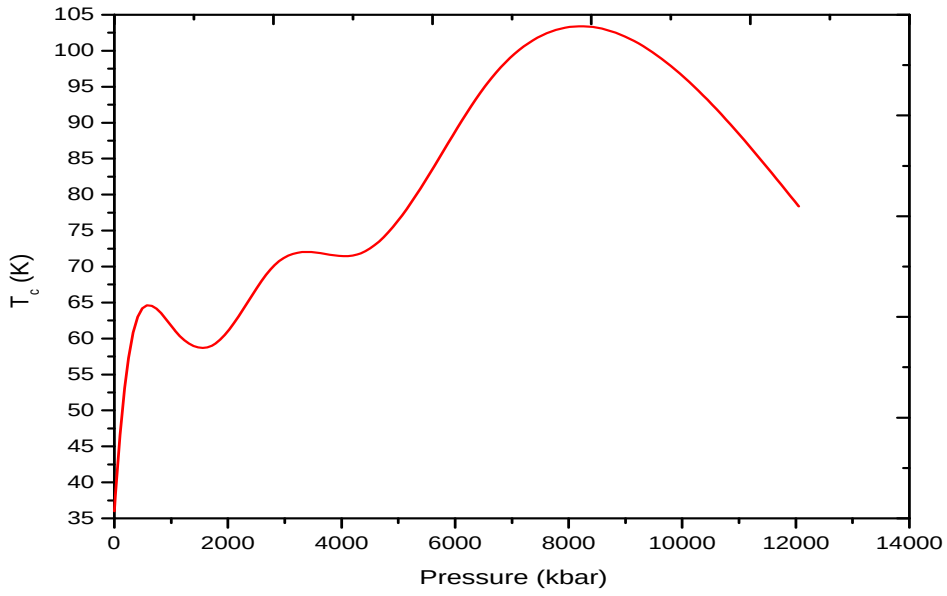


Figure 6.20: Enhancement of critical temperature of $MgB_2$ by pressure

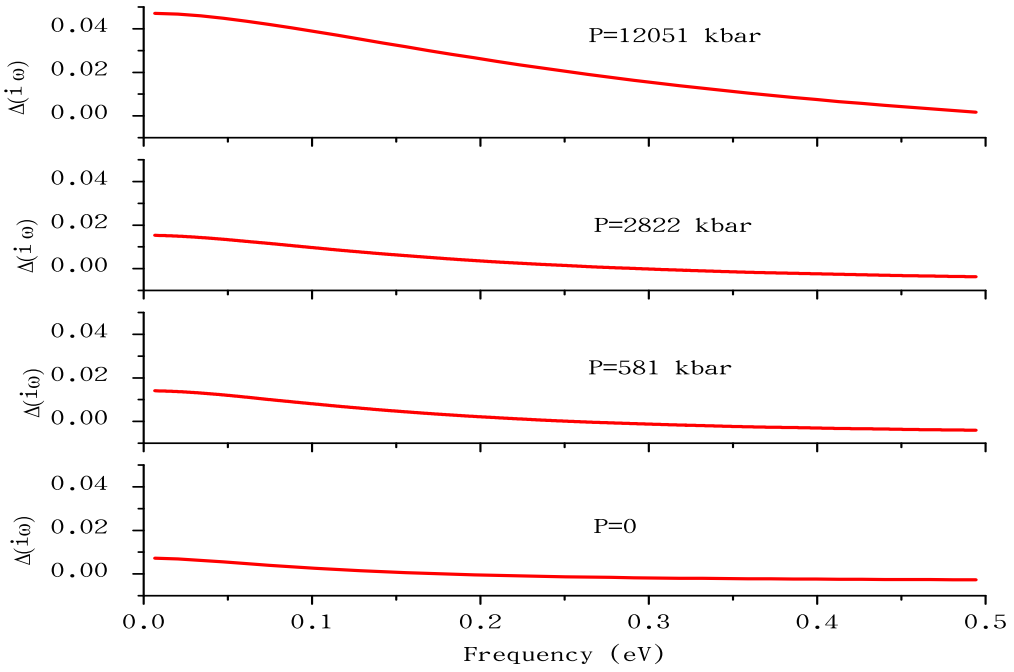


Figure 6.21: Enhancement of superconducting gap along imaginary energy axis by pressure

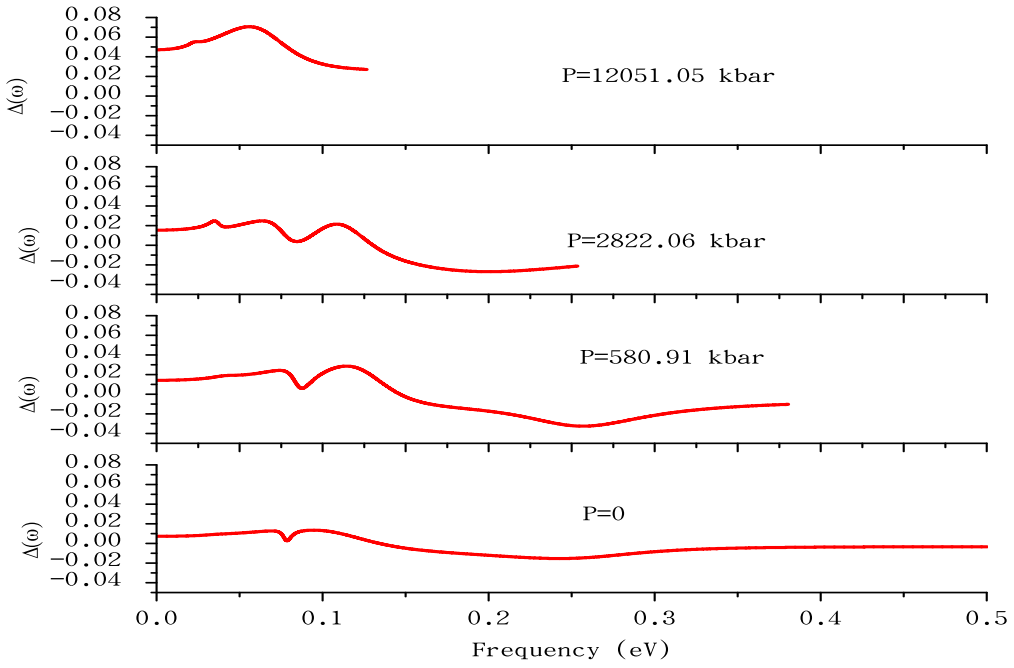


Figure 6.22: Enhancement of superconducting gap along real energy axis by pressure

# 7

# Summary, Conclusion and Future Outlook

## 7.1 Summary and conclusion

The effect of disorder due to impurity scattering on superconductivity of $Bi_2Sr_2CaCu_2O_{8+x}$ was investigated theoretically using the matrix Greens function method in Nambu formalism. The relationship between superconducting critical temperature and disorder parameters (strength of impurity potential, concentration of impurity scatterers, and strength of anisotropy) was derived analytically for both s-wave and d-wave pairing symmetries. The result obtained for s-wave pairing symmetry clearly reveals that diluted nonmagnetic disorder has no significant effect on the transition temperature of the superconductor. On the other hand, the anlytic expression derived for d-wave pairing symmetry indicates that diluted nonmagnetic disorder can significantly suppress transition temperature of the superconductor. The supression of $T_c$ depends on the strength of impurity potential, concentration of scattering centers and anisotropy of the pairing symmetry. This result is very important for the study of high-Tc superconductors because impurity dopping is always there.

The effect of disorder on superconductivity of a very thin granular superconducting films was also investigated theoretically based on the hard core boson model developed for superfluid helium. The relationship between superconductor order parameter and disorder parameters (strengths of disorder potential and two-body interaction) was derived analytically using the equation of motion method of double time retarded Greens function formalism. The obtained results clearly reveal that incrasing the strength of disorder due to randomnes in island potential and the strength of repulsive interaction

between Cooper pairs supresses superconducting order parameter of the thin film. Moreover, at some critical values of these disorder and interaction strengths the film entirely loses its superconductivity. Above this critical values the system is regarded as an insulator. These critical values divide the superconducting and insulating phases of the system. The most important result of this part is the possibility of tuning superconductivity of the system simply by varying the film size and the strength of repulsive interaction between Cooper pairs on different islands. This result is also very important in the study of strongly correlated electronic systems specifically in layered high-Tc cuprate superconductors.

The effect of pressure on superconductivity of Pb and $MgB_2$ was studied theoretically based on Eliashberg theory formulated for strongly coupled and anisotropic superconductors. The result obtaind for Pb clearly indicates that hydrostatic pressure supresses superconducting critical temperature ($T_c$) by decreasing the phonon density of states (PhDOS), Eliashberg spectral density ($\alpha^2F(\omega)$), electron-phonon coupling strength ($\lambda$). The superconducting critical temperature was supressed from 7.86 K at equilibrium where there is no pressure to almost 0 where the pressure is about 3500 kbar. In sharp contrast, the result obtained for $MgB_2$ (Figure 6.15–Figure 6.20) clearly indicates the enhancement of superconducting critical temperature. The superconducting critical temperature is enhanced from around 35 K calculated at equilibrium where the pressure is almost zero to around 95 K where the pressure is 6500 kbar. The results of this part are also very important because this approach to strain engineering, with the target of enhancing/suppressing $T_c$ as demonstrated in this work, can be applied to various strain-engineering problems.

## 7.2 Future outlook

Our prime objective, in this thesis, was investigatigating the effect of disorder on superconductivity of layered (2D) superconductors employing potential impurity solvers such as Dynamic Quantum Monte Carlo simulation. However, due to lack of skills and facilities, our investigations were limited to analytic calculations which were highly dependent on mean-field approximations. Hence, our future prospect is to investigate the interplay of superconductivity and disorder employing the more powerful mathematical

tools such as dynamical mean-field approximations and potential impurity solvers such as DQMC simulation. Moreover, due to lack of high power Computers and advanced computational skills, our DFT calculations were limited to superconductors of simple structures and bulk unit cells. Our future prospect with this regard is the investigation of superconducting properties of recently discovered and more complex high temperature superconductors using the powerful recently developed computational package, EPW. We have also a plan to extend these DFT calculations to other functional materials such as multiferoics, semiconductors, energy devices, etc.

# Bibliography


[1] H. Kamerlingh Onnes, Commun. Phys. Lab. Univ. Leiden **119b** (Feb. 1911), reprinted in Proc. K. Ned. Akad. Wet.**13**, 1107 (1911).

[2] J. Bardeen, L. N. Cooper, and J. R. Schrieffer, Phys. Rev., **106**: 162, (1957).

[3] J.Bardeen, L.N.Cooper, and J.R.Schrieffer, Phys.Rev.**108**, 1175 (1957).

[4] J G. Bednorz and K. A. Muller, Z. Phys. B **64**, 189, (1986).

[5] Y. Kamihara, T. Watanabe, M. Hirano, and H. Hosono: J. Am. Chem. Soc. **130**, 3296, (2008).

[6] A. Shalnikov, Nature, **142**, 74, 1938.

[7] P. W. Anderson, J. Phys. Chem. Solids, **11(1)**, 26-30, (1959).

[8] Abrikosov, A. A. and Gor'kov, L. P, Zh. Eksp. Teor. Fiz. **38**, 319 (1959).

[9] V. F. Gantmakher and V. T. Dolgopolov, Physics-Uspekhi, **53**(1), 1-49, (2010).

[10] V. Dobrosavljevic, N. Trivedi, and J. M. J. Valles, Conductor to Insulator Quantum Phase Transitions. OUP Oxford, (2012).

[11] E. Abrahams, P. W. Anderson, D. C. Licciardello, and T. V. Ramakrishnan, Phys. Rev. Lett., **42**, 673-676, (1979).

[12] J. Bekaert, Ab initio description of multicomponent superconductivity in bulk to atomically thin materials, PhD Thesis submitted to University of Antwerpen (2018).

[13] R. G. Sharma, Superconductivity: Basics and Applications to Magnets, Springer Series in Materials Science, 2015.

[14] W. Meissner, R. Ochsenfeld, Naturwissenschaften, **21**, 787, (1933).

[15] F. London and H. London, Proc. Roy. Soc., **A149**, 71, (1935).

[16] M. Tinkham, Introduction to Superconductivity, Dover Publications, 2004.

[17] A. B.Pippard, Proc. Roy. Soc., **A216**, 547, (1953).

[18] V.L. Ginzburg and L.D. Landau, Zh. Eksp. Teor. Fiz.,**20**, 1064, (1950).

[19] A.A. Abrikosov, Sov. Phys. JETP, **5**, 1174 (1957).

[20] E. A. Lynton, B. Serin, and M. Zucker. J. Phys. Chem. Solids, **3**, 165 (1957).

[21] B. T. Matthias, H. Suhl, E. Corenzwit. Phys. Rev. Lett., **1**, 92 (1958).

[22] D. C. Licciardello and D. J. Thouless, J. Phys. C., **8**, 4157, (1975).

[23] P. Lee, "Theory of solids 2." lecture notes available at http://ocw.mit.edu, Massachusetts Instituite of Technology, (2009).

[24] J. X. Zhu, Bogoliubov-de Gennes Method and Its Applications. Springer, (2016).

[25] J. Kwo, T. P. Orlando and M. R. Beasley, Phys. Rev. B **24**, 2506 (1981).

[26] M. Chand, G. Saraswat, A. Kamlapure, M. Mondal, S. Kumar, J. Jesudasan, V. C. Bagwe, L. Benfatto, V. Tripathi and P. Raychaudhuri, Phys. Rev. B, **85**, 014508 (2012).

[27] A. F. Ioffe and A. R. Regel, Noncrystalline, amorphous and liquid electronic semiconductors, Prog. Semicond., **4**, 237, (1960).

[28] Y. H. Lin, J. Nelson, and A. M. Goldman, Physica C Superconductivity, **514**, 130-141, (2015).

[29] Finkelstein, JETP Lett., **45**: 46 (1987).

[30] Matthew P. A. Fisher, Peter B. Weichman, G. Grinstein, and Daniel S. Fisher, Phys. Rev. B, **40**, 546-570, (1989).

[31] Matthew P.A. Fisher, Physical Review Letters, **65**(7), 923, (1990).

[32] A. Ghosal, M. Randeria, and N. Trivedi, Phys. Rev. Lett., **81**, 3940, (1998).

[33] R. T. Scalettar, N. Trivedi and C. Huscroft, (2008).

[34] Haviland, D.B., Liu, Y., and Goldman, A.M., Phys. Rev. Lett., **62**, 2180, (1989).

[35] Imry, Y. and Strongin, M., Phys. Rev. B, **24**, 6353-6360, (1981).

[36] M. Strongin, R. S. Thompson, O. F. Kammerer and J. E. Crow, Phys. Rev. B **1**, 1078, (1970).

[37] A. M. Goldman and N. Markovic, Physics Today, **39**, (1998).

[38] Valles, J.M., Dynes, R.C., and Garno, J.P., Phys. Rev. Lett., **69**, 3567, (1992).

[39] Lin, Y.H. and Goldman, A.M., Phys. Rev. B , **82**, 214511, (2010).

[40] Nguyen, H.Q., Hollen, S.M., Stewart, M.D., Shainline, J., Yin, Aijun, Xu, J.M., and Valles, J.M., Phys. Rev. Lett., **103**, 157001, (2009).

[41] Sacepe, B., Chapelier, C., Baturina, T.I., Vinokur, V.M., Baklanov, M.R., and Sanquer, M., Nat. Comms., **1**, 140, (2010).

[42] Sacepe, B., Chapelier, C., Baturina, T.I., Vinokur, V.M., Baklanov, M.R., and Sanquer, M., Phys. Rev. Lett., **101**, 157006, (2008).

[43] Shahar, D. and Ovadyahu, Z., Phys. Rev. B , **46**, 10917-10922, (1992).

[44] Mondal, M., Kamlapure, A., Chand, M., Saraswat, G., Kumar, S., Jesudasan, J., Benfatto, L., Tripathi, V., and Raychaudhuri, P., Phys. Rev. Lett., **106**, 047001, (2011).

[45] Sacepe, B., Dubouchet, T., Chapelier, C., Sanquer, M., Ovadia, M., Shahar, D., Feigelâ€man, M., and Ioffe, L., Nat. Phys., **7**, 239-244, (2011).

[46] M. Springborg, Methods of electronic structure calculations, John Wiley & Sons, 2000.

[47] R. M. Martin, Electronic Structure: Basic Theory and Practical Methods, Cambridge University Press, 2008.

[48] J. Kohanoff, Electronic structure calculations for solids and molecules: Theory and computational methods, Cambridge University Press, 2006.

[49] D. Sholl and J. A. Steckel, Density functional theory: a practical introduction, John Wiley & Sons, 2009.

[50] F. Giustino, Materials Modelling Using Density Functional Theory: Properties and Predictions, Oxford University Press, 2014.

[51] P. Hohenberg and W. Kohn, Phys. Rev. **136**, 864 (1964).

[52] W. Kohn and L. J. Sham, Phys. Rev. **140**, 1133 (1965).

[53] A. D. Becke, J. Chem. Phys. **98**, 1372 (1992).

[54] J. Heyd, G. E. Scuseria, and M. Ernzerhof, J. Chem. Phys. **118**, 8207 (2003).

[55] G. Kresse and J. FurthmÃ¼ller, Phys. Rev. B **54**, 11169 (1996).

[56] H. J. Monkhorst and J. D. Pack, Phy. Rev. B **13**, 5188 (1976).

[57] W. Nolting, Fundamentals of Many-body Physics: *Principles and Methods*. Springer, (2009).

[58] L.P. Gorkov, Sov. Phys. JETP, **7**, **505**, (1958).

[59] Y. Nambu, Phys. Rev., **117**, 648-663, (1960).

[60] P.B. Allen, B. Mitrovi, Solid State Phys., **37**, 1-92, (1983).

[61] R. A. Klemm, C. T. Rieck, and K. Scharnberg, Phys. Rev. B, **61**, 5913–5916, (2000).

[62] H. Bruus and K. Flensberg, Many-body quantum theory in condensed matter physics. Niels Bohr Institute Press, 2002.

[63] J. B. Ketterson and S.N. Song, Superconductivity. Cambridge University Press, (1999).

[64] J. J. Sakurai and San Fu Tuan.Modern quantum mechanics. Benjamin/Cummings, 1985.

[65] P. Arberg, J.P. Carbotte, Phys. Rev. B **50**, 3250, (1994)

[66] Bouadim, K., Loh, Y.L., Randeria, M., and Trivedi, N., Nat Phys., **7**, 884, ISSN 1745-2481, (2011).

[67] T. Matsubara and H. Matsuda, Prog, Theor. Phys. 16, (1956)

[68] J.-X. Zhu, Inhomogeneous Superconductors: *Granular and Quantum Effects*. Oxford University Press, (1994).

[69] A. Migdal, Sov. Phys. JETP, **34** 996 (1958).

[70] G. Eliashberg, Sov. Phys. JETP, **11**, 696, (1960).

[71] G. Eliashberg, Sov. Phys. JETP, **12**, 1000, (1961).

[72] D. J. Scalapino, J. R. Schrieffer, and J. W. Wilkins, Phys. Rev., **148**, 263, (1966).

[73] P.B. Allen, Phys. Rev. B, **18**, 5217-5224, (1978).

[74] F. Marsiglio, J.P. Carbotte, Superconductivity, Springer, (2008).

[75] A. Linscheid, A. Sanna, F. Essenberger, E.K.U. Gross, Phys. Rev. B, **92**, 024505 (2015).

[76] W.L. McMillan, Phys. Rev. **167**, 331-344, (1968).

[77] P. Giannozzi, S. Baroni, N. Bonini, M. Calandra, R. Car, C. Cavazzoni, D. Ceresoli, G.L. Chiarotti, M. Cococcioni, I. Dabo, A.D. Corso, S. de Gironcoli, S. Fabris, G. Fratesi, R. Gebauer, U. Gerstmann, C. Gougoussis, A. Kokalj, M. Lazzeri, L. Martin-Samos, N. Marzari, F. Mauri, R. Mazzarello, S. Paolini, A. Pasquarello, L. Paulatto, C. Sbraccia, S. Scandolo, G. Sclauzero, A.P. Seitsonen, A. Smogunov, P. Umari, R.M. Wentzcovitch, J. Phys. Condens. Matter **21** (39) (2009) 395502.

[78] M. Methfessel and A. T. Paxton, Phys. Rev. B **40**, 3616 (1989)

[79] P. Vashishta and J. P. Carbotte, J. Low Temp. Phys. **18**, 516 (1975).

[80] FRANCK, J. P. and KEELER, W. J., Phys. Rev. Lett. **20**, 379 (1968).

[81] P.B. Allen, R.C. Dynes, Phys. Rev. B, **12**, 905-922, (1975).

[82] Yonatan Dubi, Yigal Meir, and Yshai Avishai, Nature, **449(18)**, 876 (2007).

[83] Yen L. Loh and N. Trivedi. Theoretical Studies of Superconductor-Insulator Transitions, Columbs, Oxford University, 43210, (2013).

[84] Steiner, M. and Kapitulnik, A., Physica C, **422**, 16, (2005).

[85] Girdhar, A. The superconductor-insulator transition in resistivity-shunted Josephson-junction arrays. Urbana, University of Illinois, 2010.

[86] C. Marrache-Kikuchi. Dimensionality effects in disordered superconductors in the vicinity of the Superconductor-Insulator Transition. Paris University, Paris-XI,2014.

[87] W. E. Pickett, Phys. Rev. B, **26**, 1186, (1982).

[88] P. Morel and P. W. Anderson, Phys. Rev. B 125, 1263 (1962).

[89] A. F. Hebard and M. A. Paalanen, Phys. Rev. Lett., **65**, 927, (1990).

[90] Loh, Y.L. and Trivedi, N., Phys. Rev. Lett., **104**, 165302, (2010).

[91] J.P. Perdew, A. Zunger, Phys. Rev. B 23 (1981) 5048–5079.

[92] N. Troullier, J.L. Martins, Phys. Rev. B 43 (1991) 1993–2006.

[93] J. Bardeen and M. Stephen. Physical Review **136**, A1485 (1964).

[94] M. V. Sadovskii, Superconductivity and Localization , Physics Reports **282** , 225 (1997).

[95] S. Ponce, E.R. Margine, C. Verdi, F. Giustino, Computer Physics Communications, **209**, 116–133, (2016).

[96] R. A. Klemm, C. T. Rieck, and K. Scharnberg, Phys. Rev. B, **61**, 5913–5916, (2000).

[97] J. E. Hirsch, Physics Letters A **282**, 392 (2001).

[98] J. E. Hirsch and F. Marsiglio, Phys. Rev. B **64**, 144523 (2001).

[99] P. Haas, F. Tran, and P. Blaha, PhysicalL Review B 79, 085104 (2009).

[100] R. C. Dynes, Phys. Rev. B **2**, 644 (1970)

[101] Robert E. Hodder, Phys. Rev. **180**, 530 1969.

[102] Alan J. Bennett, Phys. Rev. **140**, A1902 1965.

[103] V.L. Ginzburg, E.A. Andryushin. Superconductivity, World Scientific, (2004).

[104] Thomas, L. H., Proc. Camb. Phil. Soc. **23**, 542–548 (1927).

[105] Jin-Cheng Zheng, Yimei Zhu. PHYSICAL REVIEW B **73**, 024509 (2006)

[106] D. N. Zubarev, Sov. Phys. Usp., **3**, 320 (1960).

[107] Mesfin Asfaw, Suprconductivity and Magnetism in Iron Based Superconducturs, PhD Thesis submitted to Addis Ababa University (2016).

# Appendix A

## A.1 Avereges of impurity potential

We consider nonmagnetic impurities from which electrons can scatter elastically. In such kinds of impurity scattring, energy is conserved but momentum is not conserved. The impurity potential due to the interaction between electrons and the scattering centers (typically short-ranged) is defined by

$$V(\mathbf{r}) = \sum_i u(\mathbf{r} - \mathbf{R}_i) \tag{1}$$

where $u(\mathbf{r} - \mathbf{R}_i)$ is the potential of individual impurities and $R_i$ denotes impurity position. The sum runs over all the impurities. In momentum basis it can be put as

$$V(\mathbf{r}) = \sum_i \frac{1}{\Omega} \sum_{\mathbf{p}} e^{i\mathbf{p}.(\mathbf{r}-\mathbf{R}_i)} u(\mathbf{p}) \tag{2}$$

where $\Omega$ denotes volume of the system.

The pertubative Hamiltonian due to the impurity potental (1), in the first quantization notation, is given by

$$H' = \sum_\sigma \int d\mathbf{r} \psi^\dagger_\sigma(\mathbf{r}) \psi_\sigma(\mathbf{r}) V(\mathbf{r}) \tag{3}$$

where $\psi^\dagger_\sigma(\mathbf{r})$ and $\psi_\sigma(\mathbf{r})$ are the usual fermionic creation and annihilation operators. In the basis of plane waves they are expressed as

$$\psi_\sigma(\mathbf{r}) = \frac{1}{\sqrt{\Omega}} \sum_{\mathbf{k}} e^{i\mathbf{k}.\mathbf{r}} c_{\mathbf{k}\sigma}, \quad \psi^\dagger_\sigma(\mathbf{r}) = \frac{1}{\sqrt{\Omega}} \sum_{\mathbf{k}} e^{-i\mathbf{k}.\mathbf{r}} c^\dagger_{\mathbf{k}\sigma}. \tag{4}$$

Upon using (2) and (4) into (3), we can put $H'$ in momentum representation as

$$H' = \sum_{\sigma} \int d\mathbf{r} \left( \frac{1}{\Omega} \sum_{\mathbf{k}\mathbf{k}'} e^{-i(\mathbf{k}'-\mathbf{k}).\mathbf{r}} c^{\dagger}_{\mathbf{k}'\sigma} c_{\mathbf{k}\sigma} \right) \left( \sum_{i} \frac{1}{\Omega} \sum_{\mathbf{p}} e^{i\mathbf{p}.(\mathbf{r}-\mathbf{R}_i)} u(\mathbf{p}) \right)$$
$$= \sum_{\sigma} \sum_{\mathbf{k}\mathbf{p}} \frac{1}{\Omega} \sum_{i} e^{-i\mathbf{p}.\mathbf{R}_i} u(\mathbf{p}) c^{\dagger}_{\mathbf{k}+\mathbf{p},\sigma} c_{\mathbf{k}\sigma}. \tag{5}$$

An electron diffusing through the system visits many different regions, in each of which the microscopic placement of impurity positions is different. Hence, in such self-averaging systems, it is possible to model impurity averaging by constructing an ensemble of systems that differ only in the placement of their impurity positions and then perform an ensemble average over all the impurity positions. Ensemble average of any function $f(\mathbf{R}_i)$ which depends on the impurity positions is given by

$$\langle f(\mathbf{R}_i) \rangle_{\text{imp}} = \frac{1}{\Omega} \int d\mathbf{R}_i f(\mathbf{R}_i). \tag{6}$$

The ensemble average of the impurity potential (1) is given by

$$\langle V(\mathbf{r}) \rangle_{imp} = \sum_{i} \frac{1}{\Omega} \sum_{\mathbf{p}} \langle e^{i\mathbf{p}.(\mathbf{r}-\mathbf{R}_i)} \rangle_{\text{imp}} u(\mathbf{p}) = n_i u_0. \tag{7}$$

Therefore the ensemble average of the impurity Hamiltonian is

$$\langle H'(\mathbf{r}) \rangle_{\text{imp}} = \sum_{\mathbf{k}\sigma} n_i u_0 c^{\dagger}_{\mathbf{k}\sigma} c_{\mathbf{k}\sigma}. \tag{8}$$

This can be absorbed into $\xi_{\mathbf{k}}$ by constant shift of chemical potential ($\mu \rightarrow \mu - n_i u_0$). Momentum is conserved after impurity averaging so that

$$\langle V(\mathbf{r}) \rangle_{\text{imp}} = n_i u_0 \equiv 0, \tag{9}$$

without loss of generality.

The second order impurity average $\langle V(\mathbf{r}_1)V(\mathbf{r}_2)\rangle_{\text{imp}}$ is

$$\begin{aligned}
\langle V(\mathbf{r}_1)V(\mathbf{r}_2)\rangle_{\text{imp}} &= \sum_{i_1 i_2}\langle u(\mathbf{r}_1-\mathbf{R}_{i1})u(\mathbf{r}_2-\mathbf{R}_{i2}) \\
&= \sum_{i_1\neq i_2}\langle u(\mathbf{r}_1-\mathbf{R}_{i_1})\rangle_{\text{imp}}\langle u(\mathbf{r}_2-\mathbf{R}_{i_2})\rangle_{\text{imp}} + \sum_{i_1}\langle u(\mathbf{r}_1-\mathbf{R}_i)u(\mathbf{r}_2-\mathbf{R}_i)\rangle_{\text{imp}} \\
&= \sum_{i_1}\langle u(\mathbf{r}_1-\mathbf{R}_i)u(\mathbf{r}_2-\mathbf{R}_i)\rangle_{\text{imp}} \\
&= \sum_i \frac{1}{\Omega}\int d\mathbf{R}_i u(\mathbf{r}_1-\mathbf{R}_i)u(\mathbf{r}_2-\mathbf{R}_i) \\
&= N_{\text{imp}}\frac{1}{\Omega}\sum_{\mathbf{p}_1\mathbf{p}_2} u(\mathbf{p}_1 u(\mathbf{p}_2))e^{i(\mathbf{p}_1.\mathbf{r}_1+\mathbf{p}_2.\mathbf{r}_2)}\frac{1}{\Omega}\int d\mathbf{R}_i e^{-i(\mathbf{p}_1+\mathbf{p}_2).\mathbf{R}_i} \\
&= n_i\frac{1}{\Omega}\sum_{\mathbf{p}_1} e^{i\mathbf{p}_1.(\mathbf{r}_1-\mathbf{r}_2)}|u(\mathbf{p}_1)|^2
\end{aligned} \tag{10}$$

Therefore, impurity averaging restores translational invariance:

$$\begin{aligned}
\langle H'H'\rangle_{\text{imp}} &= \sum_{\sigma_1\sigma_2}\int d\mathbf{r}_1\int d\mathbf{r}_2\left(\psi^\dagger_{\sigma_1}(\mathbf{r}_1)\psi_{\sigma_1}(\mathbf{r}_1)\right)\left(\psi^\dagger_{\sigma_2}(\mathbf{r}_2)\psi_{\sigma_2}(\mathbf{r}_2)\right) \\
&\quad\times\left(N_{\text{imp}}\langle u(\mathbf{r}_1-\mathbf{R})u(\mathbf{r}_2-\mathbf{R})\rangle_{\mathbf{R}}\right) \\
&= \sum_{\mathbf{k}_1\sigma_1}\sum_{\mathbf{k}_2\sigma_2}\sum_{\mathbf{p}} n_i|u(\mathbf{p})|^2 c^\dagger_{\mathbf{k}_1+\mathbf{p},\sigma_1}c_{\mathbf{k}_1,\sigma_1}c^\dagger_{\mathbf{k}_1-\mathbf{p},\sigma_1}c_{\mathbf{k}_1,\sigma_1}.
\end{aligned} \tag{11}$$

That is, total momentum of the system is conserved. Total momentum flow out of the system is zero. In general, it is reasonable to ignore the impurity averaging terms containing $n_i^m$ with $m \geq 2$ for weak disorder.

## A.2 Averaging the Green's function

In this section, we will determine the configuratioally averaged Green's function by averaging $G(\mathbf{k},\mathbf{k}')$ over all possible impurity configurations. Here we assumed that the locations of the various impurities are independent of each other so that the probability distributions for the impurity configuration is simply a product of probability distributions for the location of individual impurities, which will be taken as a uniform in space. Therefore, the impurity average simply consists of averaging the positions of the N impurities over all space. Denoting the impurity averaged Green's function by $\langle G(\mathbf{k},\mathbf{k}')\rangle$

thus we have,

$$\langle G(\mathbf{k},\mathbf{k}')\rangle = \prod_{i=1}^{N}\left(\frac{1}{\Omega}\int d^2\mathbf{R}_i\right) G(\mathbf{k}-\mathbf{k}'). \tag{12}$$

Being simply an integral over all impurity coordinates, the impurity average is clearly a linear operation, and can therefore be carried out for each term in the perturbation series separately (i.e. the average of the sum is the sum of the averages), giving

$$\langle G(\mathbf{k},\mathbf{k}')\rangle = \sum_{n=0}^{\infty}\langle G^{(n)}(\mathbf{k},\mathbf{k}')\rangle. \tag{13}$$

The only factors in the series expansion (13) which depend on the impurity positions are the function $\rho(\mathbf{k})$. Thus to find the impurity averaged Green's function we need to calculate the quantity $\langle\rho(\mathbf{k}-\mathbf{k}_1)\rho(\mathbf{k}_1-\mathbf{k}_2)\cdots\rho(\mathbf{k}_{n-1}-\mathbf{k}')\rangle$.

For $n = 1$:

$$\begin{aligned}
\langle\rho(\mathbf{k}-\mathbf{k}')\rangle_{\text{imp}} &= \prod_{i=1}^{N}\left(\frac{1}{\Omega}\int d\mathbf{R}_i\right)\rho(\mathbf{k}-\mathbf{k}') \\
&= \prod_{i=1}^{N}\left(\frac{1}{\Omega}\int d\mathbf{R}_i\right)\sum_{j=1}^{N} e^{-i(\mathbf{k}-\mathbf{k}').\mathbf{R}_j} \\
&= \sum_{j=1}^{N}\frac{1}{\Omega}\int d\mathbf{R}_j e^{i(\mathbf{k}-\mathbf{k}').\mathbf{R}_j}\prod_{i=1}^{N}\left(\frac{1}{\Omega}\int d\mathbf{R}_i\right) \\
&= \sum_{j=1}^{N}\frac{1}{\Omega}\int d\mathbf{R}_j e^{-i(\mathbf{k}-\mathbf{k}').\mathbf{R}_j} \\
&= N\delta_{\mathbf{k}\mathbf{k}'}.
\end{aligned} \tag{14}$$

For $n = 2$:

$$\begin{aligned}
\langle\rho(\mathbf{k}-\mathbf{k}_1)\rho(\mathbf{k}_1-\mathbf{k}')\rangle_{\text{imp}} &= \prod_{i=1}^{N}\left(\frac{1}{\Omega}\int d\mathbf{R}_i\right)\rho(\mathbf{k}-\mathbf{k}_1)\rho(\mathbf{k}_1-\mathbf{k}') \\
&= \prod_{i=1}^{N}\left(\frac{1}{\Omega}\int d\mathbf{R}_i\right)\sum_{j_1=1}^{N} e^{-i(\mathbf{k}-\mathbf{k}_1).\mathbf{R}_{j_1}}\sum_{j_2}^{N} e^{-i(\mathbf{k}_1-\mathbf{k}').\mathbf{R}_{j_2}} \\
&= \sum_{j_1=1}^{N}\sum_{j_2}^{N}\prod_{i=1}^{N}\left(\frac{1}{\Omega}\int d\mathbf{R}_i\right) e^{-i(\mathbf{k}-\mathbf{k}_1).\mathbf{R}_{j_1}} e^{-i(\mathbf{k}_1-\mathbf{k}').\mathbf{R}_{j_2}}.
\end{aligned} \tag{15}$$

If $j_1 \neq j_2$, $N-2$ integrals give unity while the integral over $j_1$ and $j_2$ give

$$\frac{1}{\Omega}\int d\mathbf{R}_j e^{-i(\mathbf{k}-\mathbf{k}_1).\mathbf{R}_{j_1}} e^{-i(\mathbf{k}_1-\mathbf{k}').\mathbf{R}_{j_2}} = \delta_{\mathbf{k}\mathbf{k}_1}\delta_{\mathbf{k}_1\mathbf{k}'}. \tag{16}$$

If $j_1 = j_2$, $N-1$ integrals give unity while the integral over $j_1 = j_2$ gives

$$\frac{1}{\Omega}\int d\mathbf{R}_{j_1} e^{-i(\mathbf{k}-\mathbf{k}_1).\mathbf{R}_{j_1}} e^{-i(\mathbf{k}_1-\mathbf{k}').\mathbf{R}_{j_1}} = \delta_{\mathbf{k}\mathbf{k}'}. \tag{17}$$

Therefore,

$$\begin{aligned}
\langle\rho(\mathbf{k}-\mathbf{k}_1)\rho\left(\mathbf{k}_1-\mathbf{k}'\right)\rangle_{\text{imp}} &= \sum_{j_1 j_2}\left((1-\delta_{j_1 j_2})\delta_{\mathbf{k}\mathbf{k}_1}\delta_{\mathbf{k}_1\mathbf{k}'} + \delta_{j_1 j_2}\delta_{\mathbf{k}\mathbf{k}'}\right) \\
&= \left(N^2 - N\right)\delta_{\mathbf{k}\mathbf{k}_1}\delta_{\mathbf{k}_1\mathbf{k}'} + N\delta_{\mathbf{k}\mathbf{k}'} \\
&= N\left(N-1\right)\delta_{\mathbf{k}\mathbf{k}_1}\delta_{\mathbf{k}_1\mathbf{k}'} + N\delta_{\mathbf{k}\mathbf{k}'} \\
&\simeq N^2\delta_{\mathbf{k}\mathbf{k}'}\delta_{\mathbf{k}\mathbf{k}_1} + N\delta_{\mathbf{k}\mathbf{k}'} \\
&= \left(N^2\delta_{\mathbf{k}\mathbf{k}_1} + N\right)\delta_{\mathbf{k}\mathbf{k}'}.
\end{aligned} \tag{18}$$

For $n = 3$:

$$\langle\rho(\mathbf{k}-\mathbf{k}_1)\rho(\mathbf{k}_1-\mathbf{k}_2)\rho(\mathbf{k}_2-\mathbf{k}')\rangle_{\text{imp}} = \sum_{j_1=1}^{N}\sum_{j_2}^{N}\sum_{j_3}^{N}\prod_{i=1}^{N}\left(\frac{1}{\Omega}\int d\mathbf{R}_i\right) e^{-i(\mathbf{k}-\mathbf{k}_1).\mathbf{R}_{j_1}} e^{-i(\mathbf{k}_1-\mathbf{k}_2).\mathbf{R}_{j_2}} e^{-i(\mathbf{k}_2-\mathbf{k}').\mathbf{R}_{j_3}}. \tag{19}$$

The various cases we need to consider and the delta functions obtained for each case, are

$$\begin{aligned}
j_1 \neq j_2 \neq j_3 \quad &\Longrightarrow \delta_{\mathbf{k}\mathbf{k}_1}\delta_{\mathbf{k}_1\mathbf{k}_2}\delta_{\mathbf{k}_2\mathbf{k}'} \\
j_1 = j_2 \neq j_3 \quad &\Longrightarrow \delta_{\mathbf{k}\mathbf{k}_2}\delta_{\mathbf{k}_2\mathbf{k}'} \\
j_1 \neq j_2 = j_3 \quad &\Longrightarrow \delta_{\mathbf{k}\mathbf{k}_1}\delta_{\mathbf{k}_1\mathbf{k}'} \\
j_1 = j_3 \neq j_2 \quad &\Longrightarrow \delta_{\mathbf{k}+\mathbf{k}_2,\mathbf{k}_1+\mathbf{k}'}\delta_{\mathbf{k}_1\mathbf{k}_2} \\
j_1 = j_2 = j_3 \quad &\Longrightarrow \delta_{\mathbf{k}\mathbf{k}'}.
\end{aligned} \tag{20}$$

This gives

$$\langle\rho(\mathbf{k}-\mathbf{k}_1)\rho(\mathbf{k}_1-\mathbf{k}_2)\rho(\mathbf{k}_2-\mathbf{k}')\rangle = \left(N^3\delta_{\mathbf{k}\mathbf{k}_1}\delta_{\mathbf{k}_1\mathbf{k}_2} + N^2\delta_{\mathbf{k}\mathbf{k}_2} + N^2\delta_{\mathbf{k}\mathbf{k}_1} + N^2\delta_{\mathbf{k}_1\mathbf{k}_2} + N\right)\delta_{\mathbf{k}\mathbf{k}'} \tag{21}$$

where we have made the approximations like $N(N-1) \simeq N^2$ and rewrite the delta function products in order to show that all terms contain a $\delta_{\mathbf{k}\mathbf{k}'}$ and this is also true for higher orders of $n$. Now, the impurity averaged Green's function $G(\mathbf{k}, \mathbf{k}')$ is diagonal in $\mathbf{k}$-space

$$\langle G(\mathbf{k}, \mathbf{k}') \rangle = \langle G(\mathbf{k}) \rangle \delta_{\mathbf{k}\mathbf{k}'}. \tag{22}$$

This is a consequence of the fact that the impurity averaging makes the system translationally invariant, i.e. electrons see the same average environment everywhere in the system.

## A.3 Feynman rules for diagrams contributing to impurity averaged Green function

By investigating the terms in the perturbation expansion for the impurity-averaged Green function, one can deduce the following Feynman rules.

1. Each Feynman diagram has
   - $n + 1$ directed full lines (representing electrons) laid end to end,
   - $n$ directed dashed lines (representing interactions), which end at the junction between two electron lines, and begin at one, and
   - $m \leq n$ crosses (representing impurities).
2. Construction of the diagram
   - Both the full (electron) lines and the dashed (interaction) lines are labelled by momenta.
   - To generate all diagrams for a given m one connects the n interaction lines with the m crosses in all possible topologically different ways. One carries out this procedure for each m satisfying $1 \leq m \leq n$.
3. For a given diagram, the Feynman rules are
   - For each electron line of momentum $\mathbf{k}$, associate a factor $G^{(0)}(\mathbf{k})$. The leftmost and rightmost electron lines both have momentum $\mathbf{k}$.

- For each interaction line of momentum $\mathbf{q}$, associate a factor $U(\mathbf{q})$.
- For each impurity cross, associate a factor $N$.
- At each impurity vertex (cross) the sum of the momenta of the connected outgoing interaction lines must equal zero. That is, there is momentum conservation at each impurity vertex.
- Sum over all momenta that are left undetermined by momentum conservation.

# Appendix B

## B.1 Disordered s-wave superconductors

The self energy $\Sigma_{\downarrow\uparrow}(\mathbf{k}, i\omega_n)$

$$\begin{aligned}\Sigma_{\downarrow\uparrow}(\mathbf{k}, i\omega_n) &= \frac{n_i}{(2\pi)^2}\int |u(\mathbf{k}-\mathbf{k}')|^2 G^{(0)}_{\downarrow\uparrow}(\mathbf{k}', \omega) d^2\mathbf{k}' \\ &= \frac{n_i m}{(2\pi)^2}\int_{-\infty}^{\infty}\int_0^{2\pi}\left(u_0^2 + u_1^2\cos(\phi_{kk'}) + u_2^2\cos(2\phi_{kk'})\right)\frac{\Delta^*}{\omega_n^2+\xi^2+|\Delta|^2}d\phi' d\xi. \end{aligned} \tag{23}$$

Since $\cos(n\phi')$ and $\sin(n\phi)$ both integrate to zero over $2\pi$ for any integer $n$, $u_1^2$ and $u_2^2$ terms do not contribute. Therefore, we have

$$\begin{aligned}\Sigma_{\downarrow\uparrow}(\mathbf{k}, i\omega_n) &= \frac{n_i m u_0^2 \Delta^*}{(2\pi)^2}\int_{-\infty}^{\infty}\int_0^{2\pi}\frac{1}{\omega_n^2+\xi^2+|\Delta|^2}d\phi' d\xi \\ &= \frac{n_i m u_0^2 \Delta}{2\pi}\int_{-\infty}^{\infty}\frac{1}{\omega_n^2+\xi^2+|\Delta|^2}d\xi \\ &= \frac{n_i m u_0^2 \Delta}{2\pi}\frac{\tan\left(\xi/\sqrt{\omega_n^2+|\Delta|^2}\right)}{\sqrt{\omega_n^2+|\Delta|^2}}\Bigg|_{-\infty}^{\infty} \\ &= \frac{n_i m u_0^2 \Delta^*}{2\pi}\frac{\pi}{\sqrt{\omega_n^2+|\Delta|^2}} \\ &= \frac{n_i m u_0^2 \Delta^*}{2}\frac{1}{\sqrt{\omega_n^2+|\Delta|^2}}. \end{aligned} \tag{24}$$

The self-energy $\Sigma_{\uparrow\uparrow}(\mathbf{k}, i\omega_n)$

$$\begin{aligned}\Sigma_{\uparrow\uparrow}(\mathbf{k}, i\omega_n) &= \frac{n_i}{(2\pi)^2}\int |u(\mathbf{k}-\mathbf{k}')|^2 G_{\uparrow\uparrow}(0)(\mathbf{k}', \omega) d^2\mathbf{k}' \\ &= -\frac{n_i m}{(2\pi)^2}\int_{-\infty}^{\infty}\int_0^{2\pi}\left(u_0^2 + u_1^2\cos(\phi_{kk'}) + u_2^2\cos(2\phi_{kk'})\right)\frac{i\omega_n+\xi}{\omega_n^2+\xi^2+|\Delta|^2}d\phi' d\xi. \end{aligned} \tag{25}$$

Here also, the terms $\cos(n\phi')$ and $\sin(n\phi)$ integrate to zero over $2\pi$. Besides, the term containing $\xi$ in the numinator integrates to zero. Hence, we have

$$\begin{aligned}
\Sigma_{\uparrow\uparrow}(\mathbf{k}, i\omega_n) &= -\frac{n_i m u_0^2 i\omega_n}{(2\pi)^2}\int_{-\infty}^{\infty}\int_0^{2\pi}\frac{1}{\omega_n^2+\xi^2+|\Delta|^2}d\phi' d\xi \\
&= -\frac{n_i m u_0^2 i\omega_n}{2\pi}\int_{-\infty}^{\infty}\frac{1}{\omega_n^2+\xi^2+|\Delta|^2}d\xi \\
&= -\frac{n_i m u_0^2 i\omega_n}{2\pi}\frac{\tan\left(\xi/\sqrt{\omega_n^2+|\Delta|^2}\right)}{\sqrt{\omega_n^2+|\Delta|^2}}\Bigg|_{-\infty}^{\infty} \\
&= -\frac{n_i m u_0^2 i\omega_n}{2\pi}\frac{\pi}{\sqrt{\omega_n^2+|\Delta|^2}} \\
&= -\frac{n_i m u_0^2 i\omega_n}{2}\frac{1}{\sqrt{\omega_n^2+|\Delta|^2}}.
\end{aligned} \tag{26}$$

The self-consistency condition

$$\begin{aligned}
\Delta^* &= \frac{T}{(2\pi)^2}\sum_n\int V_{\mathbf{k}\mathbf{k}'}G_{\downarrow\uparrow}(\mathbf{k}', i\omega_n)d^2\mathbf{k}' \\
&= \frac{VTm}{(2\pi)^2}\sum_n\int_0^{2\pi}\int_{-\infty}^{\infty}\frac{\tilde{\Delta}^*}{\tilde{\omega}_n^2+\xi^2+|\tilde{\Delta}|^2}d\xi d\phi' \\
&= \frac{VTm}{2\pi}\sum_n\int_{-\infty}^{\infty}\frac{\tilde{\Delta}^*}{\tilde{\omega}_n^2+\xi^2+|\tilde{\Delta}|^2}d\xi \\
&= \frac{VTm}{2}\sum_n\frac{\tilde{\Delta}^*}{\sqrt{\tilde{\omega}_n^2+|\tilde{\Delta}|^2}} \\
&= \frac{VTm}{2}\sum_n\frac{\eta_\omega\Delta^*}{\sqrt{\eta_\omega^2\omega_n^2+\eta_\omega^2|\Delta|^2}} \\
&= \frac{VTm}{2}\sum_n\frac{\Delta^*}{\sqrt{\omega_n^2+|\Delta|^2}}.
\end{aligned} \tag{27}$$

## B.2 Disordered d-wave superconductors

The self-energy $\Sigma_{\downarrow\uparrow}(\mathbf{k}, i\omega_n)$

$$\begin{aligned}
\Sigma_{\downarrow\uparrow}(\mathbf{k},\omega_n) &= \frac{n_i}{(2\pi)^2}\int |u(\mathbf{k}-\mathbf{k}')|^2 G^{(0)}_{\downarrow\uparrow}(\mathbf{k},\omega_n) d^2\mathbf{k}' \\
&= \frac{n_i m}{(2\pi)^2}\int_{-\infty}^{\infty}\int_0^{2\pi} |u(\mathbf{k}-\mathbf{k}')|^2 \frac{\Delta^*\cos(2\phi')}{\omega_n^2+\xi^2+|\Delta|^2\cos^2(2\phi')} d\phi' d\xi \\
&= \frac{n_i m}{(2\pi)^2}\int_{-\infty}^{\infty}\int_0^{2\pi} \Big(u_0^2 + u_1^2\cos(\phi_k-\phi_k') + u_2^2\cos(2(\phi_k-\phi_{k'}))\Big) \\
&\times \frac{\Delta^*\cos(2\phi')}{\omega_n^2+\xi^2+|\Delta|^2\cos^2(2\phi')} d\phi' d\xi. \qquad (28)
\end{aligned}$$

Only the $\cos(2(\phi-\phi'))$ term from the scattering potential contributes. Hence, we have

$$\begin{aligned}
\Sigma_{\downarrow\uparrow}(\mathbf{k},\omega_n) &= \frac{n_i m}{(2\pi)^2}\int_{-\infty}^{\infty}\int_0^{2\pi} u_2^2\cos(2(\phi-\phi'))\frac{\Delta^*\cos(2\phi')}{\omega_n^2+\xi^2+|\Delta|^2\cos^2(2\phi')} d\phi' d\xi \\
&= \frac{n_i m u_2^2\Delta^*}{(2\pi)^2}\int_{-\infty}^{\infty}\int_0^{2\pi} \frac{\Big(\cos(2\phi)\cos(2\phi') + \sin(2\phi)\sin(2\phi')\Big)\cos(2\phi')}{\omega_n^2+\xi^2+|\Delta|^2\cos^2(2\phi')} d\phi' d\xi \\
&= \frac{n_i m u_2^2\Delta^*}{(2\pi)^2}\int_{-\infty}^{\infty}\int_0^{2\pi} \frac{\cos(2\phi)\cos(2\phi')\cos(2\phi')}{\omega_n^2+\xi^2+|\Delta|^2\cos^2(2\phi')} d\phi' d\xi \\
&= \frac{n_i m u_2^2\Delta^*\cos(2\phi)}{(2\pi)^2}\int_{-\infty}^{\infty}\int_0^{2\pi} \frac{\cos^2(2\phi')}{\omega_n^2+\xi^2+|\Delta|^2\cos^2(2\phi')} d\phi' d\xi \\
&= \frac{n_i m u_2^2\Delta^*\cos(2\phi)}{2\pi}\int_{-\infty}^{\infty}\frac{1}{|\Delta|^2}\left[1-\frac{\sqrt{\omega_n^2+\xi^2}}{\sqrt{\omega_n^2+\xi^2+|\Delta|^2}}\right] d\xi \\
&= \frac{n_i m u_2^2\Delta^*\cos(2\phi)}{2\pi}\int_{-\infty}^{\infty}\frac{1}{|\Delta|^2}\left[1-\frac{\sqrt{\omega_n^2+\xi^2}}{\sqrt{\omega_n^2+\xi^2+|\Delta|^2}}\right] d\xi \qquad (29)
\end{aligned}$$

Expanding the square root term in the denominator in a Taylor series gives

$$\begin{aligned}
&\Sigma_{\downarrow\uparrow}(\mathbf{k},\omega_n) \\
&\quad= \frac{n_i m u_2^2 \Delta^* \cos(2\phi)}{2\pi} \int_{-\infty}^{\infty} \frac{1}{|\Delta|^2}\left[1 - \sqrt{\omega_n^2+\xi^2}\left(\frac{1}{\sqrt{\omega_n^2+\xi^2}} - \frac{|\Delta|^2}{2(\omega_n^2+\xi^2)^{3/2}}\right)\right] d\xi \\
&\quad= \frac{n_i m u_2^2 \Delta^* \cos(2\phi)}{2\pi} \int_{-\infty}^{\infty} \frac{1}{|\Delta|^2}\frac{|\Delta|^2}{2(\omega_n^2+\xi^2)} d\xi \\
&\quad= \frac{n_i m u_2^2 \Delta^* \cos(2\phi)}{4\pi} \int_{-\infty}^{\infty} \frac{1}{\omega_n^2+\xi^2} d\xi \\
&\quad= \frac{n_i m u_2^2 \Delta^* \cos(2\phi)}{4\pi} \frac{\pi}{|\omega_n|} \\
&\quad= \frac{n_i m u_2^2 \Delta^* \cos(2\phi)}{4} \frac{1}{|\omega_n|}.
\end{aligned} \tag{30}$$

Similarly, the self-energy $\Sigma_{\uparrow\uparrow}(\mathbf{k},\omega_n)$ becomes

$$\begin{aligned}
\Sigma_{\uparrow\uparrow}(\mathbf{k},\omega_n) &= \frac{n_i}{(2\pi)^2}\int |u(\mathbf{k}-\mathbf{k}')|^2 G^{(0)}_{\uparrow\uparrow}(\mathbf{k},\omega_n) d^2\mathbf{k}' \\
&= -\frac{n_i m}{(2\pi)^2}\int_{-\infty}^{\infty}\int_0^{2\pi} |u(\mathbf{k}-\mathbf{k}')|^2 \frac{i\omega_n+\xi}{\omega_n^2+\xi^2+|\Delta|^2\cos^2(2\phi')} d\phi' d\xi \\
&= -i\omega_n \frac{n_i m}{(2\pi)^2}\int_{-\infty}^{\infty}\int_0^{2\pi} \left(u_0^2 + u_1^2\cos(\phi_k-\phi_k') + u_2^2\cos(2(\phi_k-\phi_{k'}))\right) \\
&\times \frac{1}{\omega_n^2+\xi^2+|\Delta|^2\cos^2(2\phi')} d\phi' d\xi.
\end{aligned} \tag{31}$$

where we have thrown away the $\xi$ term in the numerator because we know it will integrate to zero. In this case, only the s-wave term will contribute, so that we have

$$\begin{aligned}
\Sigma_{\uparrow\uparrow}(\mathbf{k},\omega_n) &= -i\omega_n \frac{n_i m}{(2\pi)^2}\int_{-\infty}^{\infty}\int_0^{2\pi} \frac{u_0^2}{\omega_n^2+\xi^2+|\Delta|^2\cos^2(2\phi')} d\phi' d\xi \\
&= -i\omega_n \frac{n_i m u_0^2}{(2\pi)^2}\int_{-\infty}^{\infty} \frac{2\pi}{\sqrt{\omega_n^2+\xi^2}\sqrt{\omega_n^2+\xi^2+|\Delta|^2}} d\xi \\
&= -i\omega_n \frac{n_i m u_0^2}{2\pi}\int_{-\infty}^{\infty} \frac{1}{\sqrt{\omega_n^2+\xi^2}\sqrt{\omega_n^2+\xi^2+|\Delta|^2}} d\xi.
\end{aligned} \tag{32}$$

Expanding the second square root term in the integral in a Taylor series similarly to before, we have

$$\begin{aligned}\Sigma_{\uparrow\uparrow}(\mathbf{k},\omega_n) &= -i\omega_n \frac{n_i m u_0^2}{2\pi}\int_{-\infty}^{\infty}\frac{1}{\sqrt{\omega_n^2+\xi^2}}\left(\frac{1}{\sqrt{\omega_n^2+\xi^2}}-\frac{|\Delta|^2}{2(\omega_n^2+\xi^2)^{3/2}}\right)d\xi \\ &= -i\omega_n \frac{n_i m u_0^2}{2\pi}\int_{-\infty}^{\infty}\left(\frac{1}{\omega_n^2+\xi^2}-\frac{|\Delta|^2}{2(\omega_n^2+\xi^2)^2}\right)d\xi \\ &= -i\omega_n \frac{n_i m u_0^2}{2\pi}\left(\frac{\pi}{|\omega_n|}-\frac{\pi|\Delta|^2}{4|\omega_n|^3}\right) \\ &= -i\omega_n \frac{n_i m u_0^2}{2}\left(\frac{1}{|\omega_n|}-\frac{|\Delta|^2}{4|\omega_n|^3}\right). \end{aligned} \tag{33}$$

The self-consistency condition

$$\begin{aligned}\Delta^*(\mathbf{k}) &= \frac{T}{(2\pi)^2}\sum_n \int V_{\mathbf{k}\mathbf{k}'} G_{\downarrow\uparrow}(\mathbf{k}',\omega_n) d^2\mathbf{k}' \\ &= \frac{VTm}{(2\pi)^2}\sum_n \int_{-\infty}^{\infty}\int_0^{2\pi}\frac{\cos(2(\phi-\phi'))\tilde{\Delta}\cos(2\phi')}{\tilde{\omega}^2+\xi^2+\tilde{\Delta}^2\cos^2(2\phi')}d\phi' d\xi \\ &= \frac{VTm}{(2\pi)^2}\sum_n \int_{-\infty}^{\infty}\int_0^{2\pi}\frac{\eta_{\omega 2}\Delta[\cos(2\phi)\cos(2\phi')+\sin(2\phi)\sin(2\phi')]\cos(2\phi')}{\tilde{\omega}^2+\xi^2+\tilde{\Delta}^2\cos^2(2\phi')}d\phi' d\xi \\ &= \frac{VTm\Delta^*(\mathbf{k})}{(2\pi)^2}\sum_n \int_{-\infty}^{\infty}\int_0^{2\pi}\frac{\eta_{\omega 2}\cos^2(2\phi')}{\tilde{\omega}^2+\xi^2+\tilde{\Delta}^2\cos^2(2\phi')}d\phi' d\xi \\ &= \frac{VTm\Delta^*(\mathbf{k})}{(2\pi)^2}\sum_n \int_{-\infty}^{\infty}\frac{\eta_{\omega 2}2\pi}{|\tilde{\Delta}|^2}\left[1-\frac{\sqrt{\omega^2+\xi^2}}{\tilde{\omega}^2+\xi^2+|\tilde{\Delta}|^2}\right]d\xi \\ &= \frac{VTm\Delta^*(\mathbf{k})}{2\pi}\sum_n \int_{-\infty}^{\infty}\frac{\eta_{\omega 2}}{|\tilde{\Delta}|^2}\left[1-\frac{\sqrt{\omega^2+\xi^2}}{\tilde{\omega}^2+\xi^2+|\tilde{\Delta}|^2}\right]d\xi. \end{aligned} \tag{34}$$

Expanding the bottom square root in the right part of the integrand in a Taylor series as before, we have approximately that

$$\begin{aligned}\Delta^*(\mathbf{k}) &\approx \frac{VTm\Delta^*(\mathbf{k})}{4\pi}\sum_n \int_{-\infty}^{\infty}\frac{\eta_{\omega 2}}{|\tilde{\Delta}|^2}\frac{|\tilde{\Delta}|^2}{2(\tilde{\omega}^2+\xi^2)}d\xi \\ &= \frac{VTm\Delta^*(\mathbf{k})}{4\pi}\sum_n \eta_{\omega 2}\frac{\pi}{|\tilde{\omega}_n|} \\ &= \frac{VTm\Delta^*(\mathbf{k})}{4}\sum_n \eta_{\omega 2}\frac{1}{|\tilde{\omega}_n|}. \end{aligned} \tag{35}$$

# Appendix C

## Calculation of $< \theta_{ij}^2 >_{tr}$

Employing the Fourier representation of $\theta_i(\tau)$ gives

$$< \theta_{ij}^2 >_{tr} = \frac{1}{N^2} \sum_{kk'} \left( e^{i\mathbf{k}\cdot\mathbf{R}_i} - e^{i\mathbf{k}\cdot\mathbf{R}_j} \right) \left( e^{i\mathbf{k}'\cdot\mathbf{R}_i} - e^{i\mathbf{k}'\cdot\mathbf{R}_j} \right) < \theta_k \theta_{k'} >_{tr} . \tag{36}$$

where $\mathbf{R}_i$ and $\mathbf{R}_j$ denotes the position of lattice sites. The JJA arrays are assumed to be translationally invariant, and this results

$$< \theta_k \theta_{k'} >_{tr} = < \theta_k \theta_{-k} >_{tr} \delta_{k,-k}. \tag{37}$$

With this, equation (36) becomes

$$< \theta_{ij}^2 >_{tr} = \frac{2}{N^2} \sum_{k} \left[ 1 - \cos(\mathbf{k} \cdot \mathbf{R}_{ij}) \right] < \theta_k \theta_{-k} >_{tr} \tag{38}$$

where $\mathbf{R}_{ij} = \mathbf{R}_i - \mathbf{R}_j$.

The trial action $S_{tr}[\theta]$ in equation (5.36) can be written in Matsubara frequencies domain as

$$S_{CE}[\theta] = \frac{\hbar^3 \beta}{8UN} \sum_{k} \sum_{n} \theta_{k,n} \theta_{-k,-n} \omega_n^2, \tag{39}$$

where $\omega_n = \left( \frac{2\pi n}{\hbar \beta} \right)$ are Matsubara frequencies and assume integral values ($n$ being both positive and negative, including zero). Making similar substitutions in the Josephson coupling term gives

$$S_{JE}[\theta] = \frac{\beta D_s}{8N} \sum_{k} \sum_{n} \sum_{j(i)} \left[ 1 - \cos(\mathbf{k} \cdot \mathbf{R}_{ij}) \right] \theta_{k,n} \theta_{-k,-n}. \tag{40}$$

The summation over nearest neighbours $j$ of a grain site $i$ defines structure factor of the lattice as

$$f(k) = \sum_{j(i)} \Big(1 - \cos(\mathbf{k} \cdot \mathbf{R}_{ij})\Big) = z - 2 \sum_{j=1}^{d} \cos(k_j a). \tag{41}$$

where $z$ and $d$ are the coordination number and the dimensionality of the lattice respectively. Therefore, the trial action in a Fourier transformed form is given by

$$S_{tr}[\theta] = S_{CE}[\theta] + S_{JE}[\theta] = \frac{\beta}{N} \sum_{k} \sum_{n} \left(\frac{1}{8U}\omega_n^2 + \frac{D_s}{8} f(k)\right) |\theta_{k,n}|^2 \tag{42}$$

where the conditions of phase reality of the phase variable ($\theta^*_{k,n} = \theta_{-k,-n}$) has been considered. Using the stationary property of the correlation function, the equal time correlator on the right-hand-side of (38) can be written as

$$\langle \theta_k \theta_{-k} \rangle_{tr} = \sum_{n} \langle \theta_{k,n} \theta_{-k,-n} \rangle_{tr}. \tag{43}$$

The averages on the RHS of this equation can be expressed as multiple Gaussian integrals over the real and imaginary parts of the Fourier components

$$\theta_{k,n} = \theta^r_{k,n} + i\theta^i_{k,n}\,. \tag{44}$$

The real and imaginary parts of (44) for a given $(k, n)$ are not independent of those for $(-k, -n)$. Therefore, to avoid overcounting, the action in (42) is written as a sum over the space of a positive $(k, n)$ values, and also the path integral for $\sum_n \langle \theta_{k,n} \theta_{-k,-n} \rangle_{tr}$ involves only variables in this space. Thus, for a given $k_0 > 0$, $n_0 > 0$, one obtains

$$\langle \theta_{k_0,n_0} \theta_{-k_0,-n_0} \rangle_{tr} = \frac{1}{Z_{tr}} \int D\theta \exp\left(-\frac{S_0[\theta]}{\hbar}\right) (\theta_{k_0,n_0} \theta_{-k_0,-n_0})\,. \tag{45}$$

Here,

$$(\theta_{k_0,n_0} \theta_{-k_0,-n_0}) = \left(\theta_{k_0,n_0} \theta^*_{k_0,n_0}\right) = \left(\theta^r_{k_0,n_0}\right)^2 + \left(\theta^i_{k_0,n_0}\right)^2. \tag{46}$$

Wth this, equation (45) becomes

$$\langle\theta_{k_0,n_{tr}}\theta_{-k_0,-n_0}\rangle_0 = \frac{1}{Z_0}\prod_{k>0,n>0}\int_{-\infty}^{\infty}d\theta^r_{k,n}\int_{-\infty}^{\infty}d\theta^i_{k,n}\left[\left(\theta^r_{k_0,n_0}\right)^2+\left(\theta^i_{k_0,n_0}\right)^2\right]$$
$$\times\exp\left[-\frac{2\beta}{N}\left(\frac{\hbar^2}{8U}\omega_n^2+\frac{D_s}{8}f(k)\right)+\left[\left(\theta^r_{k,n}\right)^2+\left(\theta^i_{k,n}\right)^2\right]\right]. \tag{47}$$

The integrals over Fourier components with $k \neq k_0$ and $n \neq n_0$ get cancelled with corresponding integrals in $Z_{tr}$ so that

$$\begin{aligned}\langle\theta_{k_0,n_0}\theta_{-k_0,-n_0}\rangle_0 &= 2\langle\left(\theta^r_{k_0,n_0}\right)^2\rangle_{tr}\\ &= 2\frac{\int_{-\infty}^{\infty}d\theta_{k_0,n_0}\left(\theta^r_{k_0,n_0}\right)^2\exp\left[-\frac{2\beta}{N}\left(\frac{\hbar^2}{8U}\omega_n^2+\frac{D_s}{8}f(k)\right)\left(\theta^r_{k_0,n_0}\right)^2\right]}{\int_{-\infty}^{\infty}d\theta_{k_0,n_0}\exp\left[-\frac{2\beta}{N}\left(\frac{\hbar^2}{8U}\omega_n^2+\frac{D_s}{8}f(k)\right)\left(\theta^r_{k_0,n_0}\right)^2\right]}\end{aligned} \tag{48}$$

Upon using the standard integrals

$$\int_{-\infty}^{\infty}e^{-\alpha x^2}=\sqrt{\frac{\pi}{\alpha}}\quad\text{and}\quad\int_{-\infty}^{\infty}x^2e^{-\alpha x^2}=\frac{1}{2\alpha}\sqrt{\frac{\pi}{\alpha}}, \tag{49}$$

this reduces the form

$$\langle\theta_{k_0,n_0}\theta_{-k_0,-n_0}\rangle_0 = \frac{N}{2\beta}\left[\frac{\hbar^2}{8U}+\frac{D_s}{8}f(k)\right]^{-1}. \tag{50}$$

Introducing this result in (43) gives

$$\langle\theta_k\theta_{-k}\rangle_{tr} = \sum_n\frac{N}{2\beta}\left[\frac{\hbar^2}{8U}+\frac{D_s}{8}f(k)\right]^{-1}. \tag{51}$$

Again, using this last equation into (38) provides

$$\langle\theta^2_{ij}\rangle_{tr} = \frac{1}{N\beta}\sum_k\sum_n\frac{\left[1-\cos(\vec{k}\cdot\vec{R}_{ij})\right]}{\left[\frac{\hbar^2}{8U}\omega_n^2+\frac{D_s}{8}f(k)\right]}. \tag{52}$$

The bond average of $\langle\theta_{ij}^2\rangle_{tr}$ is defined as

$$\langle\bar{\theta_{ij}^2}\rangle_{tr} = \frac{1}{z}\sum_{j(i)}\langle\theta_{ij}^2\rangle_{tr} = \frac{1}{N\beta z}\sum_k\sum_n \frac{f(k)}{\frac{1}{8U}\left(\omega_n^2 + UD_s f(k)\right)}. \tag{53}$$

The structure factor for a two dimensional square latice ($d = 2, z = 4$) in the long wavelength limit becomes

$$f(k) = 4 - 2\Big[\cos(k_x a)\cos(k_y a)\Big] = k_x^2 a^2 + k_y^2 a^2 \approx k^2 a^2. \tag{54}$$

As $T \to 0$, the Matsubara sum in (53) is evaluated using

$$\sum_{n=-\infty}^{\infty}\frac{1}{\omega_n^2 + \omega_\alpha^2} = \frac{\beta}{2\omega_\alpha}. \tag{55}$$

In the present case,

$$\omega_\alpha = \sqrt{Uf(k)D_s}. \tag{56}$$

Therefore,

$$\sum_{n=-\infty}^{\infty}\frac{1}{\omega_n^2 + \omega_\alpha^2} = \frac{\beta}{2\sqrt{Uf(k)D_s}}. \tag{57}$$

Using this in (53) gives

$$\begin{aligned}
\langle\bar{\theta_{ij}^2}\rangle_0 &= \frac{1}{N}\sum_k\sqrt{\frac{f(k)U}{D_s}} \\
&= \frac{1}{N}\left(\frac{U}{D_s}\right)^{1/2}\sum_k\sqrt{f(k)} \\
&= \frac{a}{N}\left(\frac{U}{D_s}\right)^{1/2}\sum_k k \\
&= \frac{a^3}{4\pi}\left(\frac{U}{D_s}\right)^{1/2}\int_0^{k_D} k^2 dk \\
&= \frac{a^3}{12\pi}\left(\frac{U}{D_s}\right)^{1/2} k_D^3 \\
&\simeq 1.2\left(\frac{U}{D_s}\right)^{1/2}
\end{aligned} \tag{58}$$

where $k_D = 2\sqrt{\pi}/a$ is Debye frequency.

# Publication

1. Deressa, Z. & Singh, P., Effect of Hydrostatic Pressure on Superconductivity of Pb. J Supercond Nov Magn (2019). https://doi.org/10.1007/s10948-019-05168-8.

2. Zeleke Deressa and P. Singh, Effect of hydrostatic pressure on superconductivity of MgB2. AIP Advances, **9**, 095038 (2019).

# Declaration

I hereby declare that this PhD dissertation is my original work, has not been presented for a degree in any other University and that all the sources of materials used for the dissertation have been duly acknowledged.

Name: **Zeleke Deressa**

Signature: _____

This PhD dissertation has been submitted for examination with my approval as a University advisor.

Name: **Prof. Pooran Singh**

Signature: _____

**Place and date of submission**

Addis Ababa University
School of Graduate Studies Physics Department
Date: **November 8, 2019**